

THE COOPER UNION FOR THE ADVANCEMENT OF
SCIENCE AND ART

ALBERT NERKEN SCHOOL OF ENGINEERING

**Mathematical Modeling of the Role of
Electrophysiological Coupling in
Mesenchymal Stem Cell Enhancement of
Cardiomyocyte Function**

by:

Joshua Mayourian

A thesis submitted in partial fulfilment
of the requirements for the degree of
Master of Engineering

May 13, 2014

Advisor:

Dr. Ruben M. Savizky

Co-Advisor:

Dr. Kevin D. Costa

THE COOPER UNION FOR THE ADVANCEMENT OF
SCIENCE AND ART

ALBERT NERKEN SCHOOL OF ENGINEERING

This thesis was prepared under the direction of the Candidate's Thesis Advisors and has received approval. It was submitted to the Dean of the School of Engineering and the full Faculty, and was approved as partial fulfillment of the requirements for the degree of Master of Engineering.

Dean Teresa A. Dahlberg, School of Engineering 5/13/14

Professor Ruben M. Savizky 5/13/14
Candidate's Thesis Advisor

Professor Kevin D. Costa 5/13/14
Candidate's Thesis Co-Advisor

“Our obligation is to give meaning to life and in doing so to overcome the passive, indifferent life.”

Elie Wiesel

אם תרצו, אין זו אנדרה; ואם לא תרצו, אנדרה היא ואנדרה תישאר

תאודר הרצל

THE COOPER UNION FOR THE ADVANCEMENT OF SCIENCE AND ART

Abstract

Mathematical Modeling of the Role of Electrophysiological Coupling in Mesenchymal Stem Cell Enhancement of Cardiomyocyte Function

by Joshua MAYOURIAN

Human mesenchymal stem cell delivery has exhibited potential in clinical myocardial infarction therapies; however, the large-scale application of this method is limited by the fact that researchers do not fully understand the mechanisms by which mesenchymal stem cells enhance cardiomyocyte function. Mathematical modeling is a powerful tool that can predict how mesenchymal stem cells interact with cardiomyocytes. Therefore, to better understand the electrical role of mesenchymal stem cells, three novel electrophysiology models were developed. The consequences of electrical interactions between cardiomyocytes and mesenchymal stem cells were predicted by coupling the ten Tusscher cardiomyocyte model to the three novel models developed in this study. Significant electrophysiological consequences were evident when the ten Tusscher model was coupled to each of the mesenchymal stem cell models in ratios of 9:1, 4:1, and 1:1, respectively. These effects include decreases in action potential duration and plateau height, and corresponding variations in ionic current. Furthermore, there was a decrease in conduction velocity and maximum upstroke velocity. These consequences correspond to established *in vitro* electrical effects, and show mesenchymal stem cells are capable of predisposing re-entrant arrhythmias. A sensitivity analysis on the mesenchymal stem cell inputs shows the robustness of the results. Overall, this model provides promising insight into the electrical interactions between the two cell types, and can be used in future studies to optimize conditions for mesenchymal stem cell therapy.

Acknowledgments

I first would like to thank all the professors and mentors who have assisted me in the completion of this project. Specifically, I would like to thank: Dr. Ruben Savizky for his guidance, advice, and patience throughout the present work and any past project he has advised me on — his enthusiasm for this thesis topic is deeply appreciated; Dr. Kevin Costa for introducing the thesis topic to me and allowing me to work within his lab — his mentorship has inspired me to one day become a physician-scientist in the field of cardiology; Dr. Eric Sobie for kindly taking the time to review my methodology and results; Dr. Benjamin Davis for teaching me the numerical methods necessary to complete this study; Dr. Kit Nicholls for kindly and patiently reviewing my drafts; Drs. Damian Williams and Chaoqin Xie for their useful insight on patch clamping; and finally Timothy Cashman for his endless support, mentorship, and lessons.

I would also like to thank my family — מאמן, יעקב, סבנה, ואמנון, Mom, Dad, Jacob, and Arielle — for supporting me throughout my life. Your love and encouragement has motivated me to never stop trying to reach my full potential. I would also like to acknowledge all of my friends for their support and loyalty. Finally, I would like to thank Vice President Stephen Baker; my Cooper Union experience would not have been the same without you.

Table of Contents

Approval	i
Abstract	iii
Table of Contents	v
List of Figures	x
List of Tables	xiii
Physical Constants	xv
Symbols	xvi
1 Introduction	1
1.1 Background and Motivation	1
1.1.1 Mesenchymal Stem Cell Background	3
1.1.2 Clinical Applications of Mesenchymal Stem Cells	4
1.1.3 Challenges of Mesenchymal Stem Cell Delivery	5
1.1.4 Mechanisms of Mesenchymal Stem Cell Enhancement of Cardiac Function	7

1.2	Motivation for Studying the Electrophysiological Mechanism	8
1.3	Cardiac Action Potential Phases	11
1.4	Functional Ion Channels in Human Mesenchymal Stem Cells	12
1.4.1	Calcium Activated Potassium Current	13
1.4.2	Delayed Rectifier Potassium Current	14
1.4.3	L-Type Calcium Current	14
1.4.4	TTX-Sensitive Sodium Current	15
1.4.5	Transient Outward Potassium Current	16
1.5	Theory of Mathematically Modeling Electrophysiological Activity . .	16
1.5.1	Basic Electrical Properties of Cardiomyocytes and Mesenchymal Stem Cells	17
1.5.2	Single Compartment Model	23
1.5.3	Voltage-Dependent Conductances	23
1.5.4	Previously Established Electrophysiological Models	28
1.5.5	Mathematical Models of Individual Human Mesenchymal Stem Cell Channels	32
1.6	Description of Patch Clamping	34
1.6.1	Background	34
1.6.2	Types of Patch Clamping	35
2	Methodology	38
2.1	Methodology of Mathematical Modeling	38
2.2	Modeling Individual Ion Channels	39
2.2.1	TTX-Sensitive Sodium Channel Current	39

2.2.2	Transient Outward Potassium Channel Current	40
2.2.3	L-Type Calcium Current	41
2.2.4	Calcium Activated Potassium Channel Current	42
2.2.5	Delayed Rectifier Potassium Channel Current	42
2.2.6	Leakage Channel Current	44
2.2.7	Ionic Concentration Variations	45
2.3	Numerical Methods Applied for Data Fitting to Ion Channel Models .	47
2.3.1	Levenberg-Marquardt Algorithm	48
2.3.2	Runge-Kutta-Fehlberg Ordinary Differential Equation Solver .	50
2.4	Modeling of Human Mesenchymal Stem Cell Electrophysiological Activity	52
2.5	Modeling Human Mesenchymal Stem Cell-Cardiomyocyte Coupling .	54
2.5.1	Action Potential Simulation	54
2.5.2	Conduction Velocity Simulation	56
3	Results	60
3.1	Human Mesenchymal Stem Cell Individual Ion Current Models	61
3.1.1	Calcium Activated Potassium Current	61
3.1.2	Delayed Rectifier Potassium Current	63
3.1.3	Transient Outward Potassium Current	67
3.1.4	L-Type Calcium Current	71
3.1.5	TTX-Sensitive Sodium Current	73
3.1.6	Leakage Current	76
3.2	Simulation of Human Mesenchymal Stem Cell Total Currents	78

3.2.1	Type A Total Current	78
3.2.2	Type B Total Current	79
3.2.3	Type C Total Current	80
3.3	Simulation of Human Mesenchymal Stem Cell-Cardiomyocyte Coupling	81
3.3.1	Type A Total Current	81
3.3.2	Type B Total Current	87
3.3.3	Type C Total Current	93
3.3.4	Weighted Average of Total Currents	99
3.4	Simulation of Coupled Human Mesenchymal Stem Cell-Cardiomyocyte Conduction Velocity	103
3.4.1	Type A Total Current	105
3.4.2	Type B Total Current	106
3.4.3	Type C Total Current	107
3.4.4	Weighted Average of Total Currents	108
4	Discussion	110
4.1	Discussion of the Novel Models	110
4.2	Discussion of Mathematical Results	111
4.2.1	Effects on Action Potential Duration and Plateau Height	112
4.2.2	Effects on Cardiomyocyte Ionic Channel Activity	113
4.2.3	Effects on Human Mesenchymal Stem Cell Electrical Activity	113
4.2.4	Effects on Gap Junction Current	114

4.2.5	Effects on Activation Threshold	115
4.2.6	Effects on Conduction Velocity and Upstroke Velocity	115
4.3	Significance of This Study	116
4.3.1	Empirical Interactions Between Cardiomyocytes and Mesenchymal Stem Cells	116
4.3.2	Clinical Implications	117
4.4	Sensitivity Analysis	118
4.5	Limitations and Future Work	121
4.5.1	Limitations of This Study	121
4.5.2	Future Work	122
5	Conclusion	124
A	Sample MATLAB Code	126
A.1	Sample Data Fitting Code	126
A.2	Sample Individual Ion Channel Current Code	128
A.3	Sample Total Mesenchymal Stem Cell Current Code	130
A.4	Sample CM-hMSC Coupling Code	132
A.5	Sample Conduction Velocity Code	155
Bibliography		166

List of Figures

1.1	Novel Cardiotherapeutic Methods for Cardiac Repair	2
1.2	Differentiation Capabilities of Mesenchymal Stem Cells	3
1.3	Challenges of Human Mesenchymal Stem Cell Delivery	6
1.4	Potential Mechanisms of Human Mesenchymal Stem Cell Enhancement of Cardiomyocyte Function	7
1.5	Comparative Analysis of Contractile Function of Engineered Cardiac Tissue With and Without Mesenchymal Stem Cell Implementation .	9
1.6	The Five General Phases of a Cardiac Action Potential	11
1.7	Calcium Activated Potassium Channel	13
1.8	Delayed Rectifier K ⁺ Current-Like hEAG1 Channel	14
1.9	L-type Calcium Channel	15
1.10	TTX-Sensitive Sodium Channel	15
1.11	Single Compartment Model of a Cell's Capacitance and Membrane Resistance	18
1.12	Membrane Channel Gating	25
1.13	A Model of a Noninactivating Channel	26
1.14	Ion Movement Across Cardiomyocyte Cell Membrane	30

1.15 Ten Tusscher Action Potential Simulation	31
1.16 Types of Patch Clamping	35
1.17 Mesenchymal Stem Cell Whole-Cell Recording	36
2.1 Delayed-Rectifier Potassium Channel Model	43
2.2 Line-Search and Trust-Region Algorithms	48
2.3 Human Mesenchymal Stem Cell Model	53
3.1 Fitting the Calcium Activated Potassium Channel I-V Curve	62
3.2 Comparison Between Empirical and Simulation KCa Channel Activity	63
3.3 Delayed Rectifier Potassium I-V Curve	65
3.4 Comparison Between Empirical and Simulation Delayed Rectifier Potassium Channel Activity	67
3.5 Transient Outward Channel I-V Curve	69
3.6 Comparison Between Empirical and Simulation Transient Outward Potassium Channel Activity	70
3.7 L-type Calcium Channel I-V Curve	72
3.8 Comparison Between Empirical and Simulation L-type Calcium Channel Activity	73
3.9 Sodium Channel I-V Curve	75
3.10 Comparison Between Empirical and Simulation Sodium Channel Activity	76
3.11 Mesenchymal Stem Cell Membrane Potential Simulation	77
3.12 Comparison Between Simulated and Empirical Total Current “A” . .	79

3.13 Comparison Between Simulated and Empirical Total Current “B”	80
3.14 Comparison Between Simulated and Empirical Total Current “C”	80
3.15 Cardiomyocyte-Type “A” Mesenchymal Stem Cell Interaction Simulation	82
3.16 Effects on Cardiomyocyte Ionic Channels	83
3.17 Effects on Human Mesenchymal Stem Cell Electrical Activity	84
3.18 Gap Junction Current	85
3.19 Cardiomyocyte-Type “B” Mesenchymal Stem Cell Interaction Simulation	87
3.20 Effects on Cardiomyocyte Ionic Channels	89
3.21 Effects on Human Mesenchymal Stem Cell Electrical Activity	90
3.22 Gap Junction Current	91
3.23 Cardiomyocyte-Type “C” Mesenchymal Stem Cell Interaction Simulation	93
3.24 Effects on Cardiomyocyte Ionic Channels	95
3.25 Effects on Human Mesenchymal Stem Cell Electrical Activity	96
3.26 Gap Junction Current	97
3.27 Cardiomyocyte-Mesenchymal Stem Cell Interaction Simulation	99
3.28 Effects on Cardiomyocyte Ionic Channels	101
3.29 Cardiomyocyte Conduction Velocity Simulation	103
3.30 Top View of Cardiac Action Potential Propagation	104
4.1 Sensitivity Analysis of Maximum Conductance Parameters	119
4.2 Sensitivity Analysis of Activation Kinetic Parameters	120

List of Tables

1.1	Summary of Numerous Clinical <i>in vivo</i> Studies of Mesenchymal Stem Cell Delivery for Cardiac Repair	5
1.2	Functional Ion Channels in a Cardiac Action Potential	12
1.3	Functional Ion Channels in Human Mesenchymal Stem Cells	12
1.4	Transient or Persistent Behavior of Functional Ion Channels in Human Mesenchymal Stem Cells	33
2.1	Types of Total Currents for Mesenchymal Stem Cells	53
2.2	Types of Total Currents for Mesenchymal Stem Cells	54
2.3	Prevalence of Each Type of Total Currents for Mesenchymal Stem Cells	56
2.4	Parameter Values	59
3.1	Calcium Activated Potassium Channel Formulation	61
3.2	Delayed Rectifier Potassium Channel Formulation	64
3.3	Initial Conditions of Delayed Rectifier Potassium Channel	66
3.4	Transient Outward Potassium Channel Formulation	68
3.5	L-type Calcium Channel Formulation	71
3.6	Sodium Channel Formulation	74

3.7	Leakage Channel Formulation	77
3.8	Effects of Mesenchymal Stem Cell “A” on Action Potential Duration	83
3.9	Effects of Mesenchymal Stem Cell “A” on Activation Threshold . . .	86
3.10	Effects of Mesenchymal Stem Cell “B” on Action Potential Duration .	88
3.11	Effects of Mesenchymal Stem Cell “B” on Activation Threshold . . .	92
3.12	Effects of Mesenchymal Stem Cell “C” on Action Potential Duration	94
3.13	Effects of Mesenchymal Stem Cell “C” on Activation Threshold . . .	98
3.14	Effects on Action Potential Duration	100
3.15	Effects of Mesenchymal Stem Cells on Activation Threshold	102
3.16	Effects of Mesenchymal Stem Cell “A” on Conduction Velocity	105
3.17	Effects of Mesenchymal Stem Cell “A” on Maximum Upstroke Velocity	105
3.18	Effects of Mesenchymal Stem Cell “B” on Conduction Velocity	106
3.19	Effects of Mesenchymal Stem Cell “B” on Maximum Upstroke Velocity	107
3.20	Effects of Mesenchymal Stem Cell “C” on Conduction Velocity	107
3.21	Effects of Mesenchymal Stem Cell “C” on Maximum Upstroke Velocity	108
3.22	Effects on Conduction Velocity	109
3.23	Effects of Mesenchymal Stem Cells on Maximum Upstroke Velocity .	109
4.1	Parameters Modified for Sensitivity Analysis	118

Physical Constants

Gas Constant $R = 8.314462175 \frac{\text{J}}{\text{mol K}}$

Faraday Constant $F = 9.6485339924 \times 10^4 \frac{\text{C}}{\text{mol}}$

Boltzmann Constant $k = 1.3806488 \times 10^{-23} \frac{\text{m}^2\text{kg}}{\text{s}^2\text{K}}$

Symbols

In order of appearance:

I_e	Current Entering Cell	A
R_m	Membrane Resistance	Ω
ΔV	Change in Membrane Potential	V
C_m	Capacitance	F
Q	Excess Intracellular Charge	C
V	Membrane Potential	V
I	Current	A
τ_m	Membrane Time Constant	s
E_m	Equilibrium Potential	V
$\mathbf{j}_{d,p}$	Diffusional Flux Vector of Species p	$\frac{\text{mol}}{\text{m}^2\text{s}}$
D_p	Diffusivity Constant of Species p	m^2/s
C_p	Concentration of Species p	$\frac{\text{mol}}{\text{m}^3}$
u_p	Velocity of ion p	m/s
$\mathbf{j}_{e,p}$	Ionic Flux Vector of Species p	$\frac{\text{mol}}{\text{m}^2\text{s}}$
Z_p	Valence of ion p	unitless

Φ	Electric Potential	V
T	Absolute Temperature	K
r	Radial Distance	m
V^{rest}	Resting Membrane Potential	V
G_i	Conductance of Channel i	S
I_{total}	Total Current	A
I_{stim}	Stimulus Current	A
\overline{G}_i	Maximum Conductance of Channel i	S
P_i	Probability of Channel i Open	unitless
n	Activation Variable	unitless
n_∞	Steady-state n	unitless
τ_n	Time Constant	s
α_n	Gating Transition Rate	unitless
β_n	Gating Transition Rate	unitless
q	Charge of Ion	unitless
B_α	Function of Amount of Ion	unitless
	Charge and Distance Traveled	
V_T	Thermal Voltage	V
A_α	Parameter	Unitless
B_β	Function of Amount of Ion	unitless
A_β	Parameter	unitless
m	Activation Variable	unitless
h	Probability Variable	unitless

I_{ion}	Total Ionic Current	A
I_{Na}	Fast Sodium Current	A
I_{CaL}	L-type Calcium Current	A
I_{to}	Transient Outward Current	A
I_{Ks}	Slow Delayed Rectifier Current	A
I_{Kr}	Rapid Delayed Rectifier Current	A
I_{K1}	Inward Rectifier Potassium Current	A
I_{NaCa}	Sodium-Calcium Exchanger Current	A
I_{NaK}	Sodium-Potassium Exchanger Current	A
I_{pCa}	Plateau Calcium Current	A
I_{pK}	Plateau Potassium Current	A
I_{bNa}	Background Sodium Current	A
I_{bCa}	Background Calcium Current	A
ρ	Cellular Resistivity	$\Omega \text{ cm}$
S	Surface to Volume Ratio	m^{-1}
C'	Specific Capacitance	F/cm^2
V_{CM}	Cardiomyocyte Voltage	V
V_f	Fibroblast Voltage	V
I_{CM}	Cardiomyocyte Total Current	A
I_f	Fibroblast Total Current	A
G_{gap}	Gap Conductance	S
$[X_i]$	Intracellular Concentration of X ,	$\frac{\text{mol}}{\text{m}^3}$
	$\forall X = Ca^{+2}, K^+, Na^+$	

$[X_o]$	Extracellular Concentration of X	$\frac{\text{mol}}{\text{m}^3}$
	$\forall X = Ca^{+2}, K^+, Na^+$	
ϕ	Partition Coefficient	unitless
d	Activation Variable	unitless
f	Inactivation Variable	unitless
d_∞	Steady-State d	unitless
τ_d	d Time Constant	s
f_∞	Steady-State f	unitless
τ_f	f Time Constant	s
γ_α	Voltage-Dependent Rate Function	unitless
γ_β	Voltage-Dependent Rate Function	unitless
θ_α	Voltage-Dependent Rate Function	unitless
θ_β	Voltage-Dependent Rate Function	unitless
p_0	State 0 Probability	unitless
p_1	State 1 Probability	unitless
p_2	State 2 Probability	unitless
p_3	State 3 Probability	unitless
p_4	State 4 Probability	unitless
p_5	State 5 Probability	unitless
x	Activation Variable	unitless
I_L	Leakage Current	A
G_L	Leakage Conductance	S
Vol	Tissue/Individual Cell Volume	m^3

τ_{Ca}	Time Constant	s
I_{KCa}	Calcium-Activated Potassium Channel	A
I_{dr}	Delayed Rectifier Potassium Channel	A
I_{La}	Leakage Current	A
I_{Lb}	Leakage Current	A
I_{LCa}	L-type Calcium Current	A
I_{Lc}	Leakage Current	A
g_{gap}	Single Channel Conductance	S
r_c	Channel Radius	m
L_{gap}	Gap Junction Length	m

To my parents Orly and Moez, for your love, lessons, and patience.

Chapter 1

Introduction

Ischemic heart disease, which results in the reduction of blood flow to the heart, is a leading cause of both heart failure and myocardial infarctions. This insufficient oxygenation of cardiac muscles results in the death of cardiac muscles, which are incapable of regenerating substantially. Therefore, despite tremendous advancements in pharmacological and interventional therapeutic approaches, ischemic heart disease continues to be the source of nearly 1 out of 6 deaths in the United States [1, 2]. The inability of established therapeutic methods to effectively repair and regenerate myocardium has motivated novel cardiotherapeutic methods for regrowing heart muscle, including mesenchymal stem cell therapy, which is the method of interest in this study.

1.1 Background and Motivation

Researchers are currently using various approaches to encourage cardiac regeneration following myocardial infarctions, including tissue engineering, gene therapy,

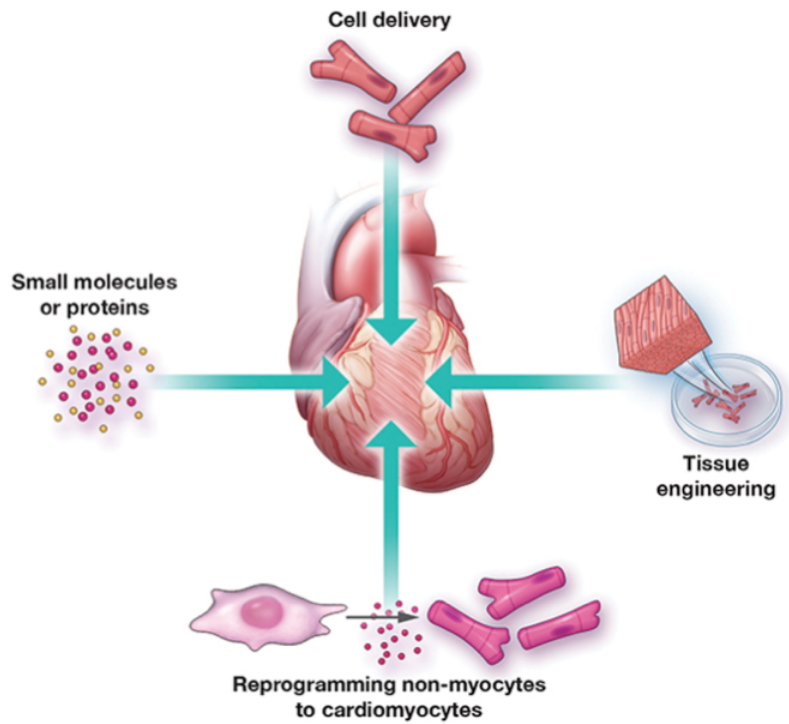


FIGURE 1.1: Gene therapy, cell delivery, tissue engineering, and growth factor delivery are new methods researchers have used to attempt to regrow cardiac muscle following myocardial infarctions [3].

growth factor implementation, and cell delivery (Figure 1.1) [3]. First, tissue engineering methods combine cells with biomaterials. Incorporating these two tools together could lead to structural and paracrine support following myocardial injury [3, 4]. Despite the great potential in this cardiotherapeutic method, it is almost nonexistent in clinical trials due to its complicated nature and underdevelopment. Second, gene therapy, which reprograms noncardiomyocytes to cardiomyocytes, is possible with microRNAs. However, this method is not perfectly controlled — unfavorable effects, such as cardiac rhythmic disturbances, may emerge [3]. This cellular reprogramming approach may be possible after rigorous safety and efficient transplantation standards are met on animal models [5]. The lack of regulation and understanding of the third method, growth factor implementation, places it in the

animal model phase for now as well. Unlike any of the other advanced cardioterapeutic methods, cell delivery, the fourth method, is regularly applied clinically [1, 6, 7], making it the method of interest. Specifically, mesenchymal stem cell transplantation has become a highly attractive clinical treatment for repopulating damaged myocardium [8].

1.1.1 Mesenchymal Stem Cell Background

Mesenchymal stem cells are multipotent stromal cells capable of differentiating into mesenchyme-derived cell types, such as adipocytes, chondrocytes, osteocytes, neurons, and muscle cells (Figure 1.2) [9]. Mesenchymal stem cells have been identified in human bone marrow [10], adipose tissue [11–14], umbilical cord endothelium [13, 15], synovial membrane [16], lung [17], amniotic membrane [18], and peripheral blood [19].

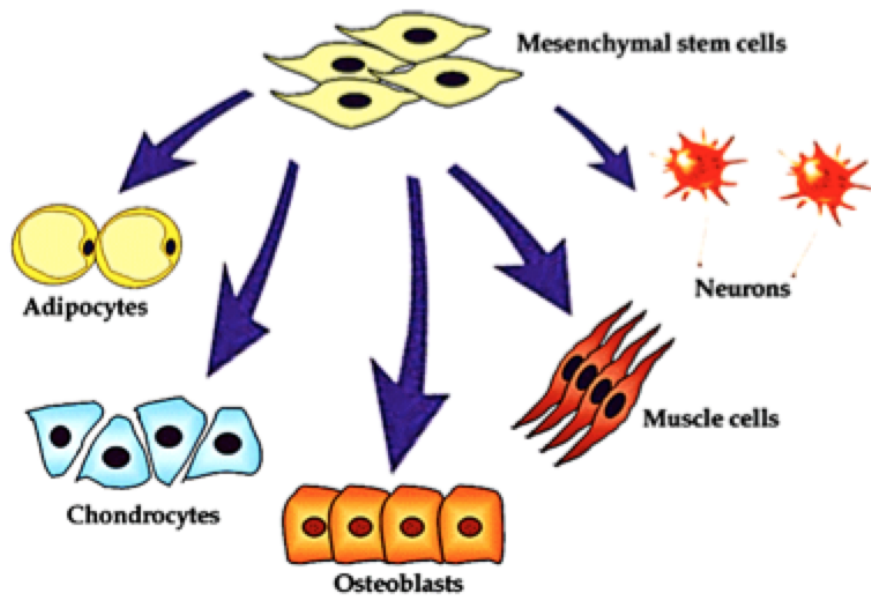


FIGURE 1.2: Mesenchymal stem cells are capable of differentiating into various cell lineages, including osteocytes, chondrocytes, adipocytes, and neurons. Mesenchymal stem cells have also been shown to differentiate into skeletal muscle. [9].

1.1.2 Clinical Applications of Mesenchymal Stem Cells

There are three main goals in cardiac tissue regeneration: 1) to replace myocardial mass; 2) to form functional and sustainable myocardial mass; and 3) to restore ventricle geometry [8]. Human mesenchymal stem cell delivery has exhibited potential in clinical myocardial infarction therapies, by improving cardiac function and limiting infarct size [20–22].

In numerous clinical trials, patients with acute or chronic myocardial infarctions received autologous mesenchymal stem cells from bone marrow [8, 23–25]. These trials indicated that mesenchymal stem cell delivery was safe and effective, as three months after injection, there was an improvement in cardiac function [25].

Various other studies have indicated that human mesenchymal stem cell delivery from an allogeneic source is safe as well. In a randomized, double-blind, placebo-controlled, dose-escalation study, patients had fewer cases of ventricular tachycardia while having improved lung function [6, 8]. In another allogeneic bone marrow derived mesenchymal stem cell clinical trial, the number of heart attacks, cardiac deaths, and coronary revascularization procedures decreased for treated patients [8, 26].

A summary of clinical *in vivo* studies of mesenchymal stem cell delivery for cardiac repair is shown in Table 1.1 [7, 27]. The vast number of clinical trials demonstrates the importance of understanding and resolving the current challenges of mesenchymal stem cell delivery.

TABLE 1.1: Summary of Numerous Clinical *in vivo* Studies of Mesenchymal Stem Cell Delivery for Cardiac Repair

Mesenchymal Stem Cell Source	Delivery Method	Observations	Reference
Autologous bone marrow	Intracoronary	Improved cardiac function	[25]
Autologous bone marrow	Intracoronary ejection factor	Left ventricular increase for \leq 18 months	[28–31]
Autologous bone marrow	Intramycocardial	Left ventricular function and exercise capacity improvement	[32]
Autologous bone marrow	Transendocardial/ Intramyocardial delivery	Improved contraction; recovery at six months	[33]
Allogenic bone marrow	Intravenous	Decreased arrhythmias; improved left ventricular ejection factor	[6]
Allogenic bone marrow	Coronary artery adventita	Improved left ventricular ejection factor; Improved left ventricular stroke volume	[34]

1.1.3 Challenges of Mesenchymal Stem Cell Delivery

Even though stem-cell therapy is regularly used to combat cardiac disease, there are still various challenges that must be considered (Figure 1.3) [35]. The clinical trials previously described, along with other trials, have suggested that variations in cell delivery methods, cell dose and timing, as well as the source for receiving mesenchymal stem cells, must be accounted for in order to improve future clinical trials.

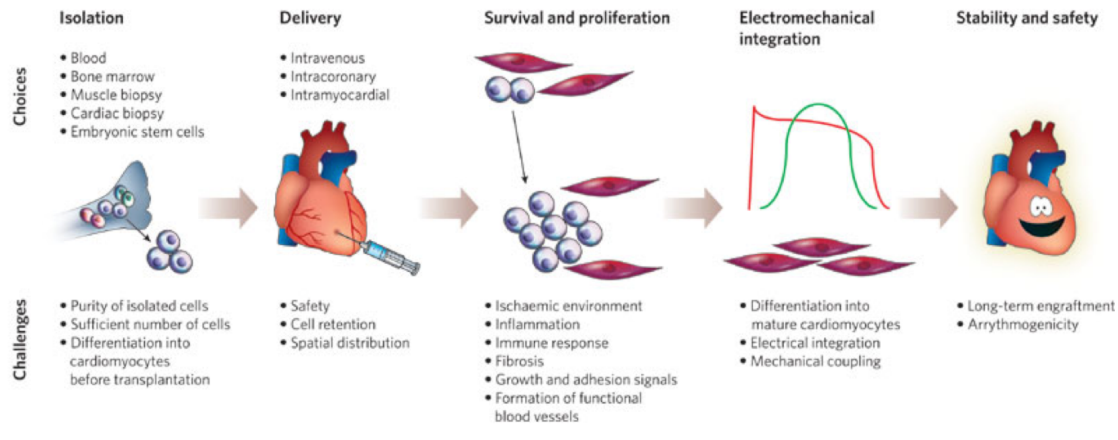


FIGURE 1.3: To rigorously and effectively regenerate cardiac tissue using stem-cell therapy, it is necessary to study isolation methods, delivery methods, levels of survival and proliferation, electromechanical integration, and stability and safety [35].

The method of delivering cells is one of the many challenges in stem cell therapy. These cells can be injected intravenously, into myocardium, or into the coronary arteries [35]. Each method of delivery has its advantages and disadvantages, as shown in clinical trials [36]. Another serious challenge is the cell dose and timing. This challenge is largely a result of the fact that researchers do not fully understand the mechanism whereby mesenchymal stem cells enhance cardiomyocyte function. This limited knowledge makes it extremely difficult to control long-term electromechanical stability, along with structural and functional electromechanical integration with host tissue [35, 37]. If the behavior of the cells delivered is not safe and stable, there is a high risk for arrhythmogenicity. In a reductionist *in vitro* controlled study of the arrhythmogenic potential of mesenchymal stem cells, it was found that co-culturing human cardiomyocytes with greater than 10 percent of mesenchymal stem cells decreases conduction velocity and predisposes re-entrant arrhythmias [37, 38]. These results are consistent with the most common cause of post-myocardial infarction arrhythmias [37, 38]. Therefore, a deeper investigation of the mechanisms of how

mesenchymal stem cells enhance cardiac function is necessary.

1.1.4 Mechanisms of Mesenchymal Stem Cell Enhancement of Cardiac Function

Through insight from clinical and laboratory studies, four viable mechanisms for mesenchymal stem cell enhancement of cardiac function have been recommended: reprogramming of cardiomyocytes, transdifferentiation, paracrine signaling, and electrophysiological coupling (Figure 1.4) [27].

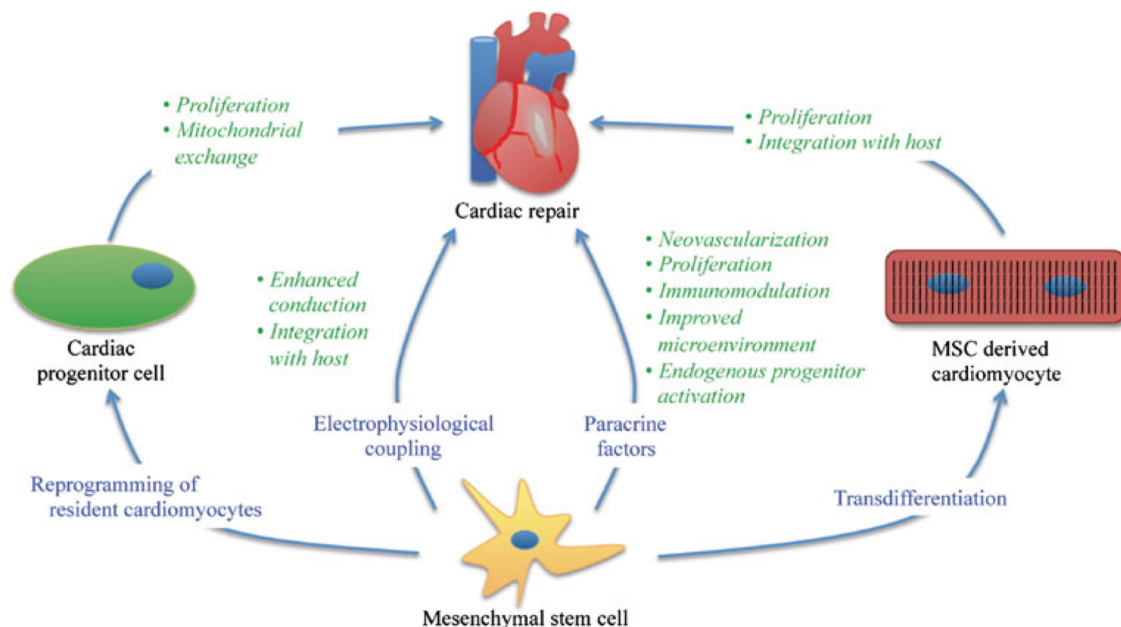


FIGURE 1.4: Viable mechanisms include paracrine signaling between mesenchymal stem cells and cardiomyocytes, reprogramming of cardiomyocytes into cardiac progenitor states, differentiation of mesenchymal stem cells into cardiomyocytes, and electrophysiological coupling of mesenchymal stem cells with cardiomyocytes [27].

The current understanding of these mechanisms is incomplete; therefore, it is possible for these mechanisms to be independent, dependent, mutually exclusive, or

accordant. It has been shown that human mesenchymal stem cells could be transdifferentiated, or delineated, into cardiomyocytes using angiotensin receptor blocker. Transdifferentiated human mesenchymal stem cells result in greater cardiac output in myocardial infarction-induced animal models than non-transdifferentiated human mesenchymal stem cells [39]. Reprogramming is the “de-differentiation” of fully differentiated adult cardiomyocytes to a cardiac progenitor state [27]. Reprogramming was suggested when progenitor markers GATA-4, Nkx-2.5, and Mef-2C increased expression after human mesenchymal stem cells were cultured with adult mouse cardiomyocytes [11].

Paracrine signaling, another proposed mechanism, is the indirect interaction between human mesenchymal stem cells and cardiomyocytes by the release of soluble trophic factors. Finally, the least understood possible mechanism is electrophysiological cardiomyocyte-mesenchymal stem cell coupling. The electrophysiological evidence apparent in clinical and laboratory studies, where human mesenchymal stem cells have exhibited electrical interactions with cardiomyocytes for myocardial infarction therapies both *in vivo* and *in vitro*, makes it necessary to investigate the electrophysiological mechanism further.

1.2 Motivation for Studying the Electrophysiological Mechanism

There is a limited understanding of electrical interactions between mesenchymal stem cells and cardiomyocytes. Furthermore, current research demonstrates electrical interaction is apparent, which affects cell delivery methods clinically and in the

laboratory setting. These factors motivated the further study of the electrophysiological coupling mechanism using mathematical modeling.

Human mesenchymal stem cells have exhibited electrical interactions with cardiomyocytes for myocardial infarction therapies both *in vivo* and *in vitro*. Bench side studies have successfully demonstrated the cardiac function effects of mesenchymal stem cells following a “pseudo”-myocardial infarction [40]. Myocyte-depleted engineered cardiac tissues, resembling post-myocardial infarction tissue, were supplemented with and without mesenchymal stem cells. The results were promising, as mesenchymal stem cell supplementation increased the developed stress of myocyte-depleted tissues, and decreased the activation threshold (Figure 1.5) [40]. These results suggested at a preliminary level that the electrical activity of supplemented mesenchymal stem cells plays a role in cardiac function, as the activation threshold decreased in mesenchymal-stem-cell-supplemented engineered cardiac tissue.

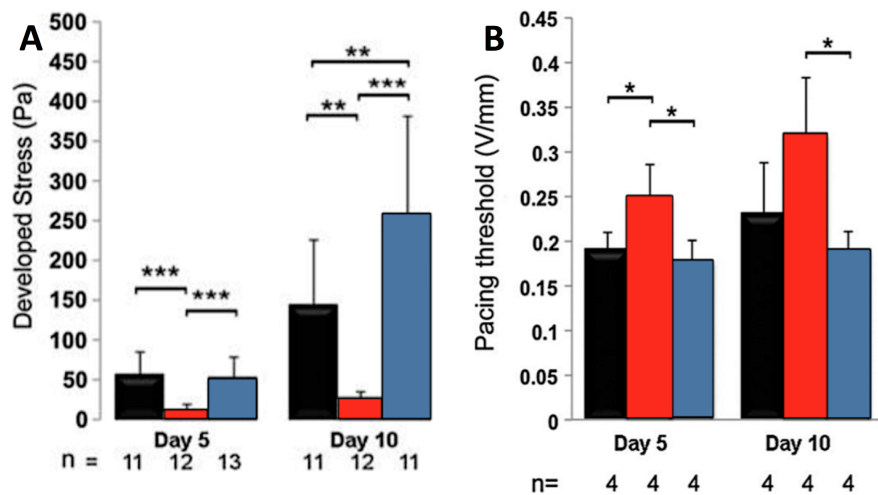


FIGURE 1.5: Control engineered cardiac tissue, myocyte-depleted engineered cardiac tissue representing a myocardial infarction, and myocyte-depleted engineered cardiac tissue supplemented with mesenchymal stem cells are represented as black, red, and blue, respectively. A) Mesenchymal stem cell supplementation increases developed stress; B) Mesenchymal stem cell supplementation decreases excitation threshold [40].

In another laboratory study, it was directly shown that mesenchymal stem cells are electrically coupled with cardiomyocytes [37]. Using immunostaining and Western blotting, researchers showed that mesenchymal stem cells form Cx43 gap junctions between each other and with surrounding cardiomyocytes [37]. This *in vitro* study suggests that mesenchymal stem cells are electrically coupled with cardiomyocytes. Chang *et al* showed in an *in vitro* controlled study the arrhythmogenic potential of mesenchymal stem cells previously discussed, as co-culturing with greater than 10 percent of mesenchymal stem cells decreases conduction velocity and predisposes re-entrant arrhythmias, which demonstrates the importance of investigating electrophysiological effects [37, 38]. An *in vivo* study on pigs also addressed the possible electrophysiological effects of mesenchymal stem cell therapy. Specifically, pro-arrhythmic consequences of mesenchymal stem cell therapy were suggested after it was found that pigs receiving mesenchymal stem cell transplantation increased heterogeneously-distributed sympathetic nerve sprouting [41].

The role of electrophysiological interaction between mesenchymal stem cells and cardiomyocytes will be studied in a novel way to address the implications of these *in vivo* and *in vitro* studies. To do so, the individual functional ion channels in human mesenchymal stem cells will be mathematically modeled. Subsequently, the electrical activity of mesenchymal stem cells will be coupled with cardiomyocytes via computer simulations. Examining the electrical effects of mesenchymal stem cells being supplied with cardiomyocytes will offer insight into how to optimize cell delivery conditions, which is currently a serious challenge faced in cell delivery cardiotherapies. Furthermore, it will offer insight into the possibility of mesenchymal

stem cells playing the role of biological pacemakers, a potential alternative to artificial electronic pacemakers [42]. To develop this insight, it is first necessary to briefly review the phases of the cardiac action potential that could be influenced by mesenchymal stem cells.

1.3 Cardiac Action Potential Phases

The cardiac action potential has five general phases (Figure 1.6): the rapid depolarization phase (Phase 0); the transient outward phase (Phase 1); the plateau phase (Phase 2); the rapid repolarization phase (Phase 3); and the resting membrane potential phase (Phase 4). The action potential duration ranges from 200 ms to 400 ms based on cardiac cell type [43]. Its resting potential and peak voltage is approximately -85 mV and 25 mV, respectively.

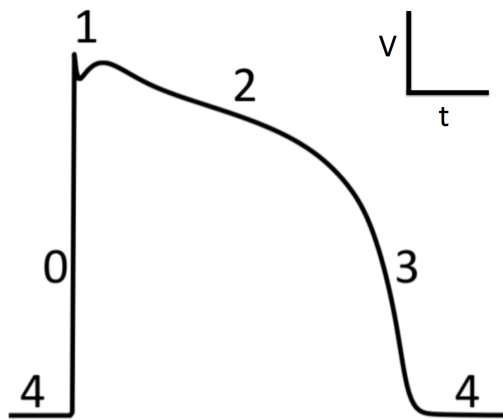


FIGURE 1.6: The five phases of a cardiac action potential include: the rapid depolarization phase (Phase 0); the transient outward phase (Phase 1); the plateau phase (Phase 2); the rapid repolarization phase (Phase 3); and the resting membrane potential phase (Phase 4). The action potential duration varies by cardiac cell type [44].

The functional cardiac ion channels that influence each phase are shown in Table 1.2.

TABLE 1.2: Functional Ion Channels in a Cardiac Action Potential

Phase	Functional Channels
0	Sodium Channel (Na^+ Influx)
1	Transient Outward Channels (K^+ and Cl^- Outflux)
2	L-type Calcium Channel (Ca^{+2} Influx) Slow Delayed Rectifier Potassium Channel (K^+ Outflux)
3	Slow Delayed Rectifier Potassium Channel (K^+ Outflux) Rapid Delayed Rectifier Potassium Channel (K^+ Outflux) Inward Rectifier Potassium Channel (K^+ Outflux)
4	Inward Rectifier Potassium Channel

1.4 Functional Ion Channels in Human Mesenchymal Stem Cells

To mathematically model the role of electrophysiological interactions between mesenchymal stem cells and cardiomyocytes, it is necessary to model the individual functional ion channels of human mesenchymal stem cells (Table 1.3) [45–48].

TABLE 1.3: Functional Ion Channels in Human Mesenchymal Stem Cells

Functional Ion Channel	mRNA Expressed
Calcium Activated Potassium Channel	MaxiK
Delayed Rectifier Potassium Channel	Kv10.1
L-type Calcium Channel	CACNA1C
Sodium Channel	SCN9A
Transient Outward Potassium Channel	Kv1.4, Kv4.2

The functional ion channels of human mesenchymal stem cells are further reviewed below. The role each of these ion channels plays in cardiomyocyte action potentials is also discussed, as it will provide a reader with some intuition into the influence of specific mesenchymal stem cell ion channel activity on cardiomyocytes.

1.4.1 Calcium Activated Potassium Current

The voltage- and calcium concentration-dependent calcium activated potassium channel was identified in all human mesenchymal stem cells via whole-cell patch clamping [45–47, 49]. The MaxiK gene was highly expressed for human mesenchymal stem cells with calcium activated potassium channels. This high conductance, high noise channel is shown below (Figure 1.7).

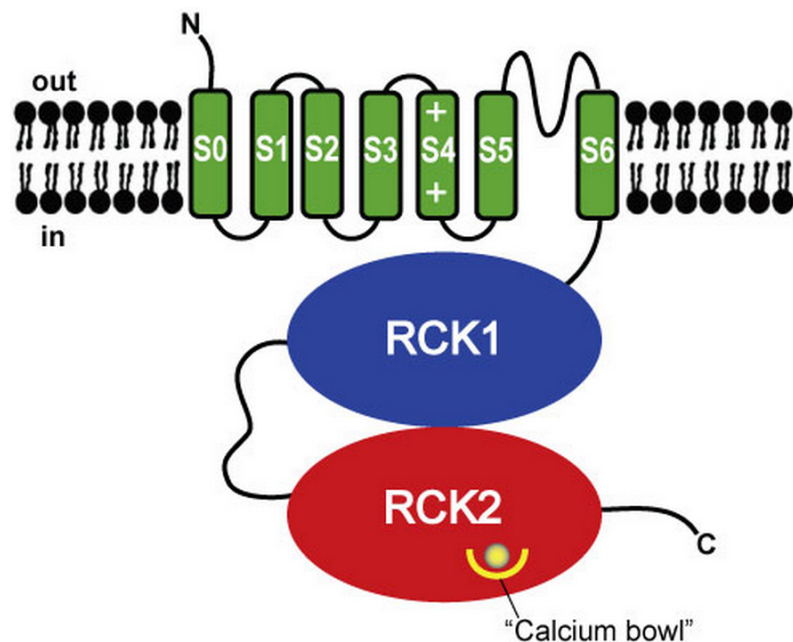


FIGURE 1.7: General structure of the Calcium Activated Potassium Channel [50]. The MaxiK channel consists a transmembrane domain (S0), a voltage-sensing domain (S1-S4), a potassium channel pore domain (S5 and S6), and a cytoplasmic C-terminal domain (CTD) with a pair of potassium conductance regulators. The CTD has calcium binding sites, known as calcium bowls, within each potassium conductance regulator. [51–57]

1.4.2 Delayed Rectifier Potassium Current

The delayed rectifier K⁺ channel is a human ether a-go-go gene potassium channel (hEAG1 or Kv10.1). It was identified in nearly 63% of human mesenchymal stem cells via whole-cell patch clamping (Figure 1.8) [45–47, 49]. This voltage gated channel is critical in the repolarization of a cardiomyocyte during an action potential [58]. Channelopathies of the delayed rectifier potassium channel include long QT syndrome, short QT syndrome, or cardiac arrhythmias [59, 60].

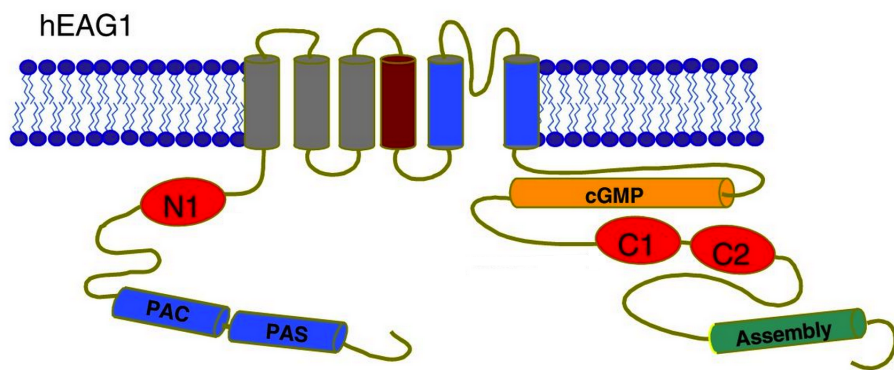


FIGURE 1.8: Structure of the delayed rectifier K⁺ current-like hEAG1 channel ([61]). The plasma membrane depicts the divide between the outside of the cell (top) and inside of the cell (bottom). This structure is analogous to a typical Kv channel, where three functional elements exist: 1) an ion conduction pore; 2) a voltage sensor; and 3) gates that open or close due to voltage changes [62].

1.4.3 L-Type Calcium Current

The voltage dependent L-Type Calcium Channel was identified in approximately 15% of human mesenchymal stem cells via whole-cell patch clamping [45–47, 49]. The general structure of this channel is shown in Figure 1.9. The CACNA1C gene is responsible for this channel, which contributes to the excitation-contraction coupling of cardiac muscle cells.

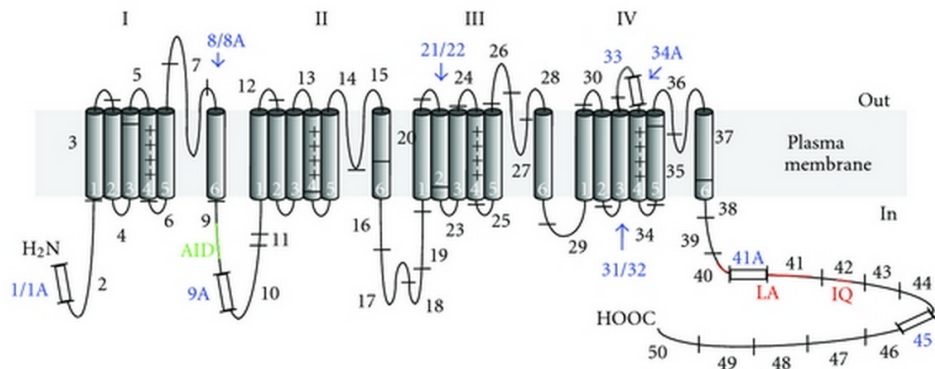


FIGURE 1.9: Schematic representation of the L-type Calcium Channel. [63]. The plasma membrane, and the inside and outside of the cell are labeled.

1.4.4 TTX-Sensitive Sodium Current

The voltage dependent TTX-sensitive sodium channel was identified in approximately 29% of human mesenchymal stem cells via whole-cell patch clamping [45–47, 49]. The SCN9A gene is responsible for this channel, a contributor to the generation and conduction of action potentials. The mutation of this gene is responsible for various pain disorders [64]. The general structure of the TTX-sensitive sodium channel is shown above (Figure 1.10).

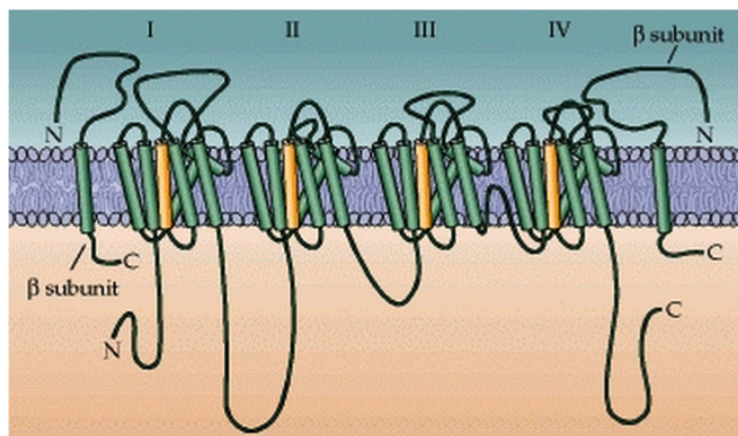


FIGURE 1.10: General structure of the TTX-sensitive Sodium Channel [49]. The plasma membrane depicts the divide between the outside of the cell (top) and inside of the cell (bottom).

1.4.5 Transient Outward Potassium Current

The transient outward potassium channel was identified in nearly 8% of human mesenchymal stem cells via whole-cell patch clamping [45–47, 49]. The general structure of the transient outward potassium channel is similar to the structure of the delayed rectifier K⁺ current-like hEAG1 channel (Figure 1.8). Specifically, the mRNA expression of Kv1.4 and Kv4.2 channels exists in a small percentage of human mesenchymal stem cells [45–47, 49]. The voltage gated transient outward potassium current contributes to the repolarization phase of the cardiac action potential.

Characterizing and developing a general understanding of the functional ion channels in human mesenchymal stem cells makes it possible to mathematically model the electrophysiology of the human mesenchymal stem cell [65].

1.5 Theory of Mathematically Modeling Electrophysiological Activity

Theoretical studies of the human heart and cardiac electrical activity are an essential and well-established area of research. The limitations of obtaining empirical studies on human hearts, and the variability of animal heart activity and function, necessitate simulations of the human heart [66]. Many electrophysiological models have been established previously, a motivating factor for this study [66, 67].

To couple a mesenchymal stem cell electrophysiological model with a cardiomyocyte electrophysiological model, it is first necessary to discuss the basic electrical properties of both mesenchymal stem cells and cardiomyocytes, including cell make-up, membrane capacitance and resistance, equilibrium and reversal potential, and

membrane current. Next, the vast amount known about the biophysical mechanisms responsible for cardiomyocyte and mesenchymal stem cell activity will be used to model channels and whole-cells electrophysiologically. Finally, previously established whole-cell models and coupling cell models will be reviewed, as the structure of these models will be analogous to the novel model developed in this study.¹

1.5.1 Basic Electrical Properties of Cardiomyocytes and Mesenchymal Stem Cells

Ions located both inside and outside of a cell create a voltage potential difference between the inside and the outside of a cell. By convention, the potential of the extracellular fluid of a cell is set to 0 V [68]. Because the intracellular voltage of a cell plays a large role in its function, it is vital to predict its electrical activity.

The response of a cell to depolarization — positively charged ions flowing into the cell or negatively charged ions out of the cell — varies greatly by cell-type. For example, cardiomyocytes and neurons initiate an action potential, or a characteristic positive feedback process when sufficient depolarization occurs beyond a threshold membrane potential level [68]. Mesenchymal stem cells, in contrast, do not have action potentials [45, 47, 69]. However, they are still capable of affecting the action potentials of coupled cardiomyocytes via gap junctions [70].

Cell Make-Up

In general, the order of magnitude of water molecules ($\sim 10^{10}$), ions ($\sim 10^8$), amino acids and nucleotides ($\sim 10^7$), and proteins ($\sim 10^5$) are consistent for various cell types. The transfer of many of these positively or negatively charged molecules

¹The structure of this section follows the useful model of Chapter 5 of Dayan and Abbott [68]

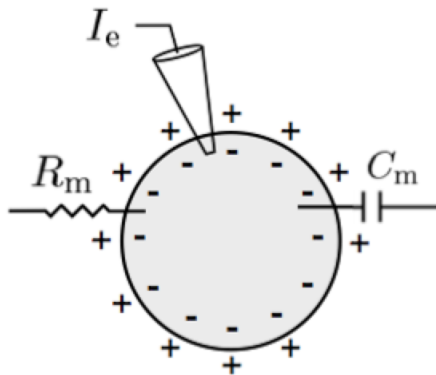


FIGURE 1.11: Single compartment model of a cell’s capacitance and membrane resistance. The excess internal charge and the membrane potential are linearly proportional to the membrane capacitance. The change in membrane potential is dependent on the current entering a cell, I_e , and the membrane resistance, R_m by $\Delta V = I_e R_m$ [68].

allows for an equivalent electrical circuit to represent individual cell electrical activity [68]. For example, the cell membrane — a lipid bilayer that has a build-up of charged molecules on the interior and exterior surfaces of the membrane due to electrostatic forces — can act as a capacitor.

Membrane Capacitance and Resistance

Normally, there is an excess of negative charge on the inside surface of the cell membrane, with a balancing amount of positive charge on the outside surface (Figure 1.11). Therefore, the cell membrane has a capacitance C_m , where the excess intracellular charge Q and the membrane voltage V are related by:

$$Q = C_m V \quad (1.1)$$

By taking the time derivative of both sides of Equation 1.1 and assuming capacitance is independent of time, the amount of current necessary to change the membrane potential over a time interval can be found:

$$\frac{d}{dt}(Q = C_m V) \quad (1.2)$$

$$I = C_m \frac{dV}{dt} \quad (1.3)$$

This implies a current is required when the membrane potential is to be held at a level different from its resting value. The difference between the resting value and the new value, ΔV is determined by Ohm's law:

$$\Delta V = IR_m \quad (1.4)$$

where I is the current necessary to be injected, and R_m is the membrane resistance. Therefore, R_m is assumed to be constant and equal to the slope of $\Delta V/I$ for small values of ΔV and I .

The analogies made between a cell's electrophysiological behavior and an equivalent RC circuit make it justifiable to define a membrane time constant, τ_m , where:

$$\tau_m = R_m C_m \quad (1.5)$$

Equilibrium Potential

Ions flow into and out of a cell due to spatial differences in concentration or electric potentials. When these two driving forces are equal and opposite, an equilibrium potential E is reached.

Fick's law of diffusion is used to relate the movement of chemical species at a location in a mixture. Fick's law of diffusion states that the rate of diffusion of chemical

species p is proportional to the concentration gradient of a species at a location, or:

$$\mathbf{j}_{d,p} = -D_p \nabla C_p \quad (1.6)$$

where $\mathbf{j}_{d,p}$ is the diffusional flux vector of species p , D_p is the diffusivity constant of species p , and C_p is the concentration of species p .

Charged ions are affected by electric field forces as well, where ion p will move at a finite velocity u_p due to intermolecular collisions. The ionic flux is given by the product of the ion concentration and its velocity, or:

$$\mathbf{j}_{e,p} = -u_p \frac{Z_p}{|Z_p|} C_p \nabla \Phi \quad (1.7)$$

where $\mathbf{j}_{e,p}$ is the ionic flux, Z_p is the valence of the ion, $\nabla \Phi$ is the electric field, and C_p is the concentration of the ion.

To relate these two driving forces, it is necessary to use Einstein's relation between the mobility u_p and the diffusivity constant D_p [71]:

$$D_p = \frac{u_p R T}{|Z_p| F} \quad (1.8)$$

where T is the absolute temperature, F is Faraday's constant, and R is the gas constant. Using each of these driving forces, it is possible to find the total flux, known as the Nernst-Planck equation [72, 73]:

$$\mathbf{j}_{total,p} = \mathbf{j}_{d,p} + \mathbf{j}_{e,p} = -D_p (\nabla C_p + \frac{Z_p C_p F}{R T} \nabla \Phi) \quad (1.9)$$

At equilibrium for species p , the electrical force balances the diffusional force, such that $\mathbf{j}_{total,p} = 0$. Therefore:

$$\mathbf{j}_{total,p} = 0 = -D_p(\nabla C_p + \frac{Z_p C_p F}{RT} \nabla \Phi) \quad (1.10)$$

making:

$$\nabla C_p = -\frac{Z_p C_p F}{RT} \nabla \Phi \quad (1.11)$$

This equation can be one-dimensionalized by assuming variation occurs only in the direction perpendicular to the membrane (call this direction r). Therefore:

$$\frac{dC_p}{dr} = -\frac{Z_p C_p F}{RT} \frac{d\Phi}{dr} \quad (1.12)$$

By rearranging and integrating Equation 1.12 from the extracellular position e to the intracellular position i :

$$\int_e^i \frac{dC_p}{C_p} = -\frac{Z_p F}{RT} \int_e^i d\Phi. \quad (1.13)$$

or:

$$\ln \frac{C_i}{C_e} = -\frac{Z F}{R T} (\Phi_i - \Phi_e) \quad (1.14)$$

However, from the convention previously established that the extracellular potential is zero, we define:

$$V = \Phi_i - \Phi_e \quad (1.15)$$

As a result, the Nernst potential [68, 74, 75], or equilibrium potential is:

$$V^{rest} = E_m = \frac{RT}{ZF} \ln \frac{C_e}{C_i} \quad (1.16)$$

The equilibrium potential is applied for one species of ion transferring across the cell membrane, such as calcium, sodium, chloride, or potassium. The equilibrium potential is vital for the driving force of a current and for the cell's overall resting potential, as discussed in the following section.

Membrane Current

For each different type of channel i with equilibrium potential E_i , there is a driving force due to the difference between the potential V and equilibrium potential E_i . By applying Ohm's law, it is apparent that the driving force is linearly proportional to the current such that:

$$I = G_i(V - E_i) \quad (1.17)$$

where G_i is the conductance of the channel. The total current is the sum of all the currents functioning within a cell, or:

$$I_{total} = \sum_i G_i(V - E_i) \quad (1.18)$$

The overall resting potential of a cell is when steady-state is achieved, where $I_{total} = dV/dt = 0$. Therefore:

$$I_{total} = \sum_i G_i(V^{rest} - E_i) = 0 \quad (1.19)$$

Rearranging, we find the overall resting potential of a cell is:

$$V^{rest} = \frac{\sum_i G_i E_i}{\sum_i G_i} \quad (1.20)$$

1.5.2 Single Compartment Model

Single compartment models are ordinary differential equations that are dependent on one variable. In this case, the membrane potential of a cell can be described by a single compartment model, as the ordinary differential equations are only functions of the cell's voltage V . The general equation for a single compartment model is:

$$C_m \frac{dV}{dt} = -(I_{total} + I_{stim}) \quad (1.21)$$

where I_{total} is the total transmembrane ionic current, and I_{stim} is a stimulus current. In this study, this general form is used for both the cardiomyocyte model and the mesenchymal stem cell model.

1.5.3 Voltage-Dependent Conductances

Empirical studies of individual channels have shown nonlinear and stochastic activity of membrane conductances, as channels fluctuate rapidly from open to closed states. Therefore, to describe the behavior of membrane conductances, a probabilistic approach is used based on the membrane potential (for voltage-dependent conductance), the presence of neurotransmitters (for synaptic conductances), ionic concentration, and/or messenger molecules. In the cardiomyocyte model [68] and the

novel model developed in this study, only voltage-dependent and ionic concentration-dependent conductances are apparent.

Two different methods can be used to describe the nonlinearity of channels: 1) voltage-dependent conductance models arising from a large number of channels; and 2) microscopic description models of the transitions between conformational states of channel molecules. Both of these methods can be applied in the models discussed in this study [68]. For simplicity, only the first method will be discussed in detail now, which holistically and deterministically describes the conductances by modeling many channels of a certain type. The second method is merely an extension of basic mathematical principles from the first method, and is discussed in further detail in Section 2.2 to model the delayed-rectifier potassium channel.

Due to a large number of independently acting channels present and the law of large numbers, the fraction of channels open is approximately the probability of one channel being open [68]. Therefore, if the probability of a channel being open is denoted as P_i , and the maximum conductance is denoted as \overline{G}_i , then the conductance at any moment is given by:

$$G_i = \overline{G}_i P_i \quad (1.22)$$

Two different mechanisms — persistent conductance and transient conductance — control how channels open and close as a function of membrane potential, thus affecting P_i .

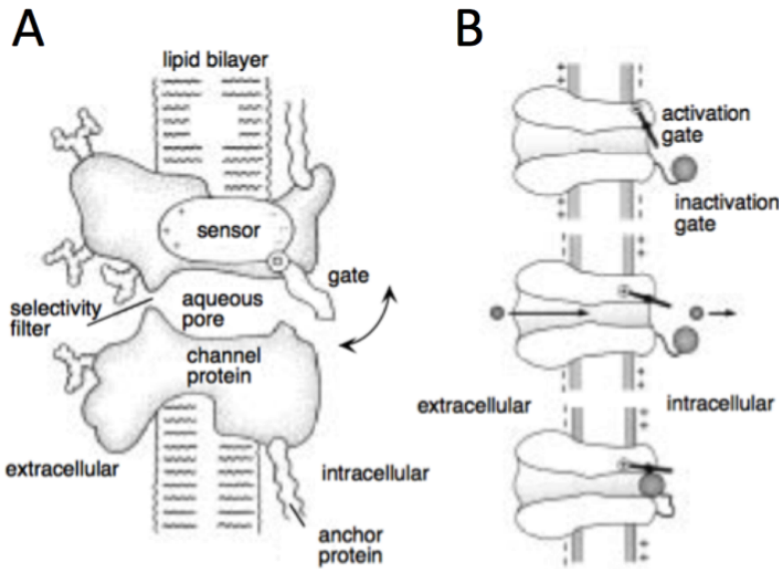


FIGURE 1.12: Membrane channel gating. A) An example of a persistent, or non-inactivating conductance is illustrated. The sensor opens or closes as a function of the membrane voltage [76]. B) An example of a transient conductance is illustrated. Two gates exist in the transient conductance model: i) An activation gate that is coupled to a voltage sensor. ii) A gate that can block a channel once it is open [75].

Persistent Conductance

In general, channel gating mechanisms involve complex structural conformations. However, since we are only interested in the conductance of a channel, it is sufficient to model a persistent, or noninactivating, channel as a swinging gate attached to a voltage sensor that opens or closes the pore of a channel (Figure 1.12). Therefore, the channel can be modeled as having two states: opened or closed. The probability of a channel being open, P_i , is given as:

$$P_i = n^k \quad (1.23)$$

where n is the probability of each k independent channel opening event occurring. Since n is the probability of the channel being open, it ranges from 0 to 1. Similarly,

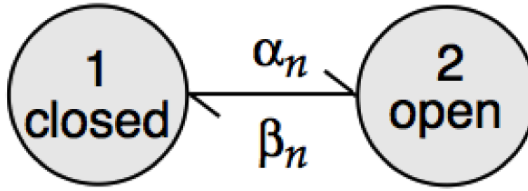


FIGURE 1.13: A model of a noninactivating channel. The channel can be modeled as in two states: opened or closed. The gating transition rates from closed-to-open and open-to-closed, $\alpha_n(V)$ and $\beta_n(V)$, respectively, are voltage-dependent. The probability of finding a gate open over a small time step is the product of the probability of finding the gate closed, or $1 - n$, multiplied by the opening rate $\alpha_n(V)$, while the probability of finding the gate closed over a small time step is the product of the probability of finding the gate open, or n , multiplied by the closing rate $\beta_n(V)$ [68].

$1 - n$ ranges from 0 to 1, which is the probability of the channel being closed.

The gating transition can be described through basic channel kinetics, as shown in Figure 1.13. The gating transition rates from closed-to-open and open-to-closed, $\alpha_n(V)$ and $\beta_n(V)$, respectively, are voltage-dependent. The probability of finding a gate open over a small time step is the product of the probability of finding the gate closed, or $1 - n$, multiplied by the opening rate $\alpha_n(V)$, while the probability of finding the gate closed over a small time step is the product of the probability of finding the gate open, or n , multiplied by the closing rate $\beta_n(V)$. Therefore:

$$\frac{dn}{dt} = \alpha_n(V)(1 - n) - \beta_n(V)n \quad (1.24)$$

This can be rewritten in a more convenient form by dividing both sides by $\alpha_n(V) + \beta_n(V)$, so that:

$$\tau_n(V) \frac{dn}{dt} = n_\infty(V) - n \quad (1.25)$$

where:

$$\tau_n(V) = \frac{1}{\alpha_n(V) + \beta_n(V)} \quad (1.26)$$

and:

$$n_\infty(V) = \frac{\alpha_n(V)}{\alpha_n(V) + \beta_n(V)} \quad (1.27)$$

The opening and closing rate functions $\alpha_n(V)$ and $\beta_n(V)$ can be described from a thermodynamic standpoint. Let B_α and B_β represent the amount of ions flowing towards the open and closed states, respectively. The transition of a charged component across a part of the membrane has an effective charge qB_α through a potential V , thus requiring an energy $qB_\alpha V$ [68]. From a statistical thermodynamics standpoint, the probability enough thermal energy will be provided to reach this energy barrier is proportional to the Boltzmann factor, making α_n to be:

$$\alpha_n(V) = A_\alpha e^{-qB_\alpha V/kT} = A_\alpha e^{-B_\alpha V/V_T} \quad (1.28)$$

where A_α is an empirical parameter and V_T is the thermal voltage, which is equal to kT/q . Using a similar argument for the closing rate $\beta_n(V)$, it is expected that $\beta_n(V)$ has the form:

$$\beta_n(V) = A_\beta e^{-qB_\beta V/kT} = A_\beta e^{-B_\beta V/V_T} \quad (1.29)$$

where A_β is an empirical parameter. Substituting Equations 1.28 and 1.29 into Equation 1.27, we find:

$$n_\infty(V) = \frac{1}{1 + (A_\beta/A_\alpha)e^{(B_\alpha - B_\beta)V/V_T}} \quad (1.30)$$

Transient Conductance

Unlike the persistent conductance, two gates exist when modeling transient conductance: 1) an activation gate that is coupled to a voltage sensor; and 2) a gate that can block a channel once it is open (Figure 1.12) [75]. The activation variable m for transient conductance is analogous to the activation variable n . The second gate, which blocks the channel pore, also requires a probability variable defined as h . h is the probability that the second gate does not block the channel pore. Therefore, the probability the gate is open, P_i is equal to:

$$P_i = m^k h^l \quad (1.31)$$

where l is an empirical power h is raised to, similar to the power k on m . Both m and h have rate functions α and β , thus requiring α_m , α_h , β_m , and β_h for transient conductances. The theory discussed in this section is the basis for previously established models and for the novel model in this study.

1.5.4 Previously Established Electrophysiological Models

Numerous models have nearly reproduced experimental cardiomyocyte action potential data, including the Priebe-Beuckelman, Luo-Rudy, and ten Tusscher models [66, 77, 78]. In this study, the ten Tusscher model, which is a very robust and computationally-efficient model, will be coupled with the novel mesenchymal stem cell model developed. Specifically, the 2006 ten Tusscher M cell model [79] will be used to mimic *in vivo* conditions [80], as clinical trials typically intramyocardially inject mesenchymal stem cells into the myocardium following an infarction [81].

Therefore, it is crucial to examine the basic dynamic equations that make up the cardiomyocyte action potential model. The whole-cell models used in these studies were modified appropriately for the novel mesenchymal stem cell model.

Ten Tusscher Cardiomyocyte Action Potential Model

The cardiomyocyte cell membrane is modeled as a capacitor in parallel with variable resistors and batteries (this is generally true independent of cell type). Specifically, the behavior of the cell can be described as:

$$\frac{dV}{dt} = -\frac{I_{ion} + I_{stim}}{C_m} \quad (1.32)$$

where I_{ion} is the net transfer of all ion movement across the cardiomyocyte cell membrane (Figure 1.14), or:

$$I_{ion} = I_{Na} + I_{K1} + I_{to} + I_{Kr} + I_{Ks} + I_{CaL} + I_{NaCa} + I_{NaK} + I_{pCa} + I_{pK} + I_{bCa} + I_{bNa} \quad (1.33)$$

where:

- I_{Na} = Fast Sodium Current
- I_{CaL} = L-type Calcium Current
- I_{to} = Transient Outward Current
- I_{Ks} = Slow Delayed Rectifier Current
- I_{Kr} = Rapid Delayed Rectifier Current
- I_{K1} = Inward Rectifier Potassium Current
- I_{NaCa} = Sodium-Calcium Exchanger Current

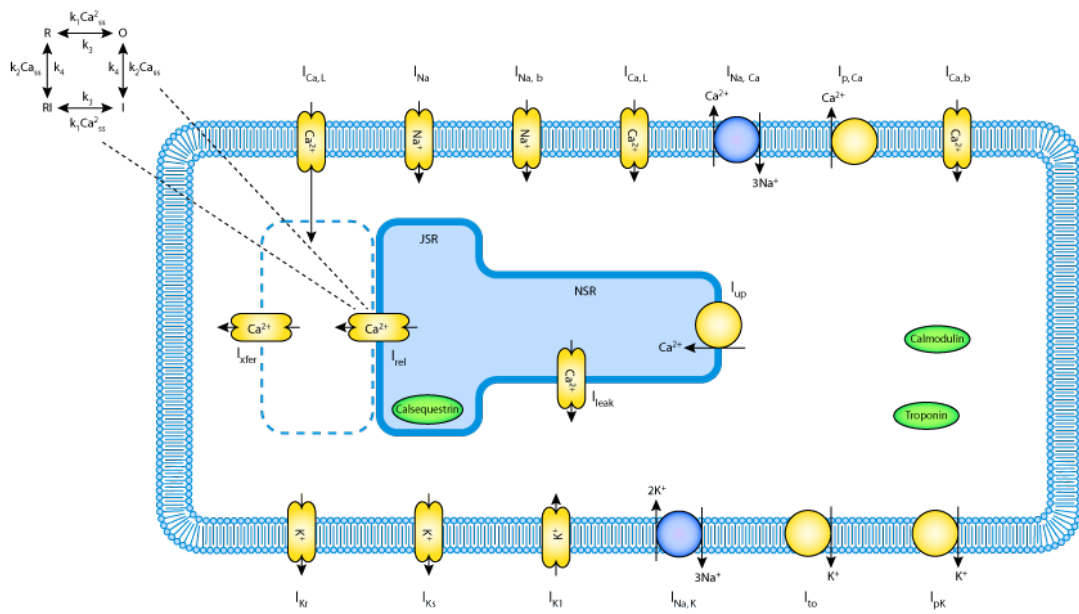


FIGURE 1.14: Ion Movement Across Cardiomyocyte Cell Membrane [82]. The following currents contribute to the total cardiomyocyte current: fast sodium, L-type calcium, transient outward, slow delayed rectifier, rapid delayed rectifier, inward rectifier potassium, sodium-calcium exchanger, sodium-potassium exchanger, plateau calcium, plateau potassium, background sodium, and background calcium.

- I_{NaK} = Sodium-Potassium Exchanger Current
- I_{pCa} = Plateau Calcium Current
- I_{pK} = Plateau Potassium Current
- I_{bNa} = Background Sodium Current
- I_{bCa} = Background Calcium Current

Each of these ion channels is voltage dependent, ion concentration dependent, or both, making the overall electrophysiology model of the cardiomyocyte transient and dynamic (for detailed models of the voltage dependence and ion concentration dependence of ion channels, see Section 2.2). Solving this dynamic model numerically resulted in the epicardial action potential shown in Figure 1.15, which is nearly

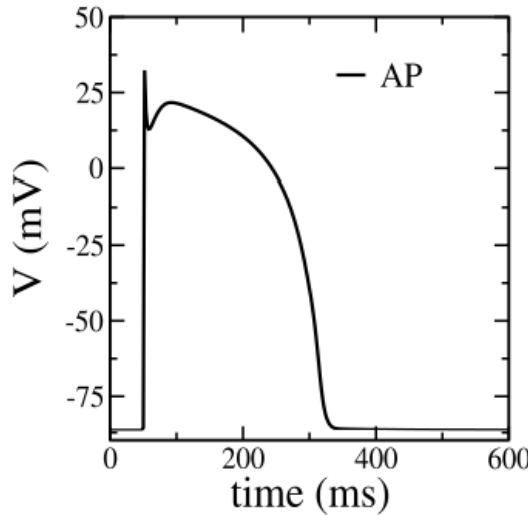


FIGURE 1.15: Ten Tusscher Action Potential Simulation. This model is extremely successful in reproducing experimental data, a motivating factor of this simulation study. [66].

identical to a human epicardial cardiomyocyte action potential [66].

Mathematical modeling enables researchers to examine other electrophysiological activity, such as the conduction velocity. ten Tusscher *et al* were also able to model the conduction velocity of the cardiomyocyte, another crucial factor in determining cardiomyocyte function, by assuming a 2-D (x - y plane) continuous system sheet of cells:

$$\frac{\partial V}{\partial t} = -\frac{I_{ion} + I_{stim}}{C_m} + \frac{1}{\rho_x S_x C'_x} \frac{\partial^2 V}{\partial x^2} + \frac{1}{\rho_y S_y C'_y} \frac{\partial^2 V}{\partial y^2} \quad (1.34)$$

where S is the surface-to volume ratio of a cell, C' is the specific capacitance in both the x and y directions, and ρ is cellular resistivity in both the x and y directions. The robustness, efficiency, and consistency of the ten Tusscher human ventricular action potential model has led other researchers to couple this cardiomyocyte model with their own novel models of differing cell types [67, 83]. The method used by various electrophysiological coupling models was used in this study.

MacCannell Myocyte-Fibroblast Coupled Model

The MacCannell model couples an electrophysiological model for mammalian ventricular fibroblasts with the ten Tusscher model of the ventricular action potential [67]. To couple the two models together, Equations 1.35 and 1.36 were used:

$$\frac{dV_{CM}}{dt} = -\frac{1}{C_{mCM}}[I_{CM} + \sum_{i=1}^n G_{gap}(V_{CM} - V_f)] \quad (1.35)$$

$$\frac{dV_f}{dt} = -\frac{1}{C_{mf}}[I_f + \sum_{i=1}^n G_{gap}(V_f - V_{CM})] \quad (1.36)$$

where CM and f subscripts represent cardiomyocytes and fibroblasts, respectively.

This method of coupling cells was applied in this study as well. In order to apply a coupling technique analogous to the method of MacCannell *et al*, it was first necessary to develop an original mesenchymal stem cell electrophysiology model by mathematically describing each individual ion channel. These ion channels can be modeled with previously established mathematical relationships, as discussed in the following section.

1.5.5 Mathematical Models of Individual Human Mesenchymal Stem Cell Channels

Like previously discussed cell channels, mesenchymal stem cell channels demonstrate nonlinear behavior. Therefore, it was necessary to consider the voltage-dependent conductances arising from a large number of channels, and the microscopic behavior of transitions between conformational states of channel molecules. The five functional ion channels previously discussed either demonstrate transient or persistent conductances (Table 1.4).

TABLE 1.4: Transient or Persistent Behavior of Functional Ion Channels in Human Mesenchymal Stem Cells

Functional Ion Channel	Persistent or Transient
Calcium Activated Potassium Channel	Persistent
Delayed Rectifier Potassium Channel	Persistent
L-type Calcium Channel	Transient
Sodium Channel	Transient
Transient Outward Potassium Channel	Transient

A sixth functional ion channel, the leakage current, is necessary to account for the transfer of all ions other than potassium, sodium, and calcium across the membrane. A detailed description of the equations used for each of these channels is shown in Section 2.2, the methodology for this computational study.

The models for the functional ion channel currents and the ionic concentration variations are the basis for the novel mesenchymal stem cell electrophysiological model. A rigorous coupled model of mesenchymal stem cells and cardiomyocytes can be developed by applying the general equations and models by ten Tusscher *et al* and MacCannell *et al*.

To test the power of this model, it is necessary to generate empirical results of the electrical activity of both mesenchymal stem cells and cardiomyocytes when coupled together. To do so, the powerful patch clamping method can be used, which is described in detail below.

1.6 Description of Patch Clamping

In order to empirically verify the novel mathematical models generated in this study, it is necessary to measure the electrophysiological activity of individual cells. Patch clamping is a state of the art technique to accomplish such a task, which will be discussed in this section.

1.6.1 Background

The 19th century discovery of bioelectricity from electrically stimulating frog muscles initially motivated the recording of physiological electrical activity. In 1952, Hodgkin and Huxley recorded squid giant axon electrical activity with crude glass electrodes [84]. By voltage clamping, or holding the membrane potential constant, they were able to model the behavior of squid giant axon electrical activity.

Translating this method from squid giant axons to individual cells was a huge challenge, and thus required nearly three decades of research in this field. In 1975, two electrode and single-electrode modes were developed [85, 86]. However, both of these methods had nonuniform contributions leading to voltage clamp problems, most of which were resolved by Neher and Sakmann in 1976 [87]. Neher and Sakmann developed the patch clamp method, which uses the strengths of microelectrodes and voltage clamping; it does so by using a large-bore pipette that forms a very tight seal with a cell membrane. This allows for individual cell and even individual channel measurements.

1.6.2 Types of Patch Clamping

There are four different patch clamping configurations where single-cell membrane recordings can be made: cell-attached, inside-out, outside-out, and whole-cell (Figure 1.16).

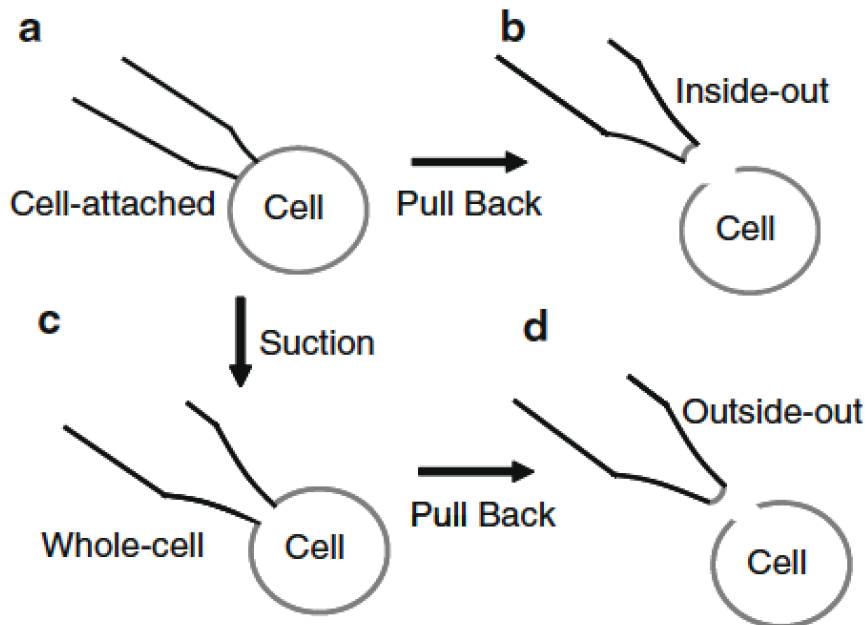


FIGURE 1.16: Types of patch clamping. A) gently pressing a pipette against a cell and applying suction to form a tight seal produces the cell-attached configuration; B) pulling the pipette away from the cell makes an inside-out configuration; C) quick suction or electrical pulses accesses the inside of the cell for whole-cell configuration; D) pulling away from whole-cell arrangement causes outside-out configuration [74, 88]

Cell-Attached

The cell-attached configuration is necessary to form the inside-out, outside-out, and whole-cell configurations. The cell-attached configuration is formed by firstly placing the pipette near the cell membrane for a low-resistance seal of approximately $50\ \Omega$, and secondly applying suction for a gigaohm resistance seal [74, 88].

Whole-cell

After the gigaseal is formed for cell-attached configuration, it is possible to apply quick suction or electrical pulses. This will result in the pipette accessing the inside of the cell for whole-cell recordings to be made [74, 88]. An example of a previous whole cell recording of mesenchymal stem cells is shown below (Figure 1.17).

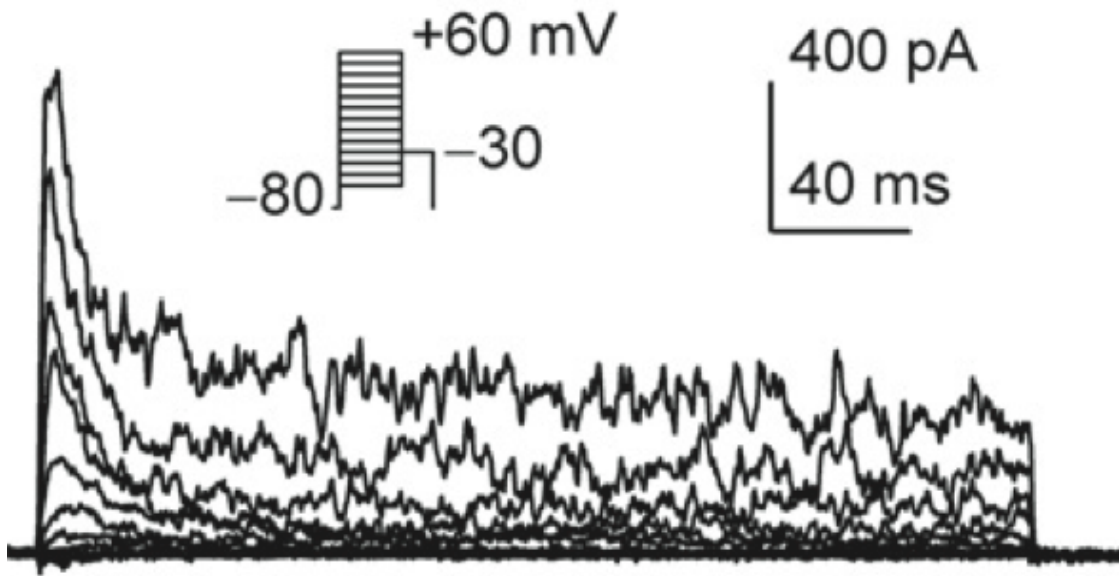


FIGURE 1.17: An example of whole-cell recording of mesenchymal stem cells. The x axis is time, and the y axis is current when the voltage is held constant at values shown [45]. The current magnitude increases as the holding voltage increases.

Inside-out

After the gigaseal is formed for a cell-attached configuration, the pipette can also be quickly withdrawn to form an inside-out arrangement. A membrane patch will still be in contact with the tip of the pipette, where the inside of the membrane will face the outside of the pipette. The pipette will then be in contact with a bathing solution for currents and transmembrane potentials to be measured of this individual patch [74, 88].

Outside-out

If the pipette is pulled away after the pipette is in the whole-cell configuration, the outside-out configuration will be achieved. The outside of the membrane will face the outside of the pipette in this case, where the extracellular surface is in contact with the bathing solution of interest [74, 88].

In this study, whole-cell patch clamp results were used to model mesenchymal stem cells. These results give a holistic look into the effect each type of ion channel has on the cell's electrical activity.

Chapter 2

Methodology

In this study, numerical results were generated to provide insight into the interaction between mesenchymal stem cells and cardiomyocytes. The methodology for this technique is discussed in detail below.

2.1 Methodology of Mathematical Modeling

To gain insight via simulations into the interaction between mesenchymal stem cells and cardiomyocytes, the following steps were taken:

1. Develop a general model for each type of functional ionic channel in mesenchymal stem cells.
2. Fit ionic channel models to corresponding empirically derived mesenchymal stem cell ion channel data.

3. Simulate whole mesenchymal stem cell electrical activity model and validate the model by comparing to empirical results.
4. Couple the mesenchymal stem cell model with the previously established cardiomyocyte model.

First, the general models used to fit mesenchymal stem cell ionic channel data will be discussed.

2.2 Modeling Individual Ion Channels

2.2.1 TTX-Sensitive Sodium Channel Current

The TTX-sensitive sodium current is known to have a transient conductance [89, 90]. Empirical TTX-sensitive sodium current data suggests the probability of open channels, P , can be related with the activation and inactivation variables m and h by:

$$P_i = m^3 h \quad (2.1)$$

where m and h vary over time as follows:

$$\frac{dh}{dt} = \frac{h_\infty - h}{\tau_h} \quad (2.2)$$

$$\frac{dm}{dt} = \frac{m_\infty - m}{\tau_m} \quad (2.3)$$

To find the driving force $V - E_{Na}$, it is necessary to find the Nernst potential:

$$E_{Na} = \frac{RT}{zF} \ln \frac{[Na_o^+]}{[Na_i^+]} \quad (2.4)$$

Therefore, the TTX-sensitive sodium current can be modeled by [68, 89, 90]:

$$I_{Na} = \overline{G_{Na}} m^3 h (V - E_{Na}) \quad (2.5)$$

2.2.2 Transient Outward Potassium Channel Current

As the name suggests, the transient outward potassium current is also known to have a transient conductance [66, 91]. Empirical transient outward potassium current data suggests the probability of open channels, P , can be related with the activation and inactivation variables r and s by:

$$P_i = rs \quad (2.6)$$

where r and s vary over time as follows:

$$\frac{dr}{dt} = \frac{r_\infty - r}{\tau_r} \quad (2.7)$$

$$\frac{ds}{dt} = \frac{s_\infty - s}{\tau_s} \quad (2.8)$$

To find the driving force $V - E_K$, it is necessary to find the Nernst potential:

$$E_K = \frac{RT}{zF} \ln \frac{[K_o^+]}{[K_i^+]} \quad (2.9)$$

Therefore, the transient outward potassium current can be modeled by:

$$I_{to} = \overline{G_{to}} rs (V - E_K) \quad (2.10)$$

2.2.3 L-Type Calcium Current

The L-type calcium current is also known to have a transient conductance. However, the standard ionic model of instantaneous linear current-voltage relation cannot be used, as the external concentration of calcium varies greatly from the internal concentration [92]. Therefore, the driving force is modeled with the Goldmann-Hodgkin-Katz equation rather than the difference between membrane potential and Nernst potential [89]. To derive the Goldmann-Hodgkin-Katz equation, it is assumed that the potential varies linearly across the cell membrane, the ion flux is constant, and the calcium concentrations are only considered. Using these assumptions and the Nernst-Planck equation (Equation 1.9), we find the driving force as:

$$V - E_{Ca} = 4 \frac{VF^2}{RT} \frac{[Ca_i^{+2}]e^{2VF/RT} - \phi[Ca_o^{+2}]}{e^{2VF/RT} - 1} \quad (2.11)$$

where ϕ is the partition coefficient for the calcium ion.

Since the L-type calcium current is also known to have a transient conductance, the activation and inactivation variables d and f , respectively, must vary over time as:

$$\frac{dd}{dt} = \frac{d_\infty - d}{\tau_d} \quad (2.12)$$

$$\frac{df}{dt} = \frac{f_\infty - f}{\tau_f} \quad (2.13)$$

Therefore, the overall L-type calcium current can be modeled as [89]:

$$I_{CaL} = \overline{G_{CaL}} df 4 \frac{VF^2}{RT} \frac{[Ca_i^{+2}]e^{2VF/RT} - \phi[Ca_o^{+2}]}{e^{2VF/RT} - 1} \quad (2.14)$$

2.2.4 Calcium Activated Potassium Channel Current

Unlike the transient outward potassium channel, the L-type calcium channel, and the TTX-sensitive sodium channel, the calcium activated potassium channel is persistent. The activation variable m , however, is both voltage-dependent and intracellular calcium concentration dependent, as described by Gerstner *et al* [89], where:

$$\frac{dm}{dt} = \alpha m - \beta(1 - m) \quad (2.15)$$

such that:

$$\alpha = \alpha_1 [Ca_i^{+2}] e^{V/\alpha_2} \quad (2.16)$$

$$\beta = \beta_1 e^{-V/\beta_2} \quad (2.17)$$

where α_1 , α_2 , β_1 , and β_2 are unitless data fitting parameters. Since $P_i = m$, and $G_i = \overline{G}_i P_i$:

$$I_{KCa} = \overline{G}_{KCa} m(V - E_K) \quad (2.18)$$

and thus the Nernst potential E_K is equal to:

$$E_K = \frac{RT}{zF} \ln \frac{[K_o^+]}{[K_i^+]} \quad (2.19)$$

2.2.5 Delayed Rectifier Potassium Channel Current

Similar to the calcium activated potassium channel, the delayed-rectifier potassium current is persistent. However, to model this channel, microscopic descriptions of the transitions between conformational states of channel molecules will be used [68].

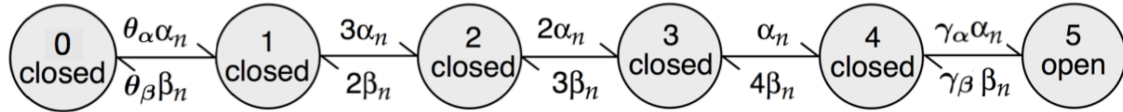


FIGURE 2.1: The states and transition rates of the persistent delayed-rectifier potassium channel model are shown [68].

The delayed-rectifier channel has a four subunit structure, each of which can be opened or closed. It is assumed that an extra transition state is required after all four subunit structures are opened for ionic flow to occur. Therefore, this model considers six states (Figure 2.1), where states 0 through 4 represent the number of subunit gates are open, and state 5 represents the extra transition state for ionic flow.

In this Markovian model, α_n and β_n are voltage-dependent rate functions; γ_α , γ_β , θ_α , and θ_β are voltage-dependent functions, which account for the possible variation in transition rates for all subunits structures to close (θ_α and θ_β) and for ionic flow to occur (γ_α and γ_β). This Markovian model is a modified version of the fibroblast Shaker Kv 1.x family channel model by Sachse *et al* [83], and of the bullfrog sympathetic neuron delayed rectifier potassium channel current model by Klemic *et al* [93].

To model this channel, it is now necessary to describe dynamic change of the probability in each state, p_i , where $i = 0, 1, 2, 3, 4$, and 5 for states 0 through 5, respectively. Using a similar reasoning to the two-state model for the persistent model, the equations for the state probabilities are [68]:

$$\frac{dp_0}{dt} = \theta_\beta \beta_n p_1 - \theta_\alpha \alpha_n p_1 \quad (2.20)$$

$$\frac{dp_1}{dt} = \theta_\alpha \alpha_n p_0 + 2\beta_n p_2 - (\theta_\beta \beta_n + 3\alpha_n) p_1 \quad (2.21)$$

$$\frac{dp_2}{dt} = 3\alpha_n p_1 + 3\beta_n p_3 - (2\beta_n + 2\alpha_n) p_2 \quad (2.22)$$

$$\frac{dp_3}{dt} = 2\alpha_n p_2 + 4\beta_n p_4 - (3\beta_n + \alpha_n) p_3 \quad (2.23)$$

$$\frac{dp_4}{dt} = \alpha_n p_3 + \gamma_\beta \beta_n p_5 - (4\beta_n + \gamma_\alpha \alpha_n) p_4 \quad (2.24)$$

$$\frac{dp_5}{dt} = \gamma_\alpha \alpha_n p_4 - \gamma_\beta \beta_n p_5 \quad (2.25)$$

From the definitions of p_i 's, it is obvious that the activation variable x for the delayed-rectifier potassium channel can be set to p_5 . Therefore, the delayed-rectifier potassium channel model is:

$$I_{dr} = \overline{G_{dr}} x (V - E_k) \quad (2.26)$$

where E_k is the Nernst potential with respect to potassium concentrations intracellularly and extracellularly.

2.2.6 Leakage Channel Current

The leakage channel current accounts for all ions crossing the cell membrane that are not accounted for by I_{KCa} , I_{dr} , I_{Na} , I_{to} , and I_{CaL} . By analogy to other currents, the form of the leakage current is [74]:

$$I_L = G_L (V - E_L) \quad (2.27)$$

where I_L is the leakage current, G_L is the conductance of the leakage channel, and E_L is the leakage resting potential. Unlike the time variant G_K , G_{Ca} , and G_{Na} , the leakage conductance has a fixed value. This current only has a significant effect when other ionic currents are small, where the leakage current is on the same magnitude as other currents [74].

For each type of mesenchymal stem cell, a different leakage current was used to satisfy its resting membrane potential (-42 mV to -12 mV) [45].

2.2.7 Ionic Concentration Variations

The intracellular (i) and extracellular (o) potassium, sodium, and calcium concentrations appear throughout the models of the functional ion channels in mesenchymal stem cells. Furthermore, the transfer of these ions across the cellular membrane can result in substantial variations in ionic concentration over time, making it necessary to discuss $\frac{d[Na_o^+]}{dt}$, $\frac{d[Na_i^+]}{dt}$, $\frac{d[K_o^+]}{dt}$, $\frac{d[K_i^+]}{dt}$, $\frac{d[Ca_o^{+2}]}{dt}$, and $\frac{d[Ca_i^{+2}]}{dt}$.

Due to the relatively large extracellular fluid volume and amount of ions, there are negligible extracellular ion concentration changes from the transfer of potassium, sodium, and calcium ions across the membrane. Therefore, it is assumed that:

$$\frac{d[Na_o^+]}{dt} \approx 0 \quad (2.28)$$

$$\frac{d[K_o^+]}{dt} \approx 0 \quad (2.29)$$

$$\frac{d[Ca_o^{+2}]}{dt} \approx 0 \quad (2.30)$$

The intracellular sodium, potassium, and calcium concentrations are sensitive to the transfer of the respective ion across the cell membrane. The transfer of both sodium and potassium ions is a direct result of an influx of the ion across its respective channel and pumps [94, 95]. However, for the purposes of this study, it is safe to assume the variations in intracellular sodium and potassium concentration are negligible. Therefore, this can be modeled by:

$$\frac{d[Na_i^+]}{dt} \approx 0 \quad (2.31)$$

$$\frac{d[K_i^+]}{dt} \approx 0 \quad (2.32)$$

There are many processes involved in the transfer of calcium ions, making it necessary to model the variation of calcium concentration differently over time. Calcium levels increase as a result of influx of calcium through the calcium channels, but they also have complicated intracellular dynamics that can be modeled as an exponentially decaying process (represented by terms 1 and 2 in the following equation, respectively). [68, 89]. Therefore, the dynamic intracellular calcium concentration is:

$$\frac{d[Ca_i^{+2}]}{dt} = \frac{I_{CaL}}{2V_c F} - \frac{[Ca_i^{+2}]}{\tau_{Ca}} \quad (2.33)$$

where τ_{Ca} is the time constant describing exponentially decaying process of the removal of calcium ions. Note the 2 in the denominator of the second term, which accounts for the +2 valence of calcium ions. However, for the purposes of this study, it is safe to assume the variations in intracellular calcium concentration are negligible, as the spontaneous decay of calcium will nearly balance out the effects

of the L-type calcium current. Therefore, this can be modeled by:

$$\frac{d[Ca_i^{+2}]}{dt} \approx 0 \quad (2.34)$$

These general models developed for each ionic channel have parameters were fit to available data by Heubach *et al* [69], Li *et al* [45], and Kawano *et al* [94]. Most patch clamp studies are conducted at room temperature (21°C - 22°C) [45, 69]. The Nernst potential, which is dependent on temperature, was therefore extrapolated to normal body temperature (37° C, or 310 K). The numerical methods used to fit the data to the ionic channel models are discussed in the following section.

2.3 Numerical Methods Applied for Data Fitting to Ion Channel Models

Due to the form of ionic channel equations, both an ordinary differential equation solver and a nonlinear optimization programming algorithm were necessary to fit the mesenchymal stem cell ion channel data. To simulate the total mesenchymal stem cell current, and the coupled mesenchymal stem cell and cardiomyocyte electrical activity, the same ordinary differential equation solver was used. To fit the mesenchymal stem cell ion channel data, both the Levenberg-Marquardt nonlinear optimization programming algorithm and the Runge-Kutta-Fehlberg ordinary differential equation solver were used.

2.3.1 Levenberg-Marquardt Algorithm

From the available data, and from the equations used to model ionic channel activity, a nonlinear least-squares optimization problem can be posed:

$$\text{minimize } f(x) = \sum_{i=1}^m [r_i(x)]^2 \quad (2.35)$$

where $r_i : \mathbb{R}^n \rightarrow \mathbb{R}$, $i = 1, \dots, m$ are functions of the difference between empirical data values and the predicted values from the non-linear fitting equation.

To solve this convex optimization problem, descent of the objective function at each iteration is necessary. To enforce the descent of an objective function at every iteration in an algorithm, two general methods are typically used: line searches and trust-regions (Figure 2.2) [96].

Line search algorithms first choose a search direction, and then the distance along this direction. Trust-regions, on the other hand, select the maximum distance to go

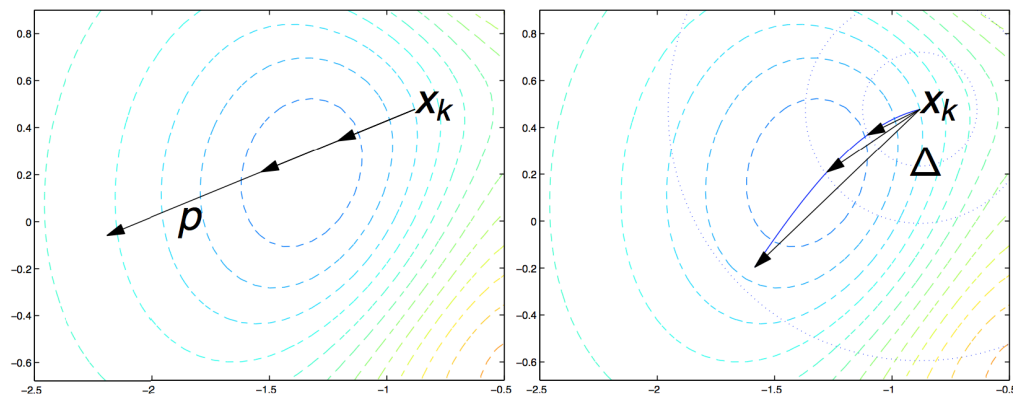


FIGURE 2.2: The difference between line-search and trust-region algorithms on input x_k are depicted above. In the figure to the left, a line-search algorithm is applied, as the search direction p is first selected, followed by the distance along this direction. In the figure to the right, a trust-region algorithm is applied, as the maximum distance to go along Δ is selected first, followed by the direction [96].

along in an iteration, followed by the direction (Figure 2.2) [96].

In order to solve this optimization problem, the Levenberg-Marquardt algorithm was applied. This algorithm is an adaptive trust-region algorithm.

To minimize the objective function $f(x)$, it is necessary to find the next point x_{i+1} that gives a smaller $f(x)$ until $f(x)$ no longer decreases. To do so, trust region algorithms in general approximate $f(x)$ by its Taylor series expansion around x_i in a neighborhood ϵ around x_i . The next step size s_i can be approximated by solving the optimization problem [97]:

$$\min q_i(s)$$

$$\text{such that } \|x\| \leq \epsilon \quad (2.36)$$

$$q_i(s) = \mathbf{g}^T s + \frac{1}{2} s^T \mathbf{H} s$$

where \mathbf{g} and \mathbf{H} are the gradient and the Hessian of $f(x)$ at x_i , respectively [97]. The optimal step size, x^* of this constrained optimization problem is the solution to:

$$(\mathbf{H} + \lambda \mathbf{I})x^* = -\mathbf{g} \quad (2.37)$$

for $\lambda \geq 0$ and a positive semi-definite matrix $\mathbf{H} + \lambda \mathbf{I}$, where \mathbf{I} is the identity matrix. Adapted trust-region sizes are typically applied for algorithms to compare the predicted and actual reduction of the objective function [96]. The reduction ratio ρ dictates the modifications of the trust-region step size, where the reduction ratio is:

$$\rho = \frac{f(x_i) - f(x_i + s_i)}{q_i(0) - q_i(s_i)} \quad (2.38)$$

If the reduction ratio is greater than $\frac{3}{4}$, the trust-region step size is increased during the next iteration. If the reduction ratio is less than $\frac{1}{4}$, the trust-region step size is decreased during the next iteration. Otherwise, the trust-region step size is not changed. It is necessary for the reduction ratio to not be too small in order for the step s to be used on an iteration [96].

In the Levenberg-Marquardt algorithm, the step size x^* is still the solution to:

$$(\mathbf{H} + \lambda \mathbf{I})x^* = -\mathbf{g} \quad (2.39)$$

However, \mathbf{H} is approximated by $\mathbf{J}^T \mathbf{J}$ in this method, where \mathbf{J} is the Jacobian of the function of interest with respect to the parameters solved for in the nonlinear least-squares optimization problem. The “fmincon” MATLAB function, which is used in this study, applies this algorithm. For sample code applying this algorithm, see Appendix A.

2.3.2 Runge-Kutta-Fehlberg Ordinary Differential Equation Solver

It is clear that ordinary differential equations exist in the general form of each mesenchymal stem cell ion channel equation. Therefore, an ordinary differential equation solver is used to numerically solve these ordinary differential equations to fit the data and simulate cellular electrical activity. The Runge-Kutta-Fehlberg method is used in this study to numerically solve the ordinary differential equations [98, 99].

The Runge-Kutta-Fehlberg method checks and compares two different approximations for the numerical solution of an ordinary differential equation to determine if the correct step size is used. If the two approximations are nearly equal, the step size is used. However, if the two approximations are not nearly equal, the step size is decreased. The calculation of the step size h requires the calculation of k_1 through k_6 :

$$k_1 = hf(t_k, y_k) \quad (2.40)$$

$$k_2 = hf(t_k + \frac{1}{4}h, y_k + \frac{1}{4}k_1) \quad (2.41)$$

$$k_3 = hf(t_k + \frac{3}{8}h, y_k + \frac{3}{32}k_1 + \frac{9}{32}k_2) \quad (2.42)$$

$$k_4 = hf(t_k + \frac{12}{13}h, y_k + \frac{1932}{2197}k_1 - \frac{7200}{2197}k_2 + \frac{7296}{2197}k_3) \quad (2.43)$$

$$k_5 = hf(t_k + h, y_k + \frac{439}{216}k_1 - 8k_2 + \frac{3680}{513}k_3 - \frac{845}{4104}k_4) \quad (2.44)$$

$$k_6 = hf(t_k + \frac{1}{2}h, y_k - \frac{8}{27}k_1 + 2k_2 - \frac{3544}{2565}k_3 + \frac{1859}{4104}k_4 - \frac{11}{40}k_5) \quad (2.45)$$

The fourth order y_{k+1} and fifth order z_{k+1} approximations of the initial value problem are then calculated by Equations 2.46 and 2.47, respectively:

$$y_{k+1} = y_k + \frac{25}{216}k_1 + \frac{1408}{2565}k_3 + \frac{2197}{4101}k_4 - \frac{1}{5}k_5 \quad (2.46)$$

$$z_{k+1} = y_k + \frac{16}{135}k_1 + \frac{6656}{12,825}k_3 + \frac{28,561}{56,430}k_4 - \frac{9}{50}k_5 + \frac{2}{55}k_6 \quad (2.47)$$

The optimal step size sh is then determined by calculating s :

$$s = \left(\frac{\epsilon h}{2|z_{k+1} - y_{k+1}|} \right)^{\frac{1}{4}} \quad (2.48)$$

where ϵ is the tolerance selected. This ordinary differential equation solver is applied with the Levenberg-Marquardt algorithm to fit the mesenchymal stem cell ion channel data from Li *et al.* The “ode45” MATLAB function, which is used in this study, applies this algorithm. For sample data fitting code, see Appendix A.

2.4 Modeling of Human Mesenchymal Stem Cell Electrophysiological Activity

After fitting the mesenchymal stem cell ion channel data, it is possible to determine the robustness of the model. This was done by simulating the whole mesenchymal stem cell electrical activity model, and comparing it to empirical results. As previously discussed, five possible functional ion channels (excluding the leakage current) exist for mesenchymal stem cells. However, these ion channels are not existent in all mesenchymal stem cells. As a result, there are three different types of total currents for mesenchymal stem cells (labeled as “Total Current A, B, and C”), as shown in Table (2.1) [45, 47]. It is assumed that a certain ionic current that is functional in different types of total currents acts equivalently.

TABLE 2.1: Types of Total Currents for Mesenchymal Stem Cells

Total Current Label	Functional Ion Channels
A	Calcium Activated Potassium Current (I_{KCa}) Delayed Rectifier Current (I_{dr}) Leakage Current A (I_{La})
B	Transient Outward Current (I_{to}) Calcium Activated Potassium Current (I_{KCa}) Leakage Current B (I_{Lb})
C	Sodium Current (I_{Na}) L-type Calcium Current (I_{LCa}) Delayed Rectifier Current (I_{dr}) Calcium Activated Potassium Current (I_{KCa}) Leakage Current C (I_{Lc})

These three types of mesenchymal stem cells only use their corresponding ion channels that are shown in Figure 2.3.

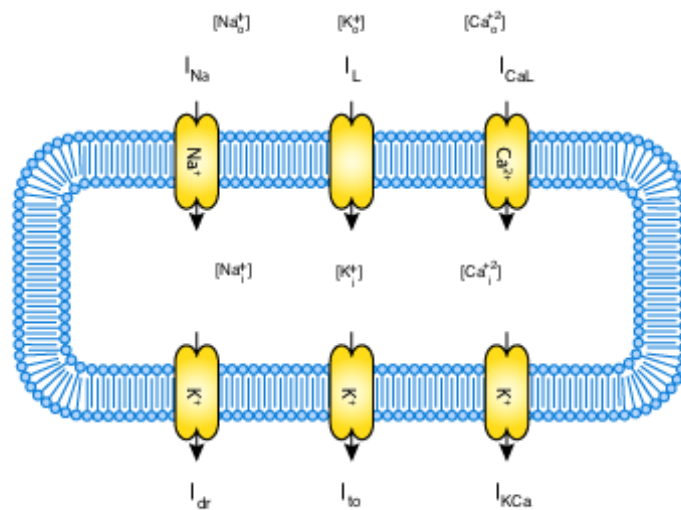


FIGURE 2.3: Human mesenchymal stem cell model. The three types of mesenchymal stem cells only operate the appropriate ion channels. “Total Current A” only operates I_{KCa} , I_{dr} , and I_{La} . “Total Current B” only operates I_{KCa} , I_{to} , and I_{Lb} . “Total Current C” operates I_{KCa} , I_{dr} , I_{Na} , I_{LCa} , and I_{Lc} . [45, 47, 69].

From this information, the three types of I_{ion} , or total currents, were modeled (Table 2.2).

TABLE 2.2: Types of Total Currents for Mesenchymal Stem Cells

Total Current Label	Total Current (I_{ion}) Equation
A	$I_{ion} = I_{KCa} + I_{dr} + I_{La}$
B	$I_{ion} = I_{KCa} + I_{to} + I_{Lb}$
C	$I_{ion} = I_{KCa} + I_{dr} + I_{Na} + I_{LCa} + I_{Lc}$

These equations were subsequently substituted into Equation 1.32 to simulate the electrical activity of a whole mesenchymal stem cell. After simulating the three types of mesenchymal stem cell electrical activity and confirming the model with empirical data [45], the model was coupled with the ten Tusscher cardiomyocyte model.

2.5 Modeling Human Mesenchymal Stem Cell-Cardiomyocyte Coupling

The novel model was coupled with the ten Tusscher cardiomyocyte model to simulate the cardiomyocyte action potential and the conduction velocity. The methods to generate such simulations are shown in the following sections.

2.5.1 Action Potential Simulation

The novel mesenchymal stem cell model was coupled with the ten Tusscher model of the ventricular action potential [67]. To couple the two models together, Equations

2.49 and 2.50 were used.

$$\frac{dV_{CM}}{dt} = -\frac{1}{C_{m,CM}}[I_{CM} + \sum_{i=1}^n G_{gap}(V_{CM} - V_{hMSC})] \quad (2.49)$$

$$\frac{dV_{hMSC}}{dt} = -\frac{1}{C_{m,hMSC}}[I_{hMSC} + \sum_{i=1}^n G_{gap}(V_{hMSC} - V_{CM})] \quad (2.50)$$

where CM and $hMSC$ subscripts represent cardiomyocytes and human mesenchymal stem cells, respectively. The cardiomyocyte and human mesenchymal stem cell total currents, I_{CM} and I_{hMSC} , along with the individual ion channel models, were previously defined in Chapters 1 and 2, respectively.

The MATLAB ordinary differential equation solver “ode45” is inadequate and unstable for stiff differential equations. Therefore, because the behavior of the cardiomyocyte action potential is stiff, the MATLAB stiff ordinary differential equation solver “ode15s” was used when coupling the two cell types together. For consistent results, the tenth action potential measured was extracted for analysis.

First, the cardiomyocyte model was coupled with each individual type of mesenchymal stem cell current in ratios of 9:1, 4:1, and 1:1, respectively. Then, the cardiomyocyte model was coupled with a weighted average (with respect to the prevalence of each mesenchymal stem cell total current) in ratios of 9:1, 4:1, and 1:1. The prevalence of each type of total current is shown below (Table 2.3) [46].

The subroutine “ode15s” on MATLAB was used to solve this system of ordinary differential equations as well.

TABLE 2.3: Prevalence of Each Type of Total Currents for Mesenchymal Stem Cells

Total Current Label	Prevalence (%)
A	63
B	8
C	29

2.5.2 Conduction Velocity Simulation

The conduction velocity, another crucial factor in determining cardiomyocyte function, was modeled by simplifying the 2-D (x - y plane) continuous system sheet of cells to a 1-D system of cardiomyocytes and mesenchymal stem cells:

$$\frac{\partial V_{CM}}{\partial t} = -\frac{I_{ion,CM} + I_{stim} + I_{gap,CM}}{C_{m,CM}} + \frac{1}{\rho_{x,CM} S_{x,CM} C'_{m,CM}} \frac{\partial^2 V_{CM}}{\partial x^2} \quad (2.51)$$

$$\frac{\partial V_{hMSC}}{\partial t} = -\frac{I_{ion,hMSC} + I_{stim} + I_{gap,hMSC}}{C_{m,hMSC}} + \frac{1}{\rho_{x,hMSC} S_{x,hMSC} C'_{m,hMSC}} \frac{\partial^2 V_{hMSC}}{\partial x^2} \quad (2.52)$$

where I_{gap} is the gap junction current between mesenchymal stem cells and cardiomyocytes (such that $I_{gap,CM} = -I_{gap,hMSC}$), S is the surface-to volume ratio of a cell, and ρ is the effective cellular resistivity. The effective cellular resistivities for mesenchymal stem cells and cardiomyocytes were determined using the method of linear scaling of intracellular conductivities with cellular volume fraction, as recommended by Sachse *et al* [100]. Specifically, the resistivities were calculated by

[100]:

$$\rho_{CM} = \frac{Vol}{Vol_{CM}} \overline{\rho_{CM}} \quad (2.53)$$

$$\rho_{hMSC} = \frac{Vol}{Vol_{hMSC}} \overline{\rho_{hMSC}} \quad (2.54)$$

such that:

$$\frac{Vol}{Vol_{CM}} = \frac{Vol_{CM,single} + n Vol_{hMSC,single}}{Vol_{myo,single}} \quad (2.55)$$

$$\frac{Vol}{Vol_{hMSC}} = \frac{Vol_{CM,single} + n Vol_{hMSC,single}}{n Vol_{hMSC,single}} \quad (2.56)$$

where n is the number of mesenchymal stem cells per cardiomyocyte, Vol is the tissue volume, Vol_{CM} is the tissue volume occupied by cardiomyocytes, Vol_{hMSC} is the tissue volume occupied by mesenchymal stem cells, $Vol_{CM,single}$ is the tissue volume occupied by a single cardiomyocyte, $Vol_{hMSC,single}$ is the tissue volume occupied by a single mesenchymal stem cell, and $\overline{\rho_{CM}}$ and $\overline{\rho_{hMSC}}$ are the conductivities of tissue composed of 100% cardiomyocytes and mesenchymal stem cells, respectively.

Empirical data was unavailable for the cellular resistivity of a mesenchymal stem cell. Therefore, the cellular resistivity of a mesenchymal stem cell was calculated by extending the cardiomyocyte single-channel gap conductance and cellular resistivity relationship [101] to the mesenchymal stem cell-mesenchymal stem cell single-channel gap conductance [70]. This inverse relationship, as suggested by Jongsma and Wilders is [102]:

$$\overline{\rho_{hMSC}} g_{gap} = \frac{\pi r_c^2}{L_{gap}} \quad (2.57)$$

where g_{gap} is the single channel conductance, r_c is the channel radius, and L_{gap} is the length of the gap junction. The length and the radius of the mesenchymal

stem cell-mesenchymal stem cell gap junction were assumed to be the same as the cardiomyocyte-cardiomyocyte gap junction.

To solve this partial differential equation, the method of lines was used via the MATLAB function “*pdepe*”, with step sizes of $\Delta x = 0.02$ cm and $\Delta t = 0.005$ ms. To mimic biological conditions best [66], Euclidian geometry was selected for the cardiomyocyte cells simulated in series. Initial conditions and Neumann-type boundary conditions were implemented to solve this partial differential equation, such that: 1) the stimulus current was applied at the first cell in the series (Boundary Condition 1); 2) no flux at the last cell in the series (Boundary Condition 2); and 3) the initial membrane voltage was the resting membrane potential (Initial Condition 1). The resulting conduction velocity was measured at the center of the system of cells. By solving this partial differential equation, it was also possible to find the maximum upstroke velocity, $\frac{dV}{dt}_{\max}$. This rapid depolarization rate was also calculated at the center of the system of cells.

The values for mesenchymal stem cell parameters within this study are shown on the next page in Table 2.4. For the ten Tusscher model parameters, see References 66, 79, and 82.

TABLE 2.4: Parameter Values

Parameter	Definition	Value	Reference
R	Gas Constant	8.314 J/mol/K	[103]
T	Temperature	310 K	[104]
F	Faraday Constant	96.485 C/mmol	[103]
$C_{m,hMSC}$	Cell Capacitance	59.7 pF	[45]
$C'_{m,hMSC}$	Specific Cell Capacitance	2.7 $\mu\text{F}/\text{cm}^2$	[105]
S_{hMSC}	Specific Area	19.4 μm^{-1}	[105]
ρ_{hMSC}	Cellular Resistivity	243 $\Omega\cdot\text{cm}$	[82]
Vol_{hMSC}	Cytoplasmic Volume	6,300 μm^3	[105]
G_{gap}	Gap Conductance	1.5 nS	[70]
g_{gap}	Single-Channel Gap Conductance	50 pS	[70]
$[K_i^+]$	Intracellular Potassium Concentration	140 mM	[104]
$[Na_i^+]$	Intracellular Sodium Concentration	5 mM	[104]
$[Ca_i^{+2}]$	Intracellular Calcium Concentration	100 nM	[104]
$[K_o^+]$	Extracellular Potassium Concentration	5.4 mM	[104]
$[Na_o^+]$	Extracellular Sodium Concentration	140 mM	[104]
$[Ca_o^{+2}]$	Extracellular Calcium Concentration	2 mM	[104]

Chapter 3

Results

Section 2.2 developed the general models for the calcium activated potassium current (I_{KCa}), delayed rectifier potassium current (I_{dr}), sodium current (I_{Na}), L-type calcium current (I_{CaL}), transient outward potassium current (I_{to}), and the leakage currents (I_{La} , I_{Lb} , and I_{Lc}). Furthermore, it described the calcium, sodium, and potassium dynamics.

The next step to develop insight into the interaction between mesenchymal stem cells and cardiomyocytes is to fit the ionic channel models to corresponding empirically derived mesenchymal stem cell ion channel data using the Levenberg–Marquardt algorithm. The resulting mesenchymal stem cell ion channel models are shown in the following section.

3.1 Human Mesenchymal Stem Cell Individual Ion Current Models

3.1.1 Calcium Activated Potassium Current

The transition rate parameters (α_n and β_n), and maximum conductance of the calcium activated potassium current were fit to the steady state current-voltage data of human mesenchymal stem cells provided by Li *et al* [45]. This was accomplished by measuring the difference between the mesenchymal stem cell current before and after the application of iberiotoxin, a selective blocker of the large-conductance potassium channel [45]. The resulting formulations were used to fully describe the calcium activated potassium current (Table 3.1).

TABLE 3.1: Calcium Activated Potassium Channel Formulation

Equations Used to Describe the Calcium Activated Potassium Channel

$$I_{KCa} = 3.0m(V - E_K)$$

$$\frac{dm}{dt} = \alpha m - \beta(1 - m)$$

$$\alpha = 687.8[Ca_i^{+2}]e^{V/15.8}$$

$$\beta = 21.1e^{-V/43.5}$$

$$E_K = -87.0 \text{ mV}$$

The ability of this model to fit the steady state current-voltage (I-V) curve of the calcium-activated potassium channel is shown below (Figure 3.1). This promising model was subsequently confirmed with dynamic empirical data.

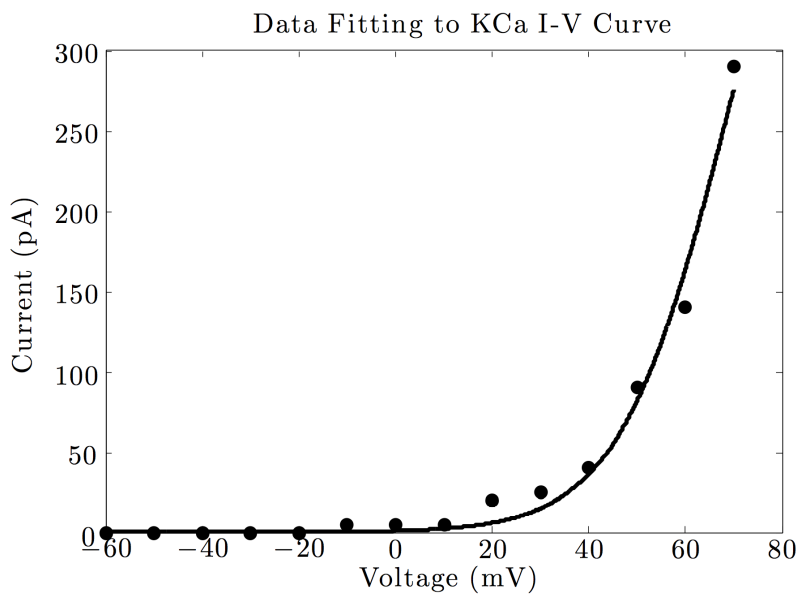


FIGURE 3.1: The calcium activated potassium channel I-V curve was derived from the difference between the mesenchymal stem cell current before and after the application of iberiotoxin, a selective blocker of large-conductance [45]. This study’s model successfully fits the I-V curve using the equations in Table 3.1. The dots and closed line represent measured data and simulated data, respectively.

The dynamic behavior of this model was confirmed by comparing it to empirical whole-cell patch clamping experiments by Li *et al* [45]. The difference between the mesenchymal stem cell current before and after the application of iberiotoxin is comparable to the calcium activated potassium channel current simulation (Figure 3.2). The noise seen in the empirical data was not accounted for, as it would have a negligible effect on the cardiac action potential behavior. The activation kinetic rate behavior and the steady state values were matched, making this calcium activated potassium channel model viable.

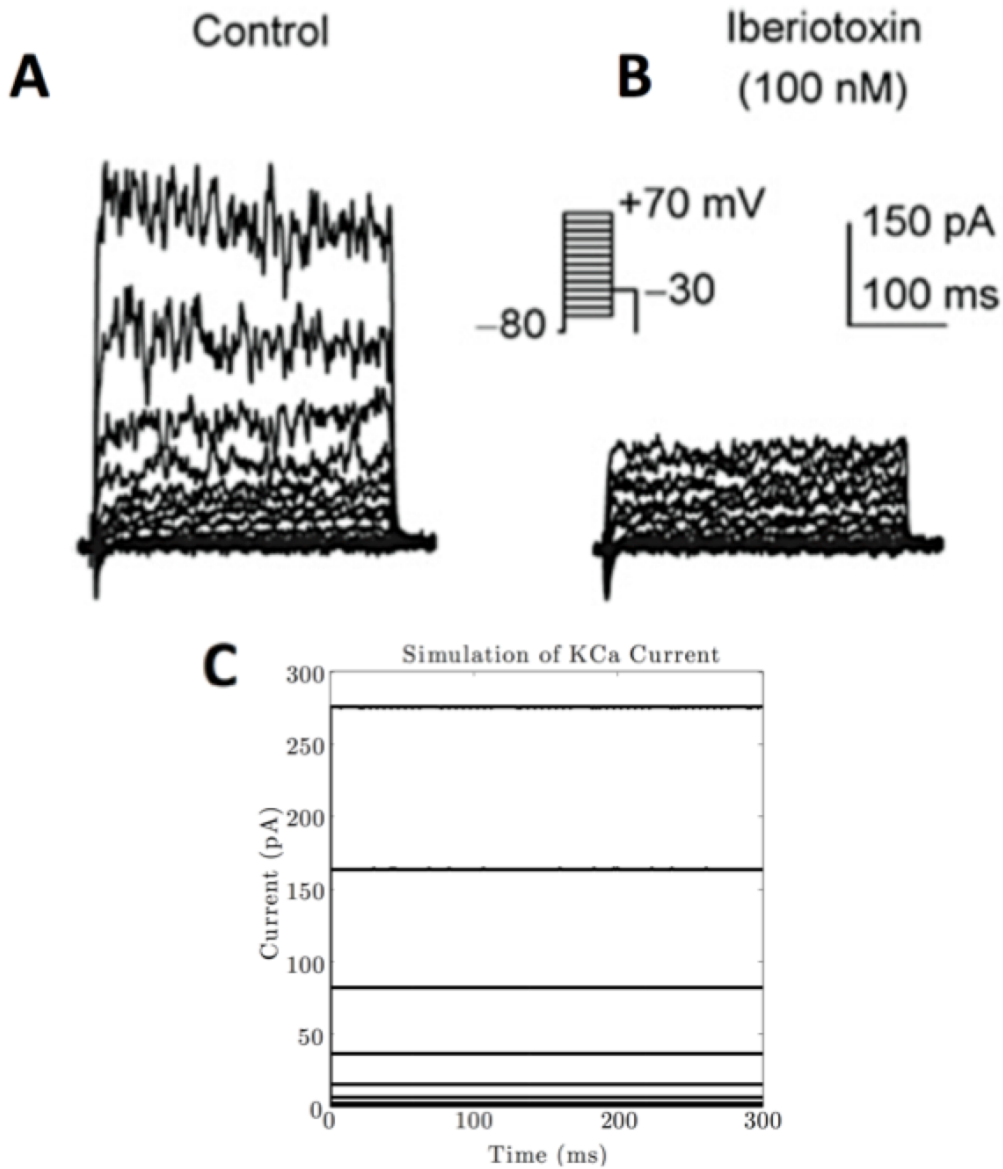


FIGURE 3.2: The difference between the mesenchymal stem cell current before (A) and after the application of iberiotoxin (B) is comparable to the calcium activated potassium channel current simulation (C) [45]. Therefore, the model for this channel was accepted.

3.1.2 Delayed Rectifier Potassium Current

Next, the delayed rectifier potassium current was modeled. The transition rate parameters, α_n and β_n , were fit to the activation time constant and the steady-state activation of human mesenchymal stem cells from Li *et al* [45]. The maximum conductance of the delayed rectifier current was fit to current-voltage data of human

mesenchymal stem cells provided by Li *et al* [45]. The resulting formulations were used to fully describe the delayed rectifier potassium current (Table 3.2).

TABLE 3.2: Delayed Rectifier Potassium Channel Formulation

Equations Used to Describe the Delayed Rectifier Potassium Channel

$$I_{dr} = 6.5x(V - E_k)$$

$$\frac{dp_0}{dt} = \theta_\beta \beta_n p_1 - \theta_\alpha \alpha_n p_1$$

$$\frac{dp_1}{dt} = \theta_\alpha \alpha_n p_0 + 2\beta_n p_2 - (\theta_\beta \beta_n + 3\alpha_n) p_1$$

$$\frac{dp_2}{dt} = 3\alpha_n p_1 + 3\beta_n p_3 - (2\beta_n + 2\alpha_n) p_2$$

$$\frac{dp_3}{dt} = 2\alpha_n p_2 + 4\beta_n p_4 - (3\beta_n + \alpha_n) p_3$$

$$\frac{dp_4}{dt} = \alpha_n p_3 + \gamma_\beta \beta_n p_5 - (4\beta_n + \gamma_\alpha \alpha_n) p_4$$

$$\frac{dp_5}{dt} = \gamma_\alpha \alpha_n p_4 - \gamma_\beta \beta_n p_5$$

$$x = p_5$$

$$\alpha_n = \frac{0.02}{1 + 0.9e^{-\frac{V-10.0}{-12.4}}}$$

$$\beta_n = \frac{2 \times 10^{-4}(125.5+V)}{1 + 26.9e^{-\frac{V-47.4}{-14.6}}}$$

$$\gamma_\alpha = 2.5e^{-\frac{(V-53.2)^2}{593.7}} + 2.4$$

$$\gamma_\beta = 8.2e^{-\frac{(V-55.2)^2}{659.9}}$$

$$\theta_\alpha = 10$$

$$\theta_\beta = 0.1$$

$$E_K = -87.0 \text{ mV}$$

The ability of this model to fit the steady state current-voltage (I-V) of the delayed rectifier potassium channel is shown in Figure 3.3. High concentrations of EGTA and Cd⁺² were used by this research group to block I_{KCa} and calcium currents, so that only the delayed rectifier current was evident in empirical data [45]. Therefore, unlike the calcium activated potassium channel, there was no need to take a difference in current before and after the application of a delayed rectifier specific blocker.

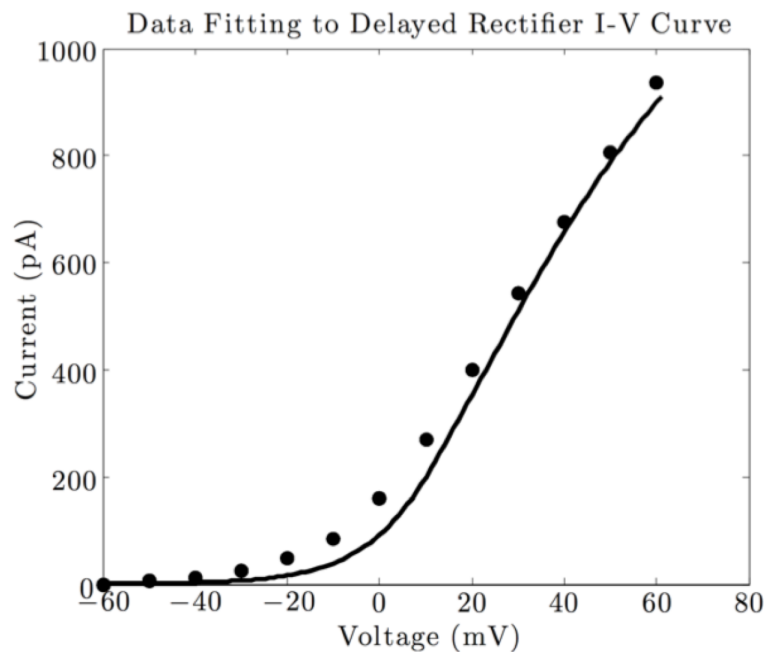


FIGURE 3.3: This model successfully fits the current-voltage curve. In this case, there was no need to take a difference before and after the application of a delayed rectifier specific blocker. The dots and closed line represent measured data and simulated data, respectively.

The initial conditions for states p_0 through p_5 , as well as the activation variables (γ_α , γ_β , θ_α , and θ_β), were derived from the time variant voltage clamp experiments by Li *et al* [45]. The initial conditions for states p_0 through p_5 are shown in Table 3.3.

TABLE 3.3: Initial Conditions of Delayed Rectifier Potassium Channel

State	Initial Condition
p_0	0
p_1	0.36
p_2	0
p_3	0
p_4	0.64
p_5	0

The delayed rectifier potassium model was compared to empirical whole cell patch clamp experiments by Li *et al* to confirm its dynamic behavior (Figure 3.4) [45]. Since high concentrations of EGTA and Cd⁺² were used by this research group to block I_{KCa} and calcium currents, only the delayed rectifier current was evident in empirical data [45]. Therefore, there was no need to measure the difference in current before and after the application of a delayed rectifier specific blocker.

The initial rapid rise over the first 25 ms, as well as the secondary gradual rise were matched. Furthermore, the steady state behavior was mainly reproduced, resulting in a model that successfully fits empirical delayed rectifier potassium channel current data. However, as seen in Figures 3.3 and 3.4, the simulated steady state current was slightly less than the corresponding empirical current for voltage clamps between -30 mV and 10 mV. Potential sources of error are discussed in Section 4.5.1. Furthermore, in Section 4.4, a sensitivity analysis was performed to demonstrate the output cardiomyocyte activity is not highly sensitive to these parameters.

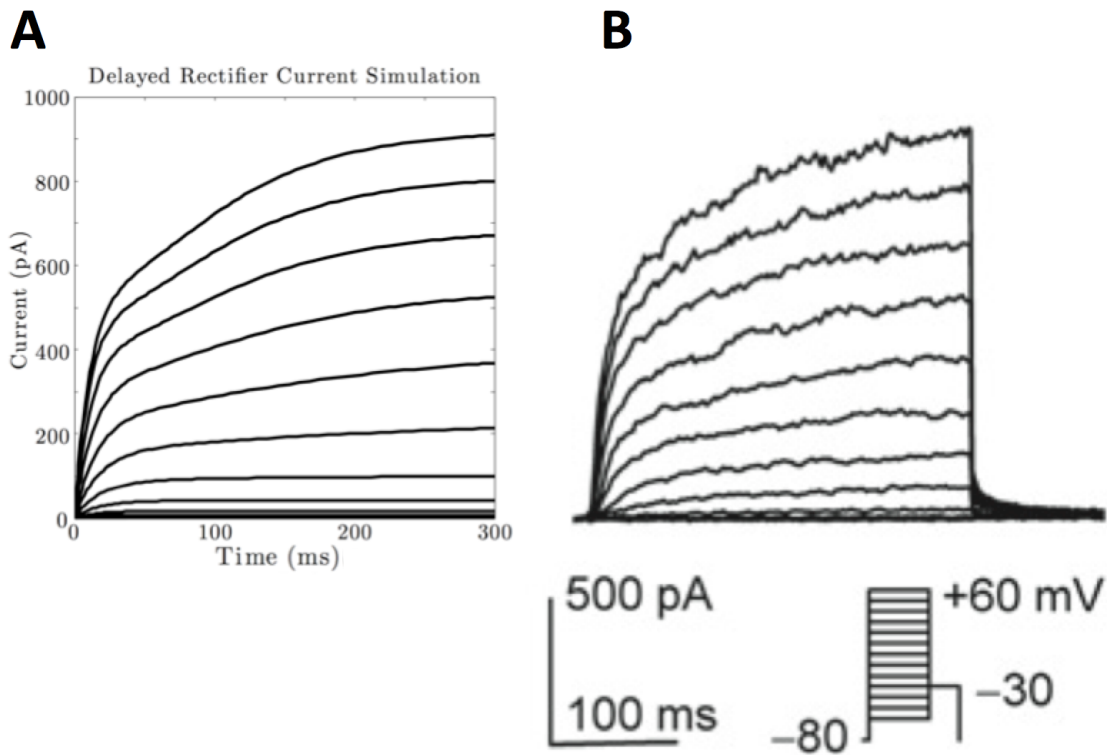


FIGURE 3.4: The model delayed rectifier channel (A) was compared to empirical delayed rectifier potassium current (B) of human mesenchymal stem cells. The model successfully fits the empirical data [45].

3.1.3 Transient Outward Potassium Current

Unlike the delayed rectifier current, the transient outward potassium current was modeled from a non-Markovian approach. Therefore, it was necessary to model the activation variable r , inactivation variable s , and their respective time constants τ_r and τ_s . The maximum conductance, as well as the activation and inactivation variables, were fit to the steady-state activation and inactivation data of human mesenchymal stem cells provided by Li *et al* [45]. Their respective time constants, τ_r and τ_s , were fit to type “B” total mesenchymal stem cell currents for greater accuracy. The resulting formulations were used to fully describe the transient outward potassium current (Table 3.4).

TABLE 3.4: Transient Outward Potassium Channel Formulation

Equations Used to Describe the Transient Outward Potassium Channel

$$I_{to} = 54.0rs(V - E_K)$$

$$\frac{dr}{dt} = \frac{r_\infty - r}{\tau_r}$$

$$\frac{ds}{dt} = \frac{s_\infty - s}{\tau_s}$$

$$r_\infty = \frac{1}{1 + e^{\frac{V - 61.8}{-18.1}}}$$

$$s_\infty = \frac{1}{1 + e^{\frac{V + 42.1}{35.0}}}$$

$$\tau_r = 20.3e^{-\frac{(V+2.9)^2}{138.4}} + 4.4e^{-\frac{(V-80.3)^2}{899.5}} + 2.9$$

$$\tau_s = 8.6e^{-\frac{(V-22.3)^2}{141.5}} + 7.0$$

$$E_K = -87.0 \text{ mV}$$

Similar to the transient outward current of human atrial myocytes and Purkinje fiber cells [106, 107], the transient outward current of mesenchymal stem cells displays both ephemeral and sustained currents [45]. Therefore, to account for both of these currents within the mesenchymal stem cell model, the slope of the inactivation curve was decreased accordingly (Table 3.4).

The ability of this model to fit the steady state current-voltage (I-V) of the transient outward potassium channel is shown in Figure 3.5. The difference between the mesenchymal stem cell current before and after the application of 4-aminopyridine, a selective blocker of the transient outward potassium channel [45], was implemented when generating this current-voltage curve.

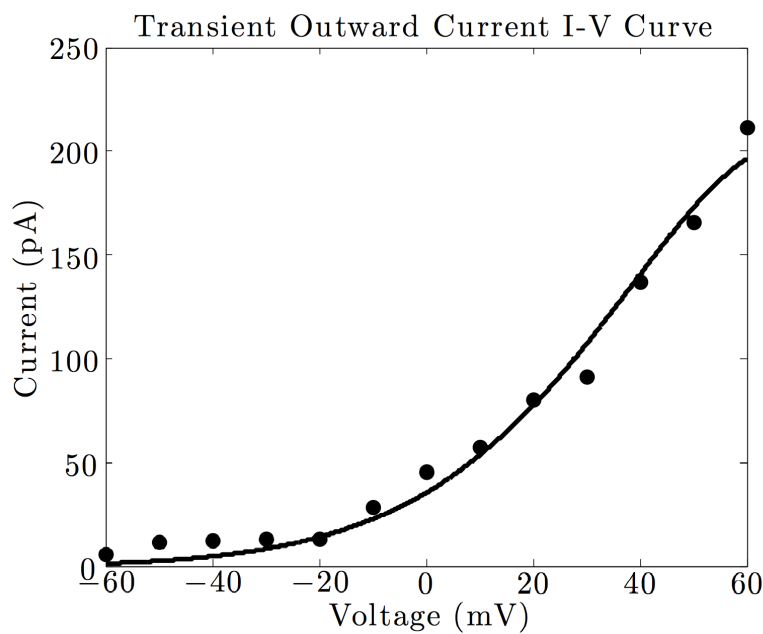


FIGURE 3.5: A comparison between the empirical and simulated transient outward channel current-voltage relationship. The difference between the mesenchymal stem cell current before and after the application of 4-aminopyridine, a selective blocker of the transient outward potassium channel [45], was implemented when generating this current-voltage curve. The dots and closed line represent measured data and simulated data, respectively.

The transient outward potassium channel model was confirmed by comparing its dynamic activity to empirical whole-cell patch clamping experiments by Li *et al* (Figure 3.6) [45]. Specifically, the transient outward potassium channel simulation was compared to the difference between the mesenchymal stem cell current before and after the application of 4-aminopyridine, a selective blocker of the transient outward potassium channel [45]. As shown in Figure 3.6, the model transient outward

potassium channel current successfully fits the empirical data. Furthermore, it fits activation and inactivation kinetics of total current “B”, which is of interest (see Section 3.2.2 for more detail).

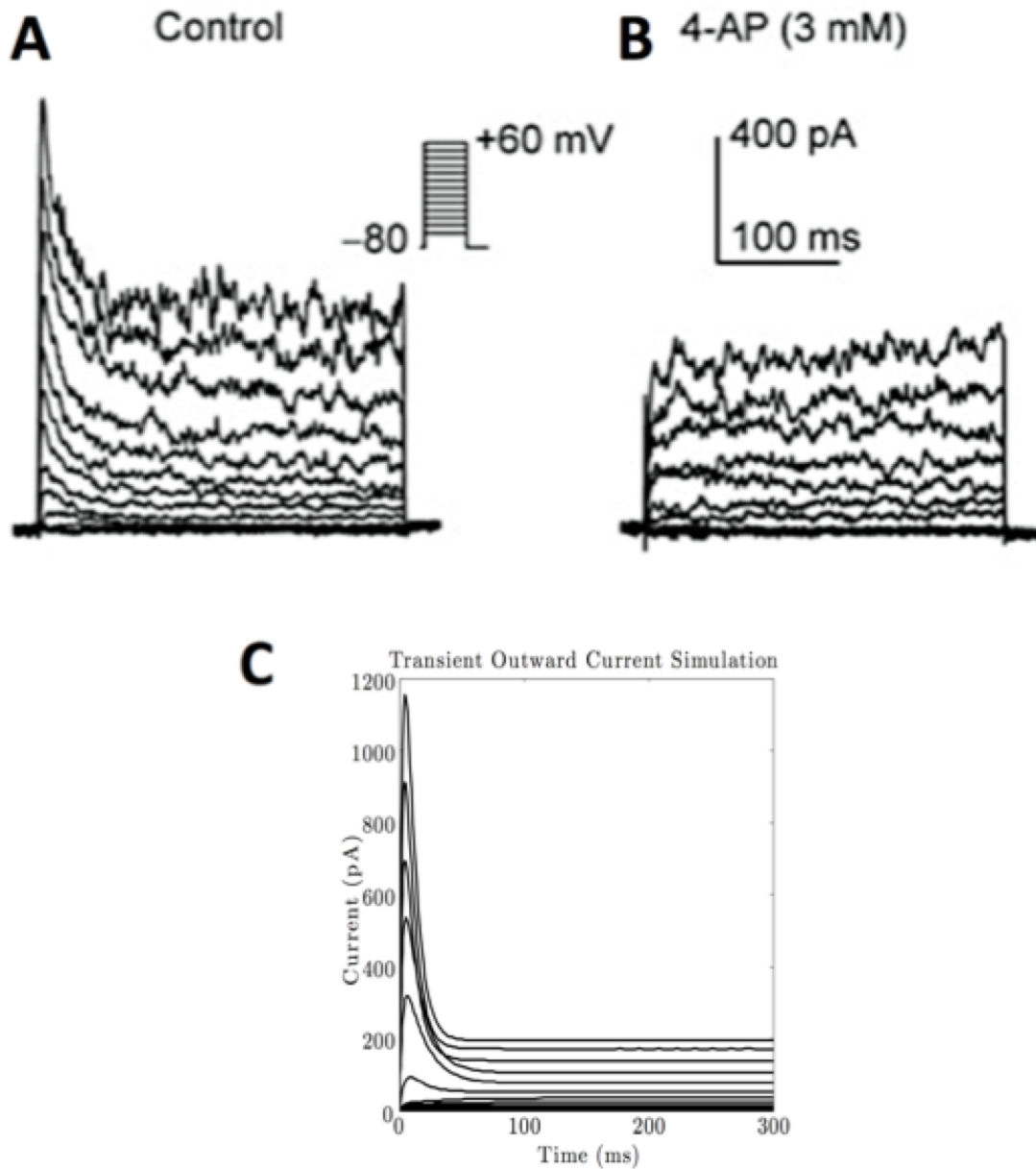


FIGURE 3.6: The transient outward potassium channel simulation (C) was compared to the difference between the mesenchymal stem cell current before (A) and after (B) the application of 4-aminopyridine, a selective blocker of the transient outward potassium channel [45]. The model transient outward potassium channel current successfully fits the empirical data [45].

3.1.4 L-Type Calcium Current

Like the transient outward potassium current, the L-type calcium current was modeled from a non-Markovian approach. Therefore, it was necessary to model the activation variable d , inactivation variable f , and their respective time constants τ_d and τ_f . The activation and inactivation variables, and their respective time constants, were fit to the peak current data, as a function of voltage, of human mesenchymal stem cell L-type calcium channels provided by Li *et al* [45]. The resulting formulations were used to describe the L-type calcium current (Table 3.5).

TABLE 3.5: L-type Calcium Channel Formulation

Equations Used to Describe the L-type Calcium Channel

$$I_{CaL} = 0.01df4 \frac{VF^2}{RT} \frac{[Ca_i^{+2}]e^{2VF/RT} - 0.341[Ca_o^{+2}]}{e^{2VF/RT} - 1}$$

$$\frac{dd}{dt} = \frac{d_\infty - d}{\tau_d}$$

$$\frac{df}{dt} = \frac{f_\infty - f}{\tau_f}$$

$$d_\infty = \frac{1}{1 + e^{\frac{V + 8.8}{-3.8}}}$$

$$f_\infty = \frac{1}{1 + e^{\frac{V + 38.1}{1.0}}}$$

$$\tau_d = \frac{6.3}{1 + e^{\frac{V - 12.6}{-120}}} + 1.2$$

$$\tau_f = \frac{11.0}{1 + e^{\frac{V - 10.1}{-120}}} + 4.2$$

$$E_{Ca} = 132.2 \text{ mV}$$

The ability of this model to fit the peak magnitude current-voltage relationship of the L-type calcium channel is shown in Figure 3.7. The difference between the mesenchymal stem cell current before and after the application of nifedipine, a selective blocker of the L-type calcium channel [45], was implemented when generating this current-voltage curve.

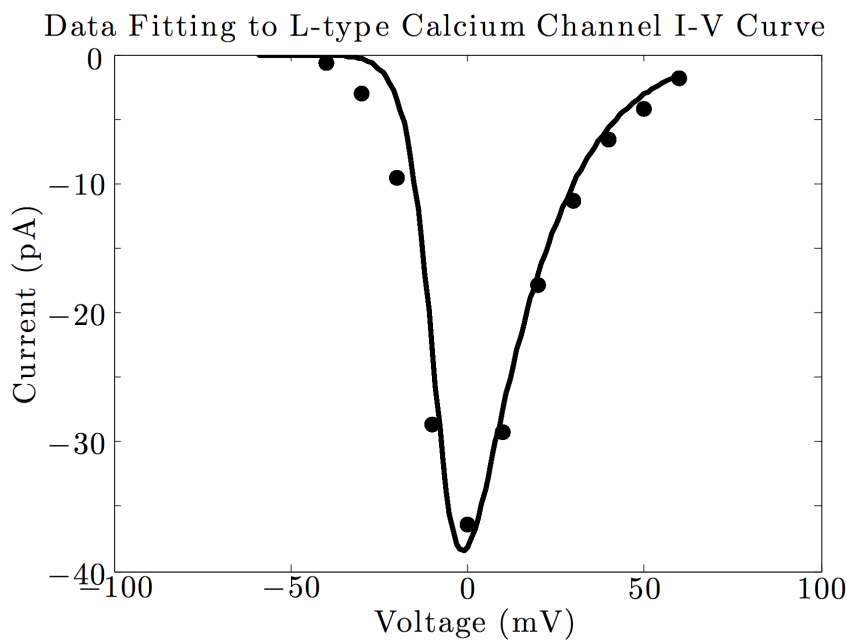


FIGURE 3.7: A comparison between the empirical and simulated L-type calcium channel current-voltage relationship. The dots and closed line represent measured data and simulated data, respectively.

The model was confirmed by comparing its dynamic behavior to the empirical whole-cell patch clamping experiments by Li *et al* (Figure 3.8) [45]. Specifically, the L-type calcium channel simulation was compared to the difference between the mesenchymal stem cell current before and after the application of the selective blocker of the L-type calcium channel [45]. As shown in Figure 3.8, the model L-type calcium channel current successfully fits the empirical data.

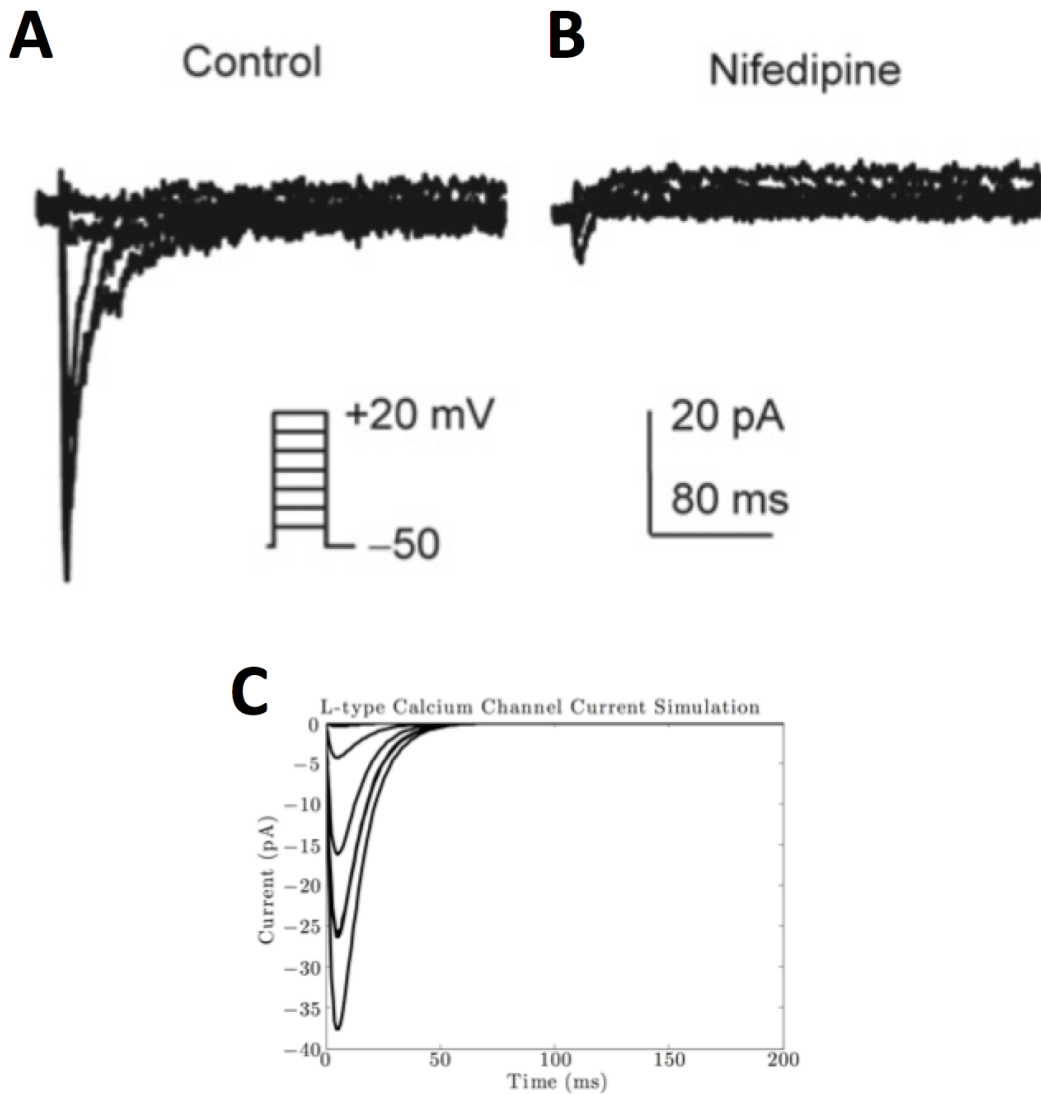


FIGURE 3.8: The L-type calcium channel simulation (C) was compared to the difference between the mesenchymal stem cell current before (A) and after (B) the application of nifedipine, a selective blocker of the L-type calcium channel [45]. The model L-type calcium channel current successfully fits the empirical data [45].

3.1.5 TTX-Sensitive Sodium Current

The sodium current was modeled from a non-Markovian approach. Therefore, it was necessary to model the activation variable m , inactivation variable h , and their

respective time constants τ_m and τ_h . The activation and inactivation variables, and their respective time constants, were fit to the peak current magnitude data (as a function of voltage) of human mesenchymal stem cell sodium channels provided by Li *et al* [45]. The resulting formulations were used to fully describe the sodium current (Table 3.6).

TABLE 3.6: Sodium Channel Formulation

Equations Used to Describe the Sodium Channel

$$I_{Na} = 7.7m^3h(V - E_{Na})$$

$$\frac{dm}{dt} = \frac{f_\infty - m}{\tau_m}$$

$$\frac{dh}{dt} = \frac{f_\infty - h}{\tau_h}$$

$$m_\infty = \frac{1}{(1+e^{\frac{V+55.0}{-10.9}})^2}$$

$$h_\infty = \frac{1}{(1+e^{\frac{V+80.0}{18.6}})^2}$$

$$\tau_m = 1.2 - 0.4e^{-\frac{(V-15.1)^2}{19.6}}$$

$$\tau_h = 2.1e^{-\frac{(V+12.0)^2}{18.8}} + 8.7e^{-\frac{(V-89.3)^2}{53.6}} + 1.2$$

$$E_{Na} = 89.0 \text{ mV}$$

The ability of this model to fit the peak magnitude current-voltage relationship of the sodium channel is shown in Figure 3.9. The difference between the mesenchymal stem cell current before and after the application of tetrodotoxin, a selective blocker of the sodium channel [45], was implemented when generating this current-voltage curve.

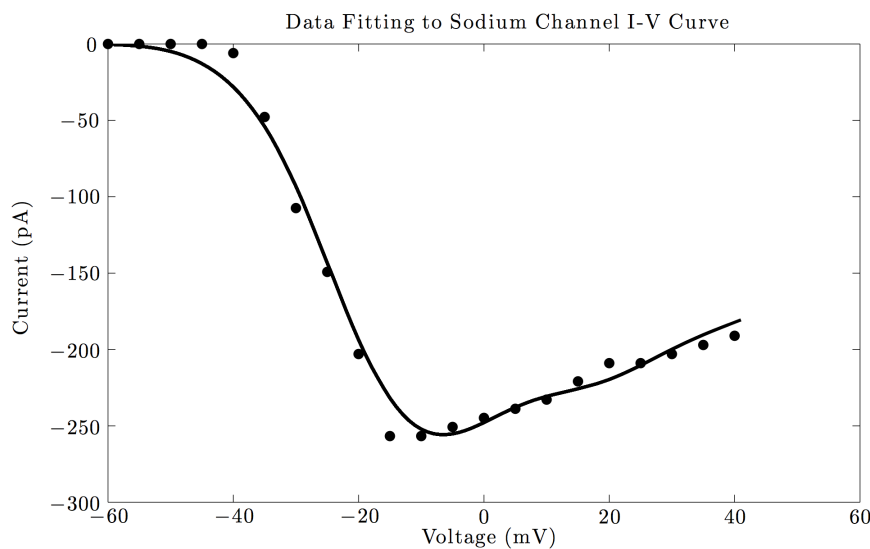


FIGURE 3.9: A comparison between the empirical and simulated sodium channel current-voltage relationship. The dots and closed line represent measured data and simulated data, respectively.

This model was confirmed by comparing its current magnitude and dynamic behavior to empirical whole-cell patch clamping experiments by Li *et al* (Figure 3.10) [45]. Specifically, the sodium channel simulation was compared to the difference between the mesenchymal stem cell current before and after the application of the selective blocker of the sodium channel [45]. As shown in Figure 3.10, the model sodium channel current successfully fits the empirical data.

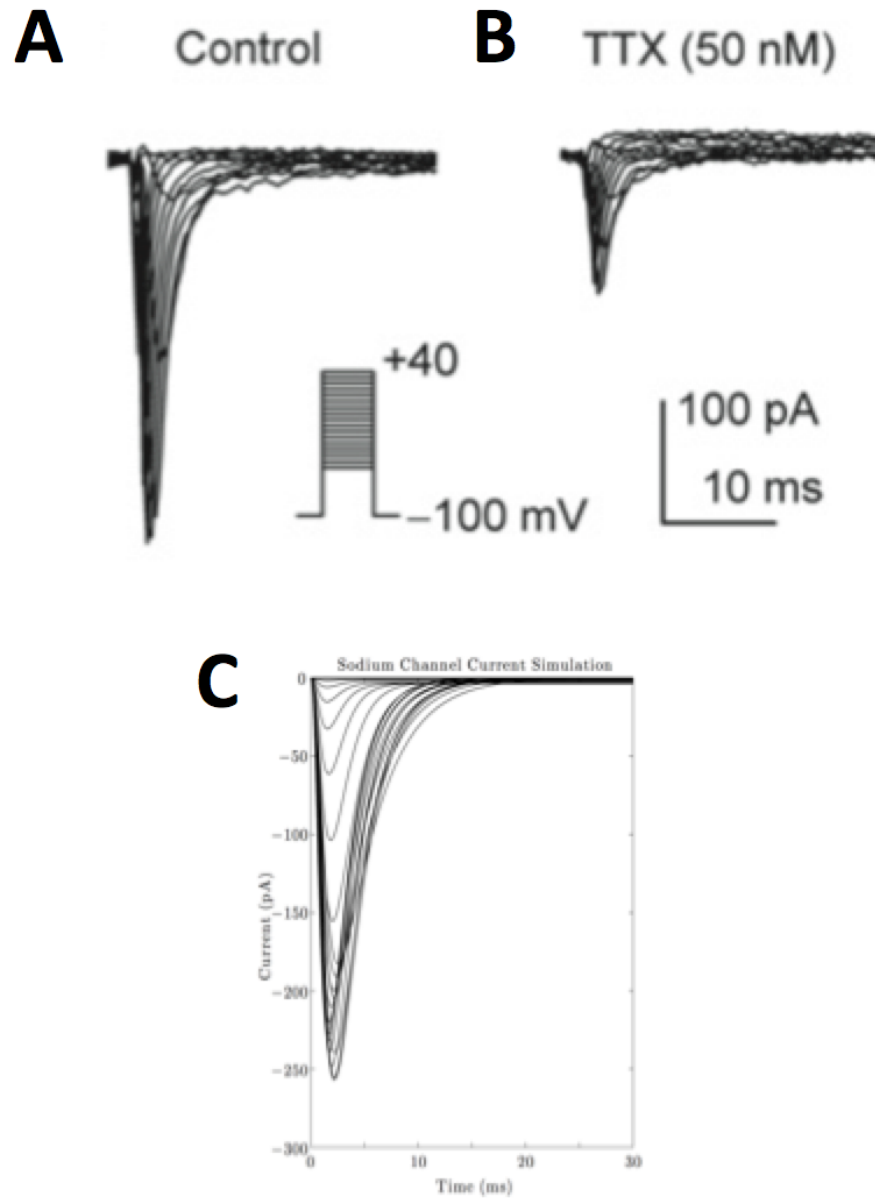


FIGURE 3.10: The sodium channel simulation (C) was compared to the difference between the mesenchymal stem cell current before (A) and after (B) the application of tetrodotoxin, a selective blocker of the sodium channel [45]. The model sodium channel current successfully fits the empirical data [45].

3.1.6 Leakage Current

The leakage current for total currents “A”, “B”, and “C” were modeled in order to have a mesenchymal stem cell resting membrane potential between -42 mV and -12 mV [45]. The resulting leakage channel formulations are shown in Table 3.7.

TABLE 3.7: Leakage Channel Formulation

Equations Used to Describe the Leakage Channel

$$I_{La} = 0.3(V - E_{Ca})$$

$$I_{Lb} = 0.03(V - E_{Ca})$$

$$I_{Lc} = 0.3(V - E_{Ca})$$

$$E_{Ca} = 132.2 \text{ mV}$$

To confirm the resting membrane potentials were between -42 mV and -12 mV, a short stimulus current was applied for each type of total current. As expected, the membrane potential increased from this stimulus current, and then approached a steady-state resting membrane potential. As shown in Figure 3.11, the resting membrane potential was within the expected range for each type of total current. The influx of sodium and calcium for total current “C” resulted in the greatest voltage spike, as expected.

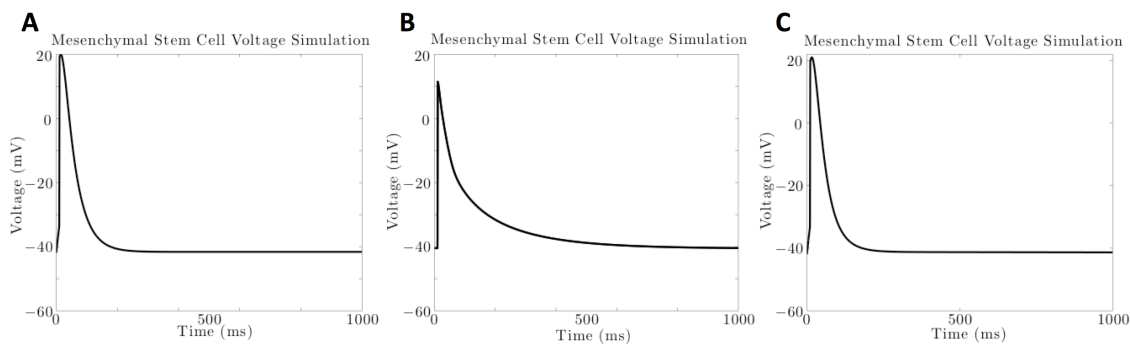


FIGURE 3.11: To confirm the resting membrane potentials were between -42 mV and -12 mV, a short stimulus current was applied for: (A) total current “A”; (B) total current “B”; and (C) total current “C”. As expected, the membrane potential increased from this stimulus current, and then approached a steady-state resting membrane potential. The resting membrane potential was within the expected range.

3.2 Simulation of Human Mesenchymal Stem Cell Total Currents

In the previous section, the Levenberg Marquardt algorithm was applied to fit empirical data of each type of functional ion channel in human mesenchymal stem cells. The resulting formulation for each type of channel was then confirmed by only simulating that individual type of ion channel, and comparing it to empirical behavior.

In this section, a comprehensive confirmation of the human mesenchymal models is made. To do so, the total currents “A”, “B”, and “C” are simulated and compared to empirical results. By confirming the total currents, it would subsequently be possible to model the interactions between mesenchymal stem cells and cardiomyocytes, the main focus of this study.

3.2.1 Type A Total Current

The calcium activated potassium, delayed rectifier potassium, and leakage currents are functional in total current “A” (Table 2.1). A comparison between the simulated and empirical total current “A” is shown in Figure 3.12. The simulated total current “A” has a longer rise time than the empirical total current; however, this model was still accepted because the activation characteristics of the delayed rectifier potassium channel are highly variable [45], which could account for the difference between the empirical and simulation results. Furthermore, the cardiomyocyte action potential

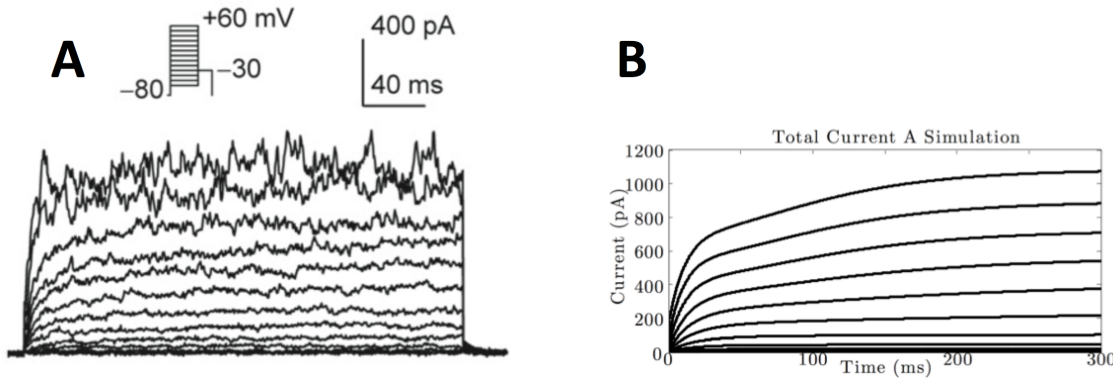


FIGURE 3.12: The empirical total current “A” (A) was compared to the simulated total current “A” (B). The simulated total current “A” has a longer rise time than the empirical total current. However, this was accepted, as the activation characteristics of the delayed rectifier potassium channel are highly variable [45].

is moderately insensitive to variations in this rise time when coupled with type “A” mesenchymal stem cells (see Section 4.4 for more detail).

3.2.2 Type B Total Current

The transient outward potassium, calcium activated potassium, and leakage currents are functional in total current “B” (Table 2.1). A comparison between the simulated and empirical total current “B” is shown in Figure 3.13. As seen, the simulated total current “B” successfully reproduces the empirical result. This implies that the transient outward potassium channel activation and inactivation time constants from Section 3.1.3 are indeed suitable for this model. Furthermore, the sustained current shown by the individual transient outward current (Section 3.1.3) was also evident in total current “B”, which implies it was fitting and necessary to decrease the slope of the inactivation curve.

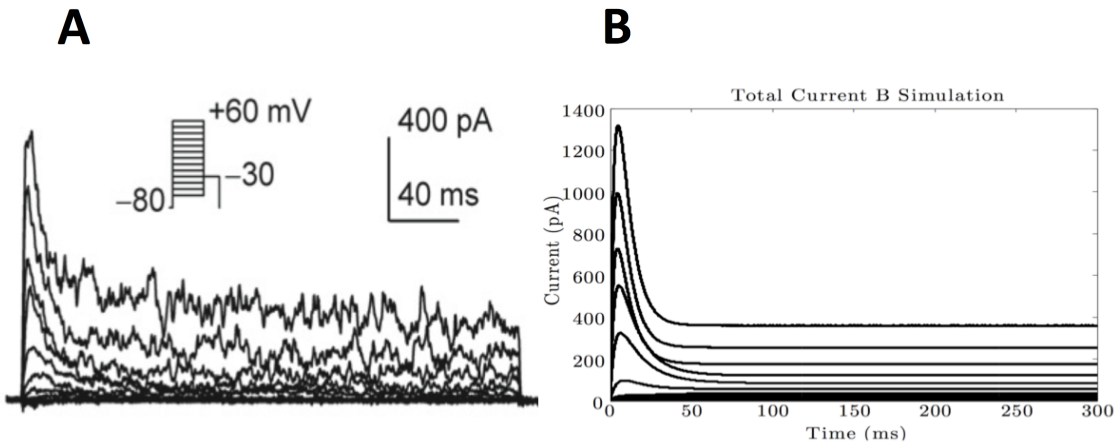


FIGURE 3.13: The empirical total current “B” (A) was compared to the simulated total current “B” (B). The simulated total current “B” successfully reproduces the empirical result. Therefore, it was accepted.

3.2.3 Type C Total Current

The sodium, L-type calcium, delayed rectifier, calcium activating potassium, and leakage currents are functional in total current “C” (Table 2.1). A comparison between the simulated and empirical total current “C” is shown in Figure 3.14.

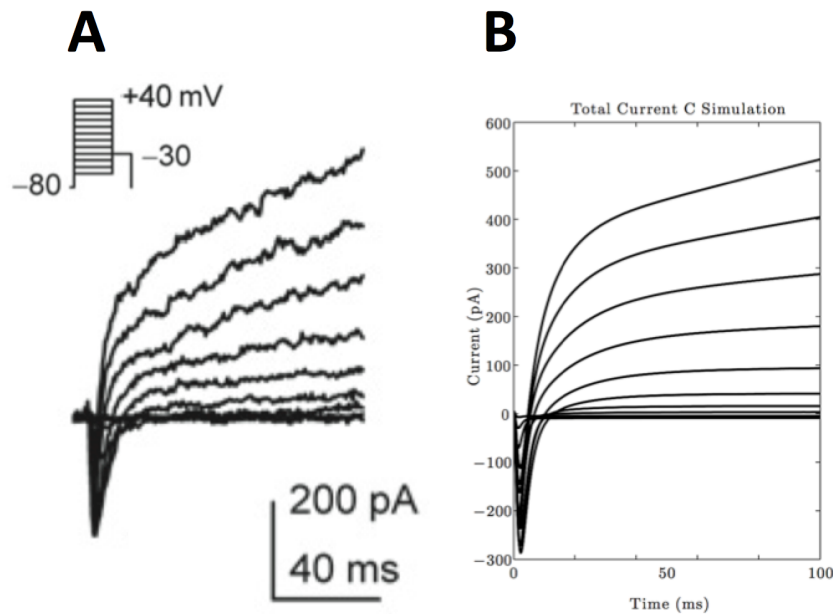


FIGURE 3.14: The empirical total current “C” (A) was compared to the simulated total current “C” (B).

As seen, the empirical delayed rectifier potassium channel activation time constant does indeed vary from cell-to-cell, which contributes to slight inaccuracies evident within the delayed rectifier potassium channel model. The total current “C” model fits the rapid inward sodium and calcium currents, as well as the outward potassium currents.

Overall, the general behavior of total currents “A”, “B”, and “C” were modeled successfully. Therefore, they were each coupled with the cardiomyocytes to develop insight into the electrical interactions between these two cell types. Specifically, the effects on the cardiomyocyte’s ion channel activity, action potential duration (APD), and conduction velocity were examined. Each of these characteristics offer insight into how electrically beneficial or harmful mesenchymal stem cells can be.

3.3 Simulation of Human Mesenchymal Stem Cell-Cardiomyocyte Coupling

Since each type of total current was confirmed, it is now possible to examine the electrical interaction between mesenchymal stem cells and cardiomyocytes. Cardiomyocytes action potentials were coupled with total currents “A”, “B”, and “C” in ratios of 9:1, 4:1, and 1:1, respectively, to develop novel insight into the electrical interactions between these cell types. This was accomplished by implementing Equations 2.49 and 2.50 to the ten Tusscher cardiomyocyte model and the novel mesenchymal stem cell models.

3.3.1 Type A Total Current

First, the ten Tusscher cardiomyocyte model was coupled with the novel type “A” mesenchymal stem cell model in ratios of 9:1, 4:1, and 1:1, respectively. The resulting

cardiomyocyte action potential behavior is shown below in Figure 3.15.

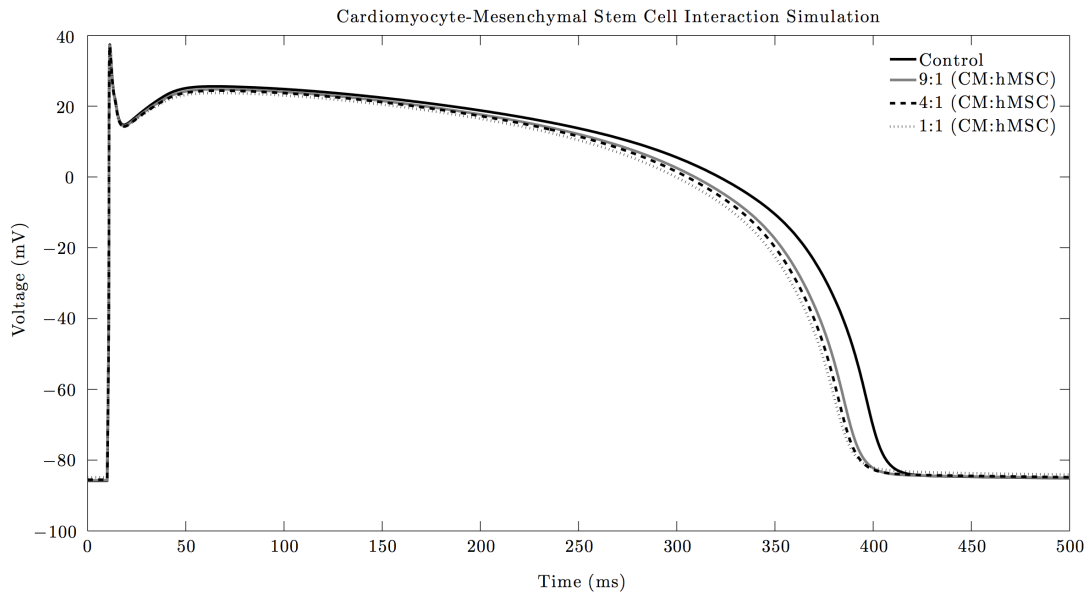


FIGURE 3.15: The ten Tusscher cardiomyocyte model was coupled with the novel type “A” mesenchymal stem cell model in ratios of 9:1, 4:1, and 1:1, respectively. As the percentage of mesenchymal stem cells increased, the action potential decreased.

As shown in Figure 3.15, there were very few effects on phases 0, 1, and 4 of the cardiac action potential. The rapid depolarization phase, the plateau phase, and the resting membrane potential phase (phases 0, 1 and 4, respectively) overlap for the varying ratios of cardiomyocytes to mesenchymal stem cells, implying there were minimal effects. However, mesenchymal stem cells affect the plateau phase and the repolarization phase (phases 2 and 3, respectively) of the cardiac action potential. As shown in Figure 3.15, as the percentage of mesenchymal stem cells increased from 10% to 50%, the action potential duration decreased. The duration for the action potential to repolarization 50% and 90% (APD_{50} and APD_{90} , respectively) was measured for these varying ratios of mesenchymal stem cells and cardiomyocytes (Table 3.8).

TABLE 3.8: Effects of Mesenchymal Stem Cell “A” on Action Potential Duration

CM : hMSC	APD ₅₀ (ms)	APD ₉₀ (ms)
1 : 0	361	392
9 : 1	349	380
4 : 1	345	378
1 : 1	342	376

As shown in the table above, both the duration for the action potential to repolarization 50% and 90% (APD₅₀ and APD₉₀) decreased, which shows phases 2 and 3 of the action potential were indeed affected by mesenchymal stem cell interaction. To better understand why the action potential duration was decreased, the cardiomyocyte ionic channels were examined (Figure 3.16).

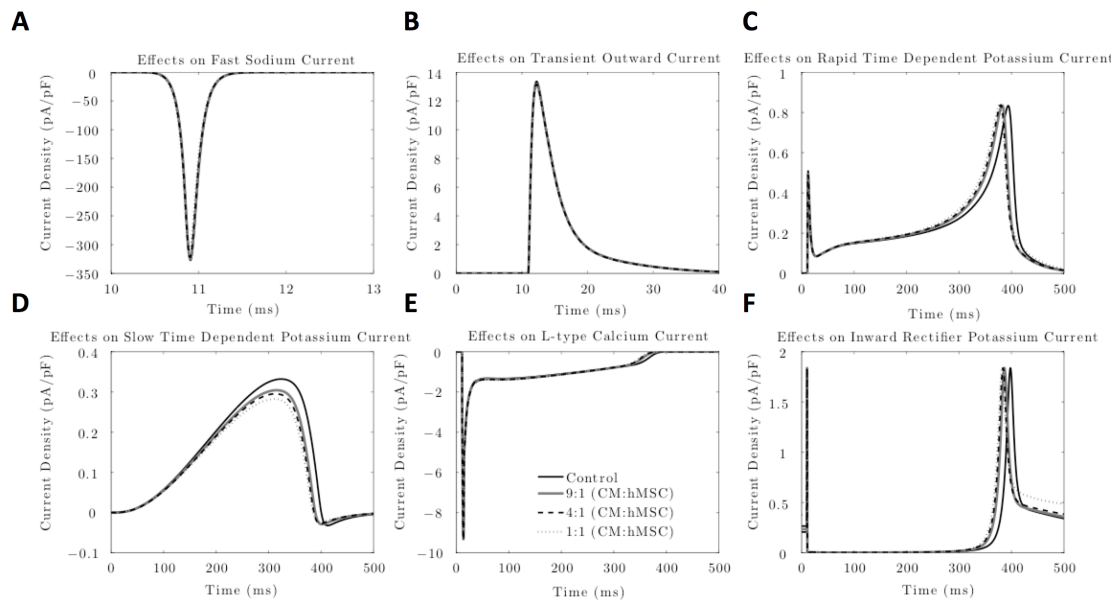


FIGURE 3.16: To better understand why the action potential duration was decreased, the cardiomyocyte: A) fast sodium; B) transient outward; C) rapid delayed rectifier potassium; D) slow delayed rectifier potassium; E) L-type calcium; and F) inward rectifier potassium currents were examined.

The cardiomyocyte ionic channel activity corresponds with the effects apparent in the overall cardiomyocyte action potential. As shown in Figures 3.16A and B, there were minimal effects on the fast sodium current and the transient outward current, which correspond to little variation in phases 0 and 1. However, there were noticeable effects on the rapid delayed rectifier channel (Figure 3.16C), the slow delayed rectifier channel (Figure 3.16D), the L-type calcium channel (Figure 3.16E), and the inward rectifier channel (Figure 3.16F). Specifically, the amplitude and duration of each of these currents decreased, which correspond with decreases in phases 2 and 3 of the cardiac action potential.

The effects of the cardiomyocytes on the human mesenchymal stem cell were also considered, as the electrical effects on the mesenchymal stem cells may give insight on functional differences of these pluripotent cells. These electrical effects are shown below (Figure 3.17).

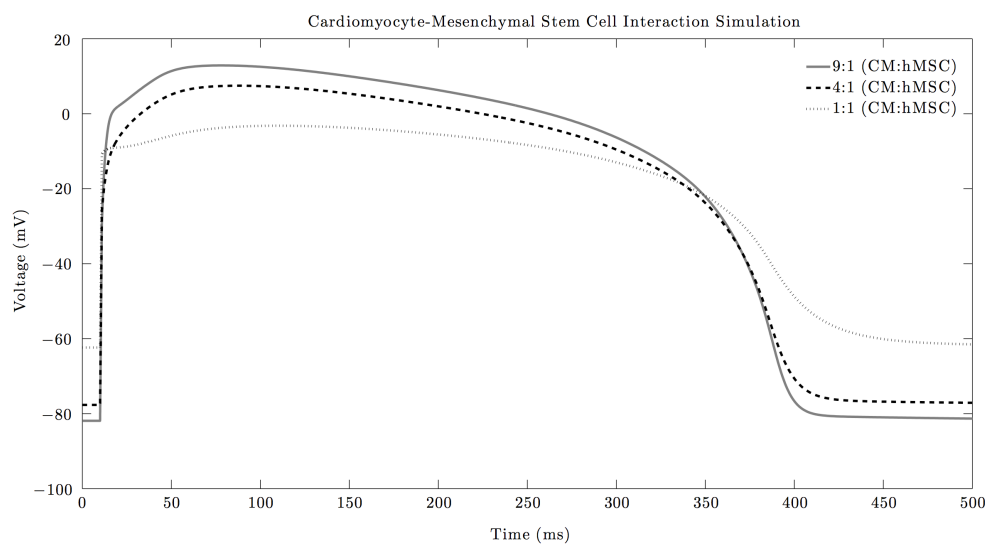


FIGURE 3.17: To develop insight into functional differences of pluripotent cells as a result of cardiomyocyte-mesenchymal stem cell coupling, the effects of the cardiomyocytes on the human mesenchymal stem cell were also considered. The mesenchymal stem cell is greatly influenced by cardiomyocyte behavior, as it approaches the general cardiac action potential behavior.

As shown in Figure 3.17, the mesenchymal stem cell is greatly influenced by cardiomyocyte behavior. As the ratio of cardiomyocytes to mesenchymal stem cells increases, the mesenchymal stem cell electrical activity approaches the cardiomyocyte action potential. This behavior is typical of non-excitible cells, where it acts as an electrical sink to the excitable source during an action potential [83].

To understand how mesenchymal stem cells are influenced by the cardiomyocytes, the mesenchymal stem cell gap junction current was examined (Figure 3.18).

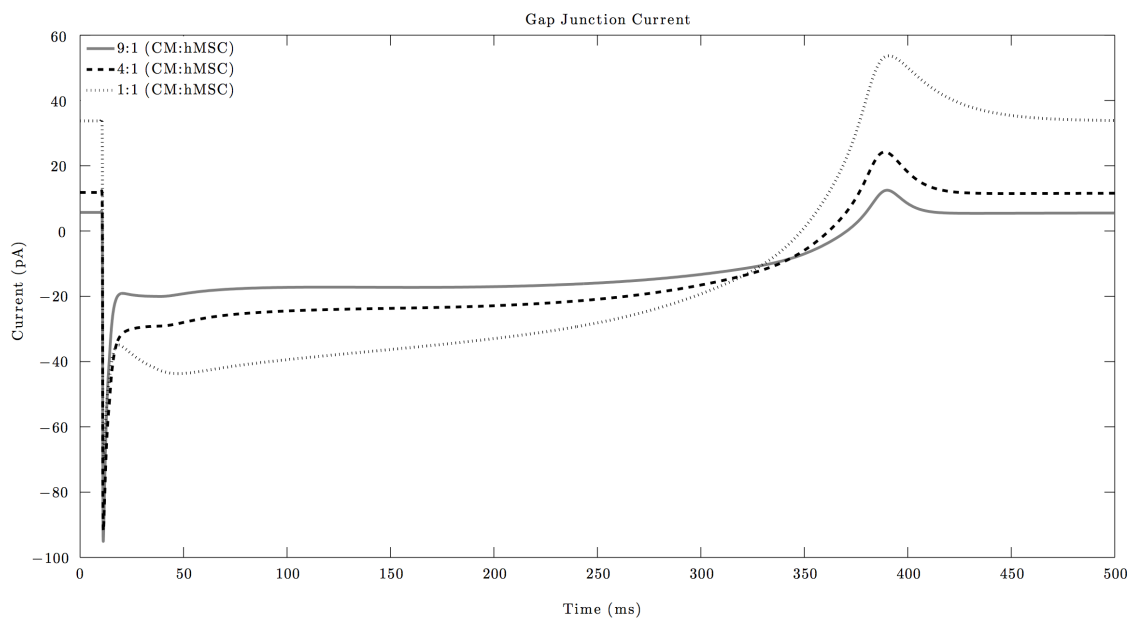


FIGURE 3.18: The mesenchymal stem cell gap junction current was examined to better understand how mesenchymal stem cells are influenced by the cardiomyocytes. The gap junction current displayed the general trends of the action potential phases, confirming the influence of the cardiomyocytes on mesenchymal stem cells. The magnitude of the current decreased as the ratio of cardiomyocytes to mesenchymal stem cells increased.

As shown above, a large influx occurred at 10 ms, as a result of the depolarization of the cardiomyocyte. This subsequently increased the voltage of the mesenchymal stem cell at 10 ms, as seen in Figure 3.17. The general trends of the action potential phases 1, 2, 3, and 4 were subsequently seen, confirming the influence of

the cardiomyocytes on mesenchymal stem cells. As the ratio of cardiomyocytes to mesenchymal stem cells increased, the magnitude of the current decreased. This is because each cardiomyocyte electrical source needed to contribute less in order for the mesenchymal stem cell to approach the cardiomyocyte electrical activity. Both positive and negative currents were evident, showing that the mesenchymal stem cell acts as a sink during phases 0 through 3 of the action potential, and a source during phase 4 of the action potential.

Finally, the activation threshold to produce a cardiomyocyte action potential was measured with and without supplementation of mesenchymal stem cells. The stimulus current was normalized to the minimum necessary pulse to create an action potential without any mesenchymal stem cells (the control condition). The effects of supplying mesenchymal stem cells are shown in Table 3.9

TABLE 3.9: Effects of Mesenchymal Stem Cell “A” on Activation Threshold

CM : hMSC	Normalized Stimulus Current (pA/pA)	Percent Change
1 : 0	1	—
9 : 1	0.99	-1
4 : 1	0.98	-2
1 : 1	0.95	-5

As expected, the activation threshold decreased with mesenchymal stem cell supplementation, as the resting membrane potential of mesenchymal stem cells (-42 to -12 mV) is less than the resting membrane potential of cardiomyocytes (-85 mV). As the percentage of mesenchymal stem cells increased, the minimum required stimulus

current decreased. The activation threshold decreased by as much as 5% when there was a 1:1 ratio of mesenchymal stem cells to cardiomyocytes.

Overall, the supplementation of mesenchymal stem cells decreased the action potential duration (APD_{50} and APD_{90}), and the activation threshold of a cardiomyocyte action potential.

3.3.2 Type B Total Current

Next, the ten Tusscher cardiomyocyte model was coupled with the novel type “B” mesenchymal stem cell model in ratios of 9:1, 4:1, and 1:1, respectively. The resulting cardiomyocyte action potential behavior is shown below in Figure 3.19.

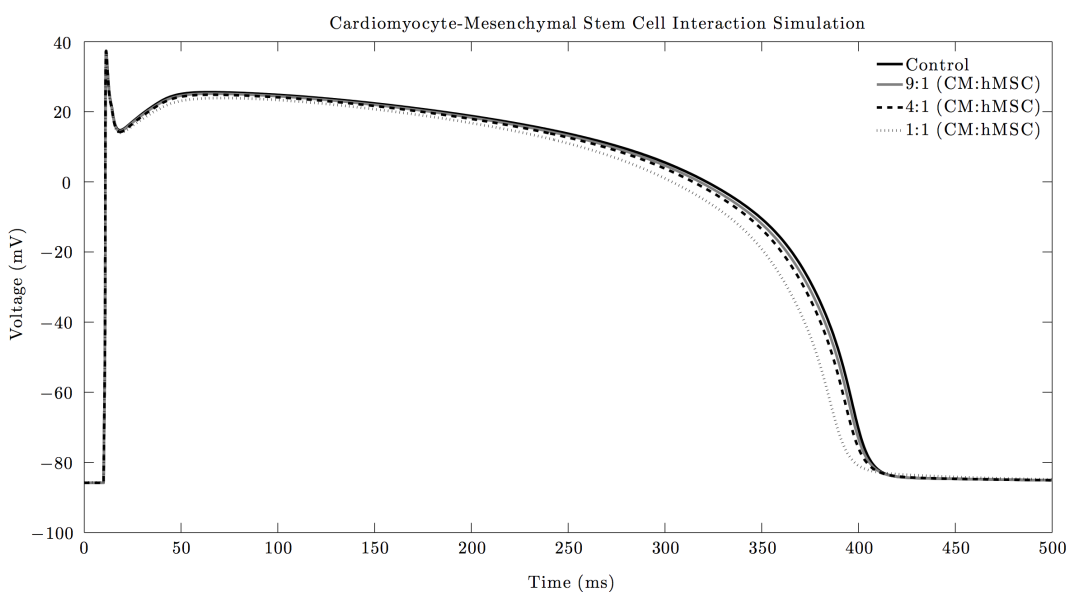


FIGURE 3.19: The ten Tusscher cardiomyocyte model was coupled with the novel type “B” mesenchymal stem cell model in ratios of 9:1, 4:1, and 1:1, respectively. As the percentage of mesenchymal stem cells increased, the action potential decreased.

As shown in Figure 3.19, a similar effect was made by mesenchymal stem cells types “A” and “B”. For example, there were very few effects on phases 0, 1, and 4 of

the cardiac action potential. The rapid depolarization phase, the plateau phase, and the resting membrane potential phase (phases 0, 1 and 4, respectively) overlap for the varying ratios of cardiomyocytes to mesenchymal stem cells, implying there were minimal effects.

Furthermore, type “B” mesenchymal stem cells affect phases 2 and 3 of the cardiac action potential. As shown in Figure 3.19, as the percentage of mesenchymal stem cells increased from 10% to 50%, the action potential decreased. The duration for the action potential to repolarization 50% and 90% (APD_{50} and APD_{90} , respectively) was measured for these varying ratios of mesenchymal stem cells and cardiomyocytes (Table 3.10).

TABLE 3.10: Effects of Mesenchymal Stem Cell “B” on Action Potential Duration

CM : hMSC	APD_{50} (ms)	APD_{90} (ms)
1 : 0	361	392
9 : 1	358	390
4 : 1	355	388
1 : 1	346	381

As shown in the table above, both the duration for the action potential to repolarization 50% and 90% (APD_{50} and APD_{90}) decreased, which shows phases 2 and 3 of the action potential were affected by mesenchymal stem cell interaction. However, APD_{50} and APD_{90} decreased less with type “B” mesenchymal stem cells than with type “A” mesenchymal stem cells. To better understand why the action potential

duration was decreased, the cardiomyocyte ionic channels were examined (Figure 3.20).

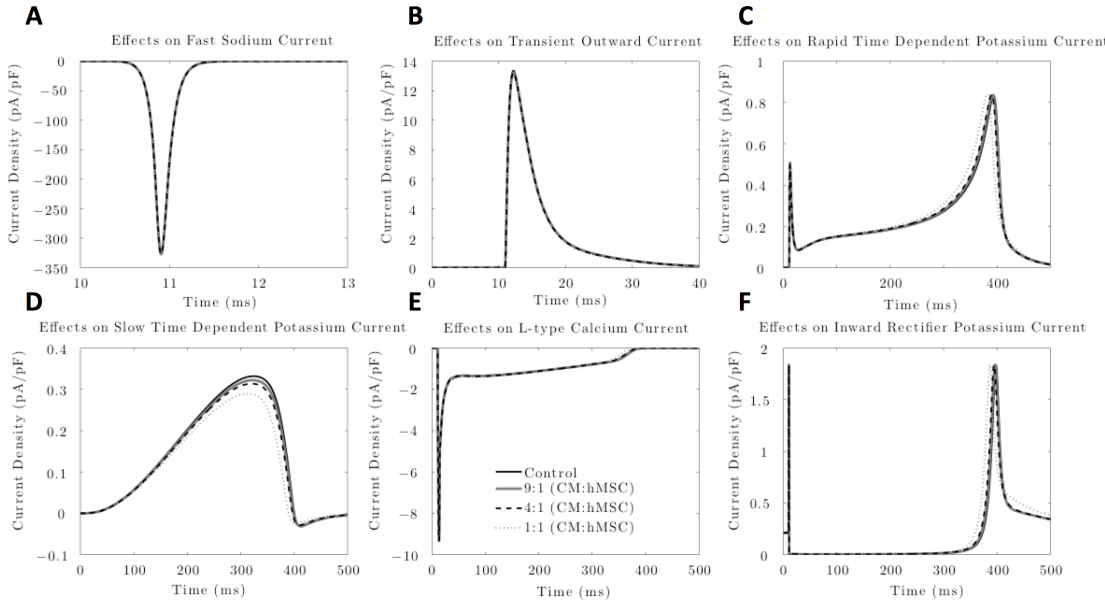


FIGURE 3.20: To better understand why the action potential duration was decreased, the cardiomyocyte: A) fast sodium; B) transient outward; C) rapid delayed rectifier potassium; D) slow delayed rectifier potassium; E) L-type calcium; and F) inward rectifier potassium currents were examined.

The cardiomyocyte ionic channel activity corresponds with the effects apparent in the overall cardiomyocyte action potential. As shown in Figures 3.20A and B, there were minimal effects on the fast sodium current and the transient outward current, which correspond to little variation in phases 0 and 1. Furthermore, there were noticeable effects on the rapid delayed rectifier channel (Figure 3.20C), the slow delayed rectifier channel (Figure 3.20D), and the inward rectifier channel (Figure 3.20F). Specifically, the amplitude and duration of each of these currents decreased, which correspond with decreases in phases 2 and 3 of the cardiac action potential. However, as expected, the amplitude and duration of each of these currents decreased

less with type “B” mesenchymal stem cells than with type “A” mesenchymal stem cells.

The effects of the cardiomyocytes on the human mesenchymal stem cell were also considered, as the electrical effects on the mesenchymal stem cells may give insight on functional differences of these pluripotent cells. These electrical effects are shown below (Figure 3.21).

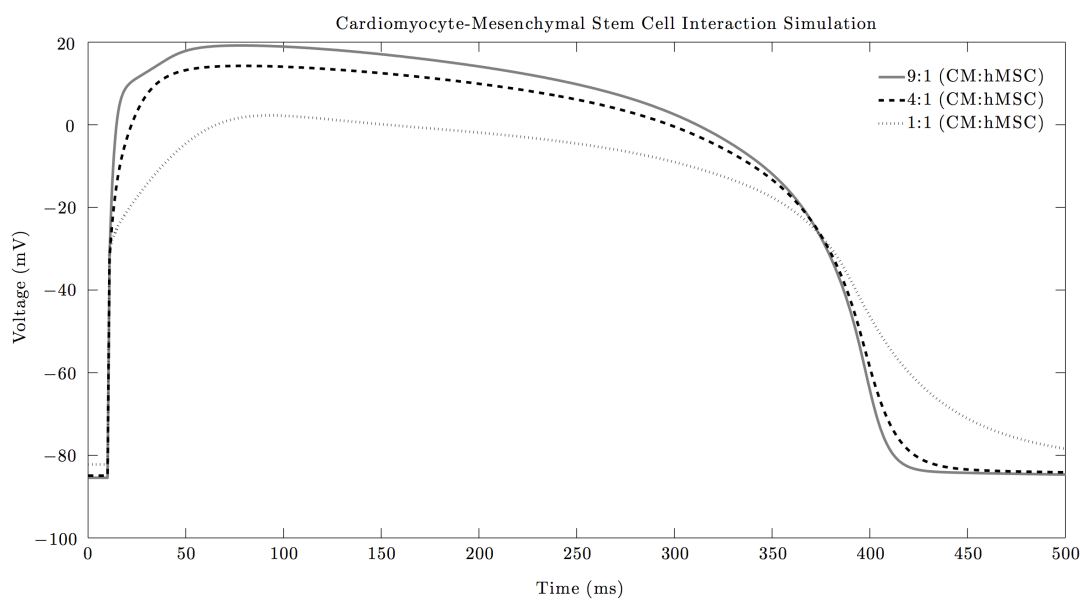


FIGURE 3.21: To develop insight into functional differences of pluripotent cells as a result of cardiomyocyte-mesenchymal stem cell coupling, the effects of the cardiomyocytes on the human mesenchymal stem cell were also considered. The mesenchymal stem cell is greatly influenced by cardiomyocyte behavior, as it approaches the general cardiac action potential behavior.

As shown in Figure 3.21, just like the type “A” mesenchymal stem cell, the type “B” mesenchymal stem cell is greatly influenced by cardiomyocyte behavior. As the ratio of cardiomyocytes to mesenchymal stem cells increases, the mesenchymal stem cell electrical activity approaches the cardiomyocyte action potential. This behavior is typical of non-excitable cells, where it inherits the excitable cell’s activity.

To understand how mesenchymal stem cells are influenced by the cardiomyocytes, the mesenchymal stem cell gap junction current was examined (Figure 3.22).

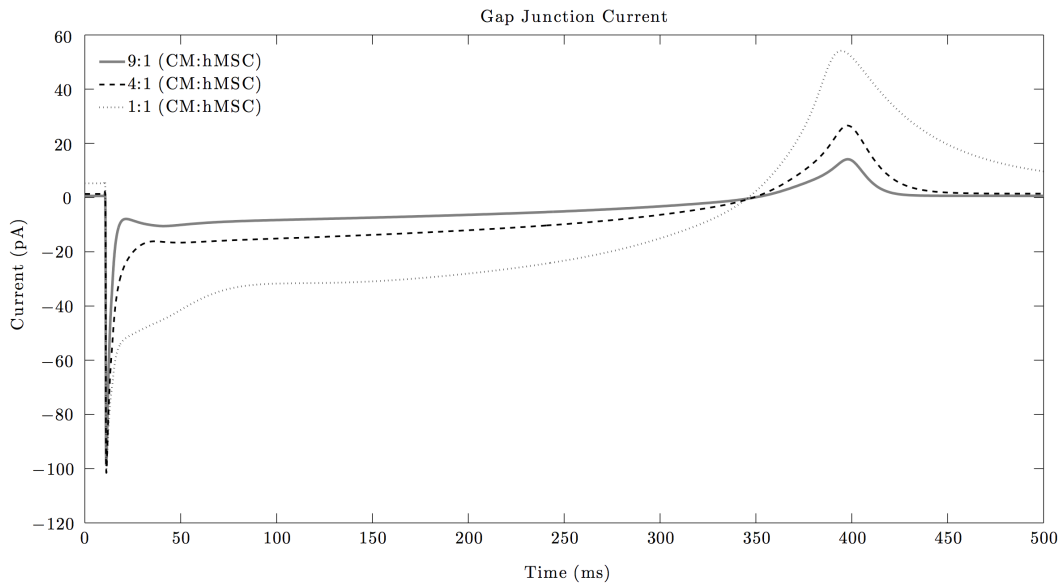


FIGURE 3.22: The mesenchymal stem cell gap junction current was examined to better understand how mesenchymal stem cells are influenced by the cardiomyocytes. The gap junction current displayed the general trends of the action potential phases, confirming the influence of the cardiomyocytes on mesenchymal stem cells. The magnitude of the current decreased as the ratio of cardiomyocytes to mesenchymal stem cells increased.

As shown above, a large influx occurred at 10 ms, as a result of the depolarization of the cardiomyocyte. This subsequently increased the voltage of the mesenchymal stem cell at 10 ms, as seen in Figure 3.21. The general trends of the action potential phases 1, 2, 3, and 4 were subsequently seen, confirming the influence of the cardiomyocytes on mesenchymal stem cells. As the ratio of cardiomyocytes to mesenchymal stem cells increased, the magnitude of the current decreased. This is because each cardiomyocyte needed to contribute less in order for the mesenchymal stem cell to approach the cardiomyocyte electrical activity. Both positive and negative currents were evident, showing that the mesenchymal stem cell acts as a sink

during phases 0 through 3 of the action potential, and a source during phase 4 of the action potential.

Finally, the activation threshold to produce a cardiomyocyte action potential was measured with and without supplementation of mesenchymal stem cells. The stimulus current was normalized to the minimum necessary pulse to create an action potential without any mesenchymal stem cells (the control condition). The effects of supplying mesenchymal stem cells are shown in Table 3.11

TABLE 3.11: Effects of Mesenchymal Stem Cell “B” on Activation Threshold

CM : hMSC	Normalized Stimulus Current (pA/pA)	Percent Change
1 : 0	1	—
9 : 1	1	0
4 : 1	1	0
1 : 1	0.99	-1

Unlike type-“A” mesenchymal stem cells, the type “B” mesenchymal stem cell had a negligible effect on the activation threshold of the cardiomyocyte action potential. Specifically, the activation threshold decreased only by as much as 1% when there was a 1:1 ratio of mesenchymal stem cells to cardiomyocytes. This could be explained by the nonexistence of functional delayed rectifier currents in type-“B” mesenchymal stem cells. As a result, the type-“B” mesenchymal stem cell adopted the resting membrane potential of the cardiomyocyte (Figure 3.21), resulting in a negligible

effect on the activation threshold. As the percentage of mesenchymal stem cells increased, the minimum required stimulus current decreased only slightly.

Overall, like type “A” mesenchymal stem cells, type “B” mesenchymal stem cells decreased the action potential duration (APD_{50} and APD_{90}), and the activation threshold of a cardiomyocyte action potential.

3.3.3 Type C Total Current

Next, the ten Tusscher cardiomyocyte model was coupled with the novel type “C” mesenchymal stem cell model in ratios of 9:1, 4:1, and 1:1, respectively. The resulting cardiomyocyte action potential behavior is shown below in Figure 3.23.

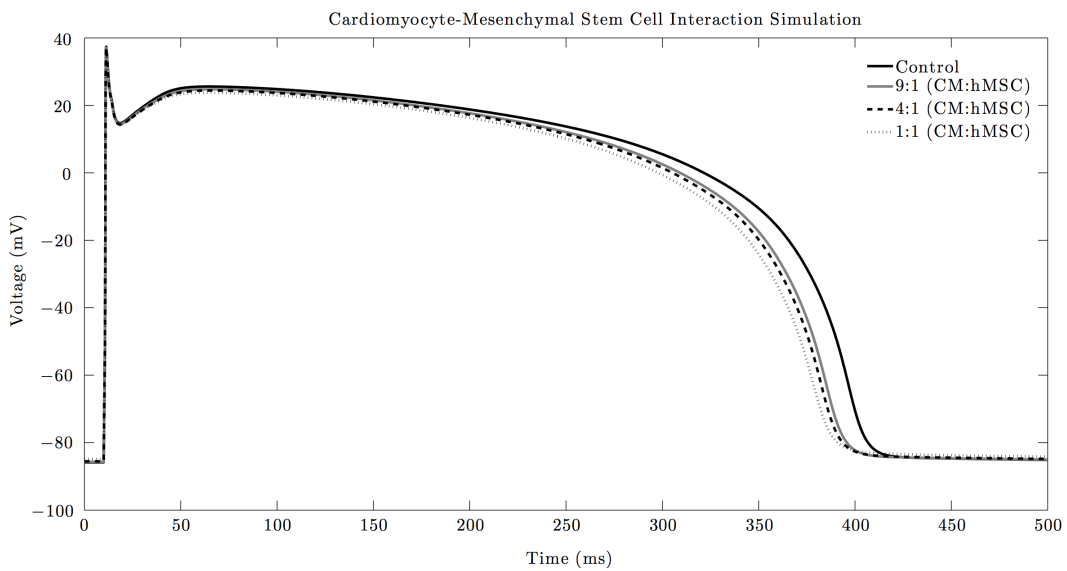


FIGURE 3.23: The ten Tusscher cardiomyocyte model was coupled with the novel type “C” mesenchymal stem cell model in ratios of 9:1, 4:1, and 1:1, respectively. As the percentage of mesenchymal stem cells increased, the action potential decreased.

As shown in Figure 3.23, the effects of type “C” mesenchymal stem cells are nearly identical to the effects by type “A” mesenchymal stem cells. There were very few

effects on phases 0, 1, and 4 of the cardiac action potential, as the rapid depolarization phase, the plateau phase, and the resting membrane potential phase overlap for the varying ratios of cardiomyocytes to mesenchymal stem cells.

Furthermore, type “C” mesenchymal stem cells affect phases 2 and 3 of the cardiac action potential. As shown in Figure 3.23, as the percentage of mesenchymal stem cells increased from 10% to 50%, the action potential decreased. The duration for the action potential to repolarization 50% and 90% (APD_{50} and APD_{90} , respectively) was measured for these varying ratios of mesenchymal stem cells and cardiomyocytes (Table 3.12).

TABLE 3.12: Effects of Mesenchymal Stem Cell “C” on Action Potential Duration

CM : hMSC	APD_{50} (ms)	APD_{90} (ms)
1 : 0	361	392
9 : 1	349	380
4 : 1	345	378
1 : 1	341	374

As shown in the table above, both the duration for the action potential to repolarization 50% and 90% (APD_{50} and APD_{90}) decreased, which shows phases 2 and 3 of the action potential were affected by mesenchymal stem cell interaction. Type “C” mesenchymal stem cells decreased the action potential duration more than type “B” mesenchymal stem cells, but nearly the same as type “A” mesenchymal stem cells. This was expected, as both type “A” and type “C” mesenchymal stem cells have functional delayed rectifier currents. To better understand why the action potential

duration was decreased, the cardiomyocyte ionic channels were examined (Figure 3.24).

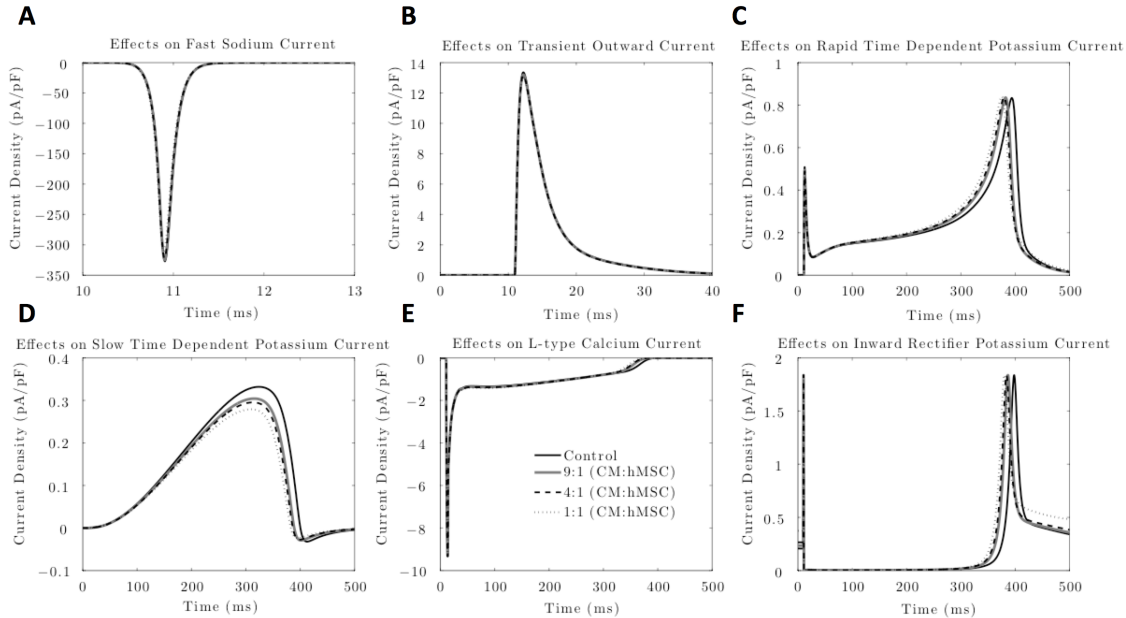


FIGURE 3.24: To better understand why the action potential duration was decreased, the cardiomyocyte: A) fast sodium; B) transient outward; C) rapid delayed rectifier potassium; D) slow delayed rectifier potassium; E) L-type calcium; and F) inward rectifier potassium currents were examined.

The cardiomyocyte ionic channel activity corresponds with the effects apparent in the overall cardiomyocyte action potential. As shown in Figures 3.24A and B, there were minimal effects on the fast sodium current and the transient outward current, which correspond to little variation in phases 0 and 1. Furthermore, there were noticeable effects on the rapid delayed rectifier channel (Figure 3.24C), the slow delayed rectifier channel (Figure 3.24D), the L-type calcium channel (Figure 3.24E), and the inward rectifier channel (Figure 3.24F). Specifically, the amplitude and duration of each of these currents decreased, which correspond with decreases in phases 2 and 3 of the cardiac action potential.

The effects of the cardiomyocytes on the human mesenchymal stem cell were also considered, as the electrical effects on the mesenchymal stem cells may give insight on functional differences of these pluripotent cells. These electrical effects are shown below (Figure 3.25).

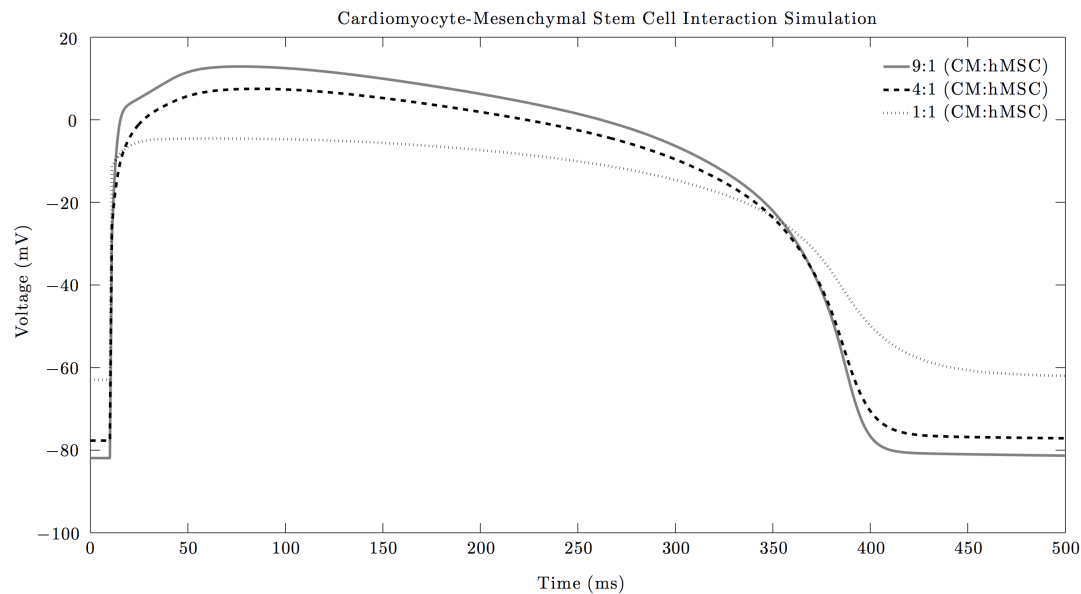


FIGURE 3.25: To develop insight into functional differences of pluripotent cells as a result of cardiomyocyte-mesenchymal stem cell coupling, the effects of the cardiomyocytes on the human mesenchymal stem cell were also considered. The mesenchymal stem cell is greatly influenced by cardiomyocyte behavior, as it approaches the general cardiac action potential behavior.

As shown in Figure 3.25, the mesenchymal stem cell is greatly influenced by cardiomyocyte behavior. As the ratio of cardiomyocytes to mesenchymal stem cells increases, the mesenchymal stem cell electrical activity approaches the cardiomyocyte action potential. This behavior is typical of non-excitable cells, where it inherits the excitable cell's activity.

To understand how mesenchymal stem cells are influenced by the cardiomyocytes, the mesenchymal stem cell gap junction current was examined (Figure 3.26). As

shown below, a large influx occurred at 10 ms, as a result of the depolarization of the cardiomyocyte. This subsequently increased the voltage of the mesenchymal stem cell at 10 ms, as seen in Figure 3.25. The general trends of the action potential phases 1, 2, 3, and 4 were subsequently seen, confirming the influence of the cardiomyocytes on mesenchymal stem cells. As the ratio of cardiomyocytes to mesenchymal stem cells increased, the magnitude of the current decreased. This is because each cardiomyocyte needed to contribute less in order for the mesenchymal stem cell to approach the cardiomyocyte electrical activity. Both positive and negative currents were evident, showing that the mesenchymal stem cell acts as a sink during phases 0 through 3 of the action potential, and a source during phase 4 of the action potential.

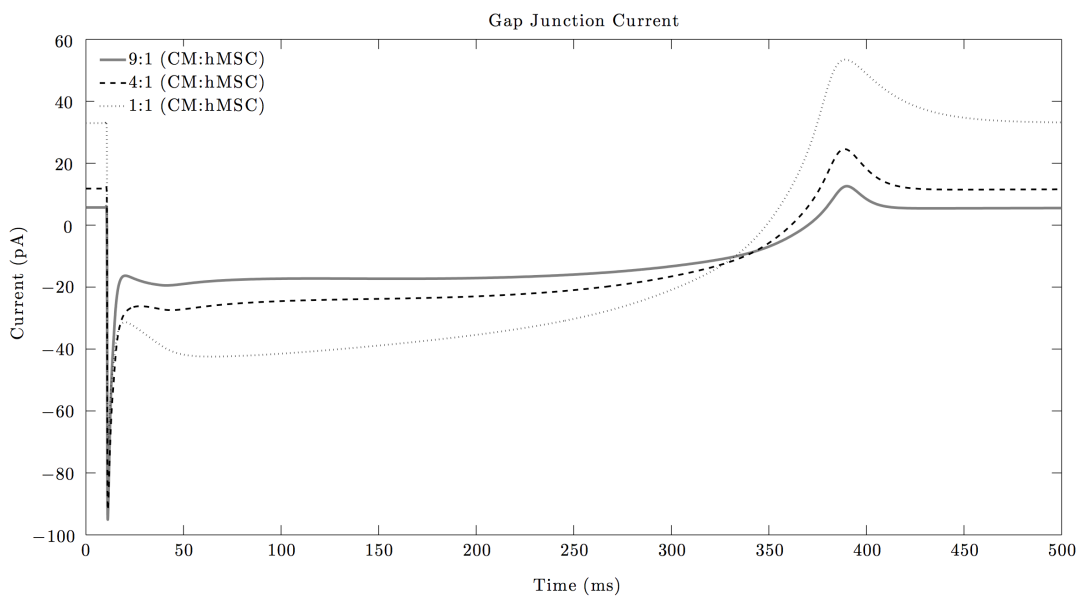


FIGURE 3.26: The mesenchymal stem cell gap junction current was examined to better understand how mesenchymal stem cells are influenced by the cardiomyocytes. The gap junction current displayed the general trends of the action potential phases, confirming the influence of the cardiomyocytes on mesenchymal stem cells. The magnitude of the current decreased as the ratio of cardiomyocytes to mesenchymal stem cells increased.

Finally, the activation threshold to produce a cardiomyocyte action potential was measured with and without supplementation of mesenchymal stem cells. The stimulus current was normalized to the minimum necessary pulse to create an action potential without any mesenchymal stem cells (the control condition). The effects of supplying mesenchymal stem cells are shown in Table 3.13

TABLE 3.13: Effects of Mesenchymal Stem Cell “C” on Activation Threshold

CM : hMSC	Normalized Stimulus Current (pA/pA)	Percent Change
1 : 0	1	—
9 : 1	0.99	-1
4 : 1	0.98	-2
1 : 1	0.95	-5

As expected, the activation threshold decreased with mesenchymal stem cell supplementation, as the resting membrane potential of mesenchymal stem cells (-42 to -12 mV) is less than the resting membrane potential of cardiomyocytes (-85 mV). As the percentage of mesenchymal stem cells increased, the minimum required stimulus current decreased. The activation threshold decreased by as much as 5% when there was a 1:1 ratio of mesenchymal stem cells to cardiomyocytes. The activation threshold just as much for type “C” mesenchymal stem cells as for type “A” mesenchymal stem cells.

Overall, like types “A” and “B” mesenchymal stem cells, type “C” mesenchymal stem cells decreased the action potential duration (APD_{50} and APD_{90}), and the

activation threshold of a cardiomyocyte action potential. The effects of type “C” mesenchymal stem cells were nearly identical to the effects of type “A” mesenchymal stem cells, mainly due to the delayed rectifier current functional in both cell types.

3.3.4 Weighted Average of Total Currents

Finally, the ten Tusscher cardiomyocyte model was coupled with all three mesenchymal stem cell models (using a weighted average of the prevalence of each total current) in ratios of 9:1, 4:1, and 1:1, respectively. The resulting cardiomyocyte action potential behavior is shown below in Figure 3.27.

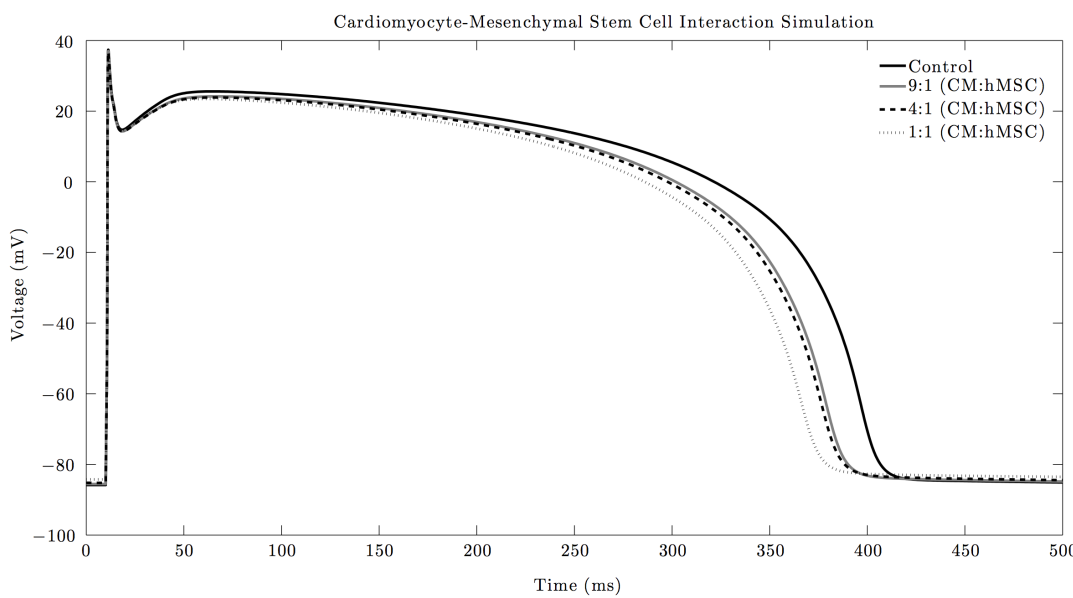


FIGURE 3.27: The ten Tusscher cardiomyocyte model was coupled with all three mesenchymal stem cell models (using a weighted average) in ratios of 9:1, 4:1, and 1:1, respectively. As the percentage of mesenchymal stem cells increased, the action potential decreased.

As shown in Figure 3.27, there were very few effects on phases 0, 1, and 4 of the cardiac action potential. The rapid depolarization phase, the plateau phase, and the resting membrane potential phase (phases 0, 1 and 4, respectively) overlap for

the varying ratios of cardiomyocytes to mesenchymal stem cells, implying there were minimal effects.

However, the weighted average of mesenchymal stem cells affected phases 2 and 3 of the cardiac action potential greatly. As shown in Figure 3.27, as the percentage of mesenchymal stem cells increased from 10% to 50%, the action potential decreased. The duration for the action potential to repolarization 50% and 90% (APD_{50} and APD_{90} , respectively) was measured for these varying ratios of mesenchymal stem cells and cardiomyocytes (Table 3.14).

TABLE 3.14: Effects on Action Potential Duration

CM : hMSC	APD ₅₀ (ms)	APD ₉₀ (ms)
1 : 0	361	392
9 : 1	342	374
4 : 1	339	373
1 : 1	328	362

As shown in the table above, both the duration for the action potential to repolarization 50% and 90% (APD_{50} and APD_{90}) decreased, which shows phases 2 and 3 of the action potential were affected by mesenchymal stem cell interaction. These effects were greater for the weighted average of mesenchymal stem cells than for any individual type of mesenchymal stem cell. To better understand why the action potential duration was decreased, the cardiomyocyte ionic channels were examined (Figure 3.28).

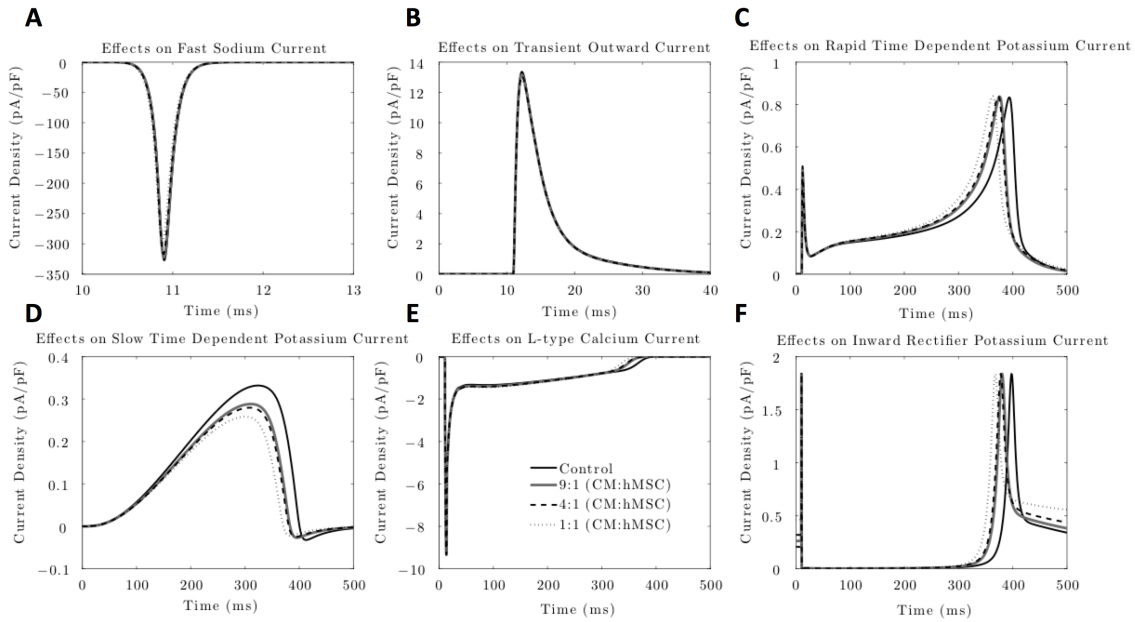


FIGURE 3.28: To better understand why the action potential duration was decreased, the cardiomyocyte: A) fast sodium; B) transient outward; C) rapid delayed rectifier potassium; D) slow delayed rectifier potassium; E) L-type calcium; and F) inward rectifier potassium currents were examined.

The cardiomyocyte ionic channel activity corresponds with the effects apparent in the overall cardiomyocyte action potential. As shown in Figures 3.28A and B, there were minimal effects on the fast sodium current and the transient outward current, which correspond to little variation in phases 0 and 1. Furthermore, there were noticeable effects on the rapid delayed rectifier channel (Figure 3.28C), the slow delayed rectifier channel (Figure 3.28D), the L-type calcium channel (Figure 3.28E), and the inward rectifier channel (Figure 3.28F). Specifically, the amplitude and duration of each of these currents decreased, which correspond with decreases in phases 2 and 3 of the cardiac action potential. These effects were greater for the weighted average of mesenchymal stem cells than for any individual type of mesenchymal stem cell, which corresponds with a shorter action potential duration.

Finally, the activation threshold to produce a cardiomyocyte action potential was

measured with and without supplementation of mesenchymal stem cells. The stimulus current was normalized to the minimum necessary pulse to create an action potential without any mesenchymal stem cells (the control condition). The effects of supplying mesenchymal stem cells are shown in Table 3.15

TABLE 3.15: Effects of Mesenchymal Stem Cells on Activation Threshold

CM : hMSC	Normalized Stimulus Current (pA/pA)	Percent Change
1 : 0	1	—
9 : 1	0.98	-2
4 : 1	0.97	-3
1 : 1	0.91	-9

As the percentage of mesenchymal stem cells increased, the minimum required stimulus current decreased. The activation threshold decreased by as much as 9% when there was a 1:1 ratio of mesenchymal stem cells to cardiomyocytes.

Overall, like types “A”, “B”, and “C” mesenchymal stem cells, the weighted average of mesenchymal stem cell types decreased the action potential duration (APD_{50} and APD_{90}), and the activation threshold of a cardiomyocyte action potential. The effects of this mixed mesenchymal stem cell makeup were more severe than any individual stem cell type.

3.4 Simulation of Coupled Human Mesenchymal Stem Cell-Cardiomyocyte Conduction Velocity

The effects of mesenchymal stem cells on the cardiac action potential conduction velocity were also determined for further insight into the therapeutic or pro-arrhythmic effects of these pluripotent cells. First, the control conduction velocity (i.e. no mesenchymal stem cells) was measured and compared to previously published results [66]. To do so, voltage was plotted as a function of time and distance, as seen in Figure 3.29, with the following initial condition and Neumann-type boundary conditions: 1) the stimulus current was applied at the first cell in the series (Boundary Condition 1); 2) no flux condition at the last cell in the series (Boundary Condition 2); and 3) the initial membrane voltage was the resting membrane potential (Initial Condition 1).

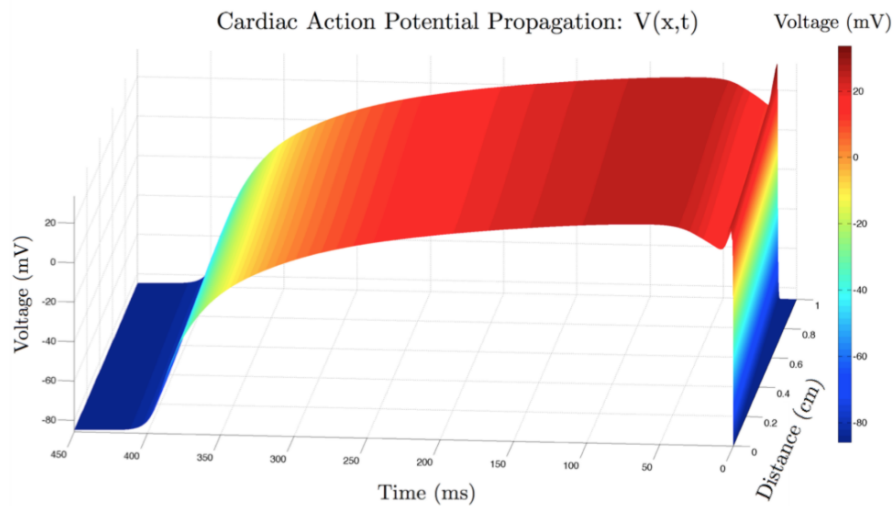


FIGURE 3.29: The voltage of a cardiomyocyte was plotted as a function of time and distance, with one initial condition and two Neumann-type boundary conditions: 1) the stimulus current was applied at the first cell in the series; 2) the last cell in the series was at the resting membrane potential; and 3) the initial membrane voltage was the resting membrane potential.

To see the propagation velocity of the action potential, a top view of Figure 3.29 was made (Figure 3.30).

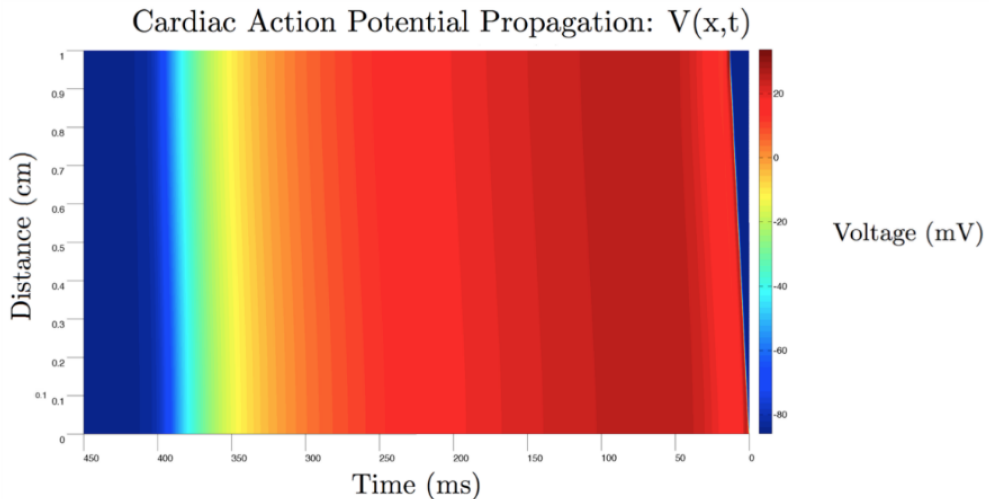


FIGURE 3.30: To see the propagation velocity of the action potential, a top view of the voltage as a function of distance and time was made. As seen, voltage contours are evident throughout this cell system, which allows for a calculation of the conduction velocity. To calculate the conduction velocity, the chain rule is used at constant voltage contours.

As seen in the top view, a certain amount of time elapses in order for the action potential to propagate along a constant voltage. To obtain accurate results, the conduction velocity was measured along the center of the cardiomyocyte-only cell strands only at the peak voltage contour line. The conduction velocity along the center of the cardiomyocyte-only cell strands (at the peak voltage contour line) was measured at 74.1 cm/s, which was within the range of 61.7 - 75.4 cm/s for the ten Tusscher model [66]. Therefore, this methodology was accepted, and was applied for various ratios of cardiomyocytes and mesenchymal stem cells with a step size of 0.02 cm in the x direction, and 0.005 ms in the t direction.

3.4.1 Type A Total Current

First, the effects of type-“A” mesenchymal stem cells on cardiomyocyte action potential conduction velocity were examined. This was performed for ratios of 9:1, 4:1, and 1:1 of cardiomyocytes to mesenchymal stem cells, respectively. The resulting conduction velocities are shown in Table 3.16.

TABLE 3.16: Effects of Mesenchymal Stem Cell “A” on Conduction Velocity

CM : hMSC	Conduction Velocity (cm/s)	Percent Change
1 : 0	74.1	—
9 : 1	72.7	-1.9
4 : 1	70.8	-4.5
1 : 1	63.0	-15.0

As shown above, as the ratios of mesenchymal stem cells to cardiomyocytes increased, the conduction velocity decreased. To develop further insight into the electrical effects of mesenchymal stem cells, the maximum upstroke velocity ($\frac{dV}{dt}_{\max}$) was calculated at the center of the cell system (Table 3.17).

TABLE 3.17: Effects of Mesenchymal Stem Cell “A” on Maximum Upstroke Velocity

CM : hMSC	Upstroke Velocity (V/s)	Percent Change
1 : 0	144.4	—
9 : 1	142.9	-1.0
4 : 1	142.1	-1.6
1 : 1	136.7	-5.3

As the ratios of mesenchymal stem cells to cardiomyocytes increased, the upstroke velocity decreased. This was expected, as upstroke velocity and conduction velocity are positively correlated [108].

3.4.2 Type B Total Current

Next, the effects of type-“B” mesenchymal stem cells on cardiomyocyte action potential conduction velocity were examined. This was performed for ratios of 9:1, 4:1, and 1:1 of cardiomyocytes to mesenchymal stem cells, respectively. The resulting conduction velocities are shown in Table 3.18.

TABLE 3.18: Effects of Mesenchymal Stem Cell “B” on Conduction Velocity

CM : hMSC	Conduction Velocity (cm/s)	Percent Change
1 : 0	74.1	—
9 : 1	72.7	-1.9
4 : 1	70.8	-4.5
1 : 1	63.5	-14.3

As the ratios of mesenchymal stem cells to cardiomyocytes increased, the conduction velocity decreased. To develop further insight into the electrical effects of mesenchymal stem cells, the maximum upstroke velocity ($\frac{dV}{dt}_{\max}$) was calculated at the center of the cell system (Table 3.19).

TABLE 3.19: Effects of Mesenchymal Stem Cell “B” on Maximum Upstroke Velocity

CM : hMSC	Upstroke Velocity (V/s)	Percent Change
1 : 0	144.4	—
9 : 1	142.9	-1.0
4 : 1	142.1	-1.6
1 : 1	136.7	-5.3

As the ratios of mesenchymal stem cells to cardiomyocytes increased, the upstroke velocity decreased. This was expected, as upstroke velocity and conduction velocity are positively correlated [108].

3.4.3 Type C Total Current

Next, the effects of type-“C” mesenchymal stem cells on cardiomyocyte action potential conduction velocity were examined. This was performed for ratios of 9:1, 4:1, and 1:1 of cardiomyocytes to mesenchymal stem cells, respectively. The resulting conduction velocities are shown in Table 3.20.

TABLE 3.20: Effects of Mesenchymal Stem Cell “C” on Conduction Velocity

CM : hMSC	Conduction Velocity (cm/s)	Percent Change
1 : 0	74.1	—
9 : 1	72.7	-1.9
4 : 1	70.8	-4.5
1 : 1	63.5	-14.3

As the ratios of mesenchymal stem cells to cardiomyocytes increased, the conduction velocity decreased. To develop further insight into the electrical effects of mesenchymal stem cells, the maximum upstroke velocity ($\frac{dV}{dt}_{\max}$) was calculated at the center of the cell system (Table 3.21).

TABLE 3.21: Effects of Mesenchymal Stem Cell “C” on Maximum Upstroke Velocity

CM : hMSC	Upstroke Velocity (V/s)	Percent Change
1 : 0	144.4	—
9 : 1	143.0	-1.0
4 : 1	142.2	-1.5
1 : 1	137.0	-5.1

As the ratios of mesenchymal stem cells to cardiomyocytes increased, the upstroke velocity decreased. This was expected, as upstroke velocity and conduction velocity are positively correlated [108].

3.4.4 Weighted Average of Total Currents

Finally, the effects of a weighted average of mesenchymal stem cells (with respect to prevalence of each type of total current) on cardiomyocyte action potential conduction velocity were examined. This was performed for ratios of 9:1, 4:1, and 1:1 of cardiomyocytes to mesenchymal stem cells, respectively. The resulting conduction velocities are shown in Table 3.22.

TABLE 3.22: Effects on Conduction Velocity

CM : hMSC	Conduction Velocity (cm/s)	Percent Change
1 : 0	74.1	—
9 : 1	72.3	-2.4
4 : 1	70.8	-4.5
1 : 1	63.0	-15.0

As the ratios of mesenchymal stem cells to cardiomyocytes increased, the conduction velocity decreased. To develop further insight into the electrical effects of mesenchymal stem cells, the maximum upstroke velocity ($\frac{dV}{dt}_{\max}$) was calculated at the center of the cell system (Table 3.23).

TABLE 3.23: Effects of Mesenchymal Stem Cells on Maximum Upstroke Velocity

CM : hMSC	Upstroke Velocity (V/s)	Percent Change
1 : 0	144.4	—
9 : 1	143.3	-0.8
4 : 1	142.5	-1.3
1 : 1	137.0	-5.1

As the ratios of mesenchymal stem cells to cardiomyocytes increased, the upstroke velocity decreased. This was expected, as upstroke velocity and conduction velocity are positively correlated [108].

Overall, each cell type, along with the weighted average of cell types, decreased the conduction velocity and upstroke velocity of a system of cardiomyocytes.

Chapter 4

Discussion

In this study, two original and clinically relevant studies were conducted: 1) the development of a mesenchymal stem cell electrophysiology model; and 2) the electrophysiological role of mesenchymal stem cells interacting with cardiomyocytes. The insight drawn from each of these studies, as well as future directions for enhancing this study, are discussed below.

4.1 Discussion of the Novel Models

Three novel electrophysiology models were developed mainly with data provided by Li *et al* [45]. These models apply both Markovian and non-Markovian methods, as well as the Nernst and Goldman-Hodgkin-Katz equations, to describe the functional transient outward, L-type calcium, delayed rectifier potassium, TTX-sensitive sodium, and calcium-activated potassium channels.

This model is capable of predicting individual functional ion channels (Figures 3.2, 3.4, 3.6, 3.8, and 3.10), as well as total currents for three different types of mesenchymal stem cell behavior (Figures 3.12, 3.13, and 3.14). Furthermore, all three models are capable of receiving a stimulus current, and approaching their expected membrane potentials (Figure 3.11). Therefore, these models are not limited only to interactions with cardiomyocytes; mesenchymal stem cells are widely applied throughout medical therapies, and their electrical interactions with various cellular systems can be described with this powerful model. The promising description of mesenchymal stem cell electrophysiological behavior using these simulations makes it worthwhile to enhance the models in the future. More detail on how to improve these models are shown in Section 4.5.1.

4.2 Discussion of Mathematical Results

Overall, the general behavior of total currents “A”, “B”, and “C” were modeled successfully. Therefore, they were each coupled with the cardiomyocytes to develop insight into the electrical interactions between these two cell types. Specifically, the effects on the cardiomyocyte’s ion channel activity, action potential duration, and conduction velocity were examined.

The consequences of electrical interactions between cardiomyocytes and mesenchymal stem cells were predicted by coupling the ten Tusscher cardiomyocyte model to the three novel models developed in this study. Significant electrophysiological consequences were evident when the ten Tusscher model was coupled to each of the mesenchymal stem cell models in ratios of 9:1, 4:1, and 1:1, respectively. These

effects include decreases in action potential duration and plateau height, and corresponding variations in ionic current. Furthermore, there was a decrease in both conduction velocity and maximum upstroke velocity. As the ratio of mesenchymal stem cells to cardiomyocytes increased, these effects became even more drastic. Since the membrane potential for mesenchymal stem cells (-42 mV to -12 mV) is greater than for cardiomyocytes (-85 mV), the activation threshold decreased for a cardiomyocyte action potential. A detailed description on the effects on the cardiomyocyte action potential duration, plateau height, ionic current, conduction velocity, and maximum upstroke velocity is shown below.

4.2.1 Effects on Action Potential Duration and Plateau Height

Total currents “A”, “B”, and “C”, as well as the weighted currents, all decreased the action potential duration and plateau height of the cardiomyocyte action potential duration. For each type of mesenchymal stem cell model, as the percentage of mesenchymal stem cells increased from 10% to 50%, the action potential duration and plateau height decreased, as expected. The weighted currents exhibited the most substantial effects, followed by total currents “A” and “C”, all of which have functional delayed rectifier potassium channels. This implies the delayed rectifier potassium channel of mesenchymal stem cells is largely influential on the cardiomyocyte action potential duration and plateau height. There were very few effects on phases 0, 1, and 4 of the cardiac action potential for total currents “A”, “B”, and “C”, as well as the weighted currents. The rapid depolarization phase, the plateau phase, and the resting membrane potential phase (phases 0, 1 and 4, respectively)

overlap for the varying ratios of cardiomyocytes to mesenchymal stem cells, implying there were minimal effects. To better understand why the action potential duration was decreased, the cardiomyocyte ionic channels were examined for each type of mesenchymal stem cell electrophysiological behavior.

4.2.2 Effects on Cardiomyocyte Ionic Channel Activity

The cardiomyocyte ionic channel activity corresponds with the effects apparent in the overall cardiomyocyte action potential. For example, for total currents “A”, “B”, and “C”, as well as the weighted currents, there were minimal effects on the fast sodium current and the transient outward currents, which correspond to little variation in phases 0 and 1. However, there were noticeable effects on the rapid delayed rectifier channel, the slow delayed rectifier channel, the L-type calcium channel, and the inward rectifier channel. Specifically, the amplitude and duration of each of these currents decreased, which correspond with decreases in phases 2 and 3 of the cardiac action potential. These effects were more evident when the action potential duration and plateau height decreased more drastically.

4.2.3 Effects on Human Mesenchymal Stem Cell Electrical Activity

The effects of the cardiomyocytes on the human mesenchymal stem cell were also considered, as the electrical effects on the mesenchymal stem cells may give insight on functional differences of these pluripotent cells. For total currents “A”, “B”, and “C”, as well as the weighted currents, the mesenchymal stem cell is greatly influenced by cardiomyocyte behavior. Total current “B” approaches the membrane

potential of cardiomyocytes more than any other mesenchymal stem cell-type, because it does not have functional delayed rectifier potassium currents. As the ratio of cardiomyocytes to mesenchymal stem cells increases, the mesenchymal stem cell electrical activity approaches the cardiomyocyte action potential. This behavior is typical of non-excitatory cells, where it acts as an electrical sink to the excitable source during an action potential. To further understand how the cardiomyocytes affect mesenchymal stem cells (and vice versa), the gap junction current was simulated.

4.2.4 Effects on Gap Junction Current

For each mesenchymal stem cell type, a large influx occurred at 10 ms, as a result of the depolarization of the cardiomyocyte. This subsequently increased the voltage of the mesenchymal stem cell at 10 ms. The general trends of the action potential phases 1, 2, 3, and 4 were subsequently seen, confirming the influence of the cardiomyocytes on mesenchymal stem cells. As the ratio of cardiomyocytes to mesenchymal stem cells increased, the magnitude of the current decreased. This is because each cardiomyocyte electrical source needed to contribute less in order for the mesenchymal stem cell to approach the cardiomyocyte electrical activity. Both positive and negative currents were evident, showing that the mesenchymal stem cell acts as a sink during phases 0 through 3 of the action potential, and a source during phase 4 of the action potential. The lower gap junction current for type-“B” mesenchymal stem cells during phase 4 explained why the membrane potential of this pluripotent cell approached the cardiomyocyte membrane potential.

4.2.5 Effects on Activation Threshold

The activation threshold to produce a cardiomyocyte action potential was measured with and without supplementation of mesenchymal stem cells. As expected, the activation threshold decreased with mesenchymal stem cell supplementation, as the resting membrane potential of mesenchymal stem cells (-42 to -12 mV) is less than the resting membrane potential of cardiomyocytes (-85 mV). As the percentage of mesenchymal stem cells increased, the minimum required stimulus current decreased. The activation threshold decreased by as much as 5% when there was a 1:1 ratio of mesenchymal stem cells to cardiomyocytes for the weighted currents, as well as total currents “A” and “C”. A negligible effect on activation threshold was evident with type-“B” mesenchymal stem cells, as this cell type adopted the membrane potential of cardiomyocytes.

4.2.6 Effects on Conduction Velocity and Upstroke Velocity

Significant effects were evident for all mesenchymal stem cell types on cardiomyocyte conduction velocity. This effect was independent of the type of mesenchymal stem cell; it was mainly dependent on the cellular resistivity and volume of mesenchymal stem cell. Upstroke velocity was also affected by mesenchymal stem cells, but in a less substantial way. This was expected, as upstroke velocity and conduction velocity are positively correlated [108].

4.3 Significance of This Study

To determine how meaningful this model is, the results were compared to empirical interactions between cardiomyocytes and mesenchymal stem cells. The similarities between the simulations and the empirical results make it possible to draw clinical implications.

4.3.1 Empirical Interactions Between Cardiomyocytes and Mesenchymal Stem Cells

Human mesenchymal stem cells have exhibited electrical interactions with cardiomyocytes for myocardial infarction therapies both *in vivo* and *in vitro*. For example, mesenchymal stem cell supplementation decreased the activation threshold (Figure 1.5) [40]. These results suggested at a preliminary level that the electrical activity of supplemented mesenchymal stem cells plays a role in cardiac function, as the activation threshold decreased in mesenchymal-stem-cell-supplemented engineered cardiac tissue. Furthermore, in various other studies, it the arrhythmogenic potential of mesenchymal stem cells was shown, as co-culturing with greater than 10 percent of mesenchymal stem cells decreases conduction velocity and action potential duration, and predisposes re-entrant arrhythmias [37, 38, 109, 110]. Finally, mesenchymal stem cells are capable of inheriting cardiomyocyte action potential behavior [110]. These consequences correspond to the *in vitro* electrical effects previously described, and show mesenchymal stem cells are indeed capable of predisposing re-entrant arrhythmias. Furthermore, it implies the models generated are promising for future studies.

4.3.2 Clinical Implications

Human mesenchymal stem cell delivery has exhibited potential in clinical myocardial infarction therapies; however, the large-scale application of this method is limited by the fact that researchers do not fully understand the mechanisms by which mesenchymal stem cells enhance cardiomyocyte function. This limited knowledge makes it extremely difficult to control long-term electromechanical stability, along with structural and functional electromechanical integration with host tissue [35, 37]. This promising model makes it possible to better understand the electrical consequences of this therapeutic method. Overall, based on the results of this mathematical study, as well as various *in vitro* studies, mesenchymal stem cells have arrhythmogenic potential. Fortunately, this model makes it possible to generate regenerative medicine therapeutics that account for cardiomyocyte-mesenchymal stem cell coupling.

For example, mesenchymal stem cells can be used as a vector of gene engineering for treatment of heart disease [109]. Mesenchymal stem cells are attractive for gene delivery because they are pluripotent even with integrated vectors that affect gene expression [109]. This provides opportunities to modify the functional ion channels expressed in mesenchymal stem cells (to positively influence cardiomyocyte action potential and conduction velocity characteristics), while delivering vascular endothelial growth factor (VEGF) via VEGF gene-transfected mesenchymal stem cells [109]. This would result in major improvement of cardiac function, while minimizing potential arrhythmogenic effects of mesenchymal stem cells. Section 4.5.2 describes potential methods to discover which functional ion channels should be modified in the future.

4.4 Sensitivity Analysis

To study the robustness of the results, a sensitivity analysis was performed. Specifically, the variations in action potential duration (APD₉₀) were examined when various mesenchymal stem cell electrical characteristics were modified (Table 4.1). Each parameter was increased and decreased by 25% and 50% individually. The activation and inactivation parameters of the delayed rectifier potassium channel and the sodium channel were varied to ensure that their uncertainty would not affect the cardiomyocyte action potential characteristics. This analysis was performed for cardiomyocytes coupled to the weighted mesenchymal stem cell currents in a ratio of 9:1.

TABLE 4.1: Parameters Modified for Sensitivity Analysis

Parameter	Meaning
$\overline{G_{Na}}$	Maximum Sodium Current Conductance
$\overline{G_{dr}}$	Maximum Delayed Rectifier Current Conductance
$\overline{G_{CaL}}$	Maximum L-type Calcium Current Conductance
$\overline{G_{to}}$	Maximum Transient Outward Current Conductance
$\overline{G_{KCa}}$	Maximum Calcium Activated Potassium Current Conductance
$\alpha_{n,dr}$	Delayed Rectifier Current Activation Parameter
$\beta_{n,dr}$	Delayed Rectifier Current Activation Parameter
τ_m	Sodium Current Activation Parameter
τ_h	Sodium Current Inactivation Parameter

The effects of varying maximum conductances on the action potential duration of cardiomyocytes are shown in Figure 4.1.

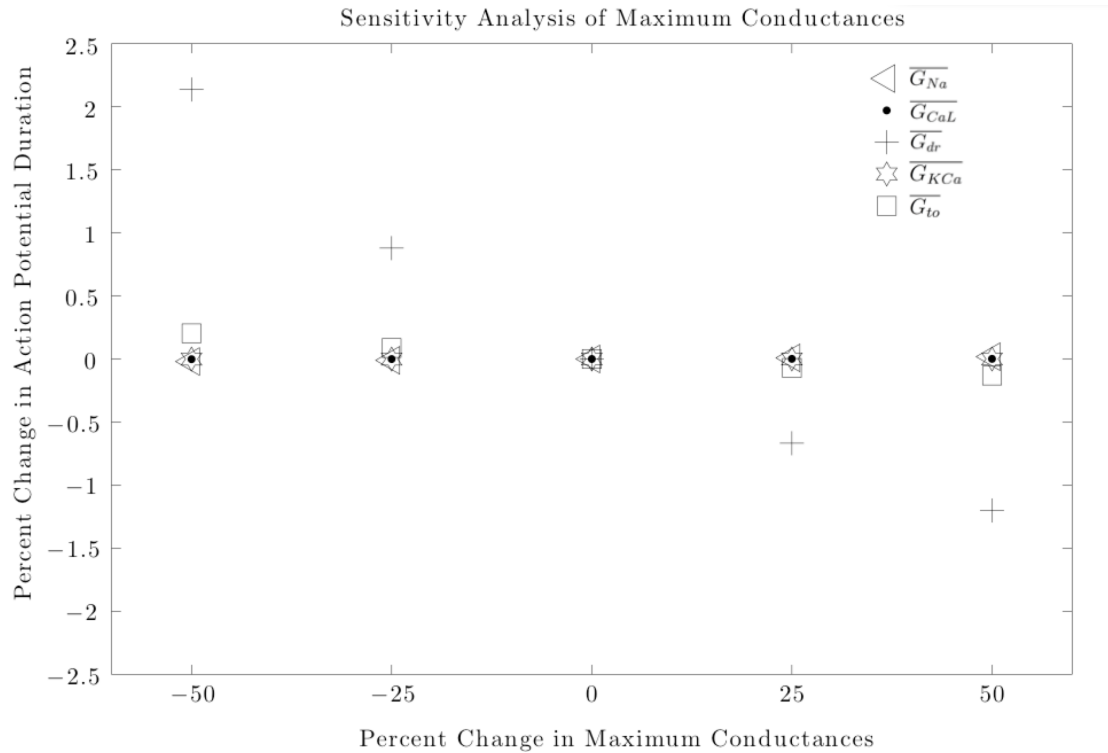


FIGURE 4.1: To study the robustness of the results, a sensitivity analysis was performed. Each maximum conductance parameter was increased and decreased by 25% and 50% individually.

As evident in Figure 4.1, this sensitivity analysis on the mesenchymal stem cell inputs shows the robustness of the results. The action potential duration varies by 2% at most, even when the maximum conductances are increased or decreased by 50%. The maximum action potential duration achieved was still lower than the control action potential duration, which reinforces the fact that mesenchymal stem cells decrease action potential duration. As expected, the maximum conductance of the delayed rectifier potassium channel was most sensitive, as total currents “A” and “C” affect action potential duration most, and they express this channel.

Next, the effects of varying the delayed rectifier and sodium channel kinetic parameters on the action potential duration of cardiomyocytes were studied (Figure 4.2).

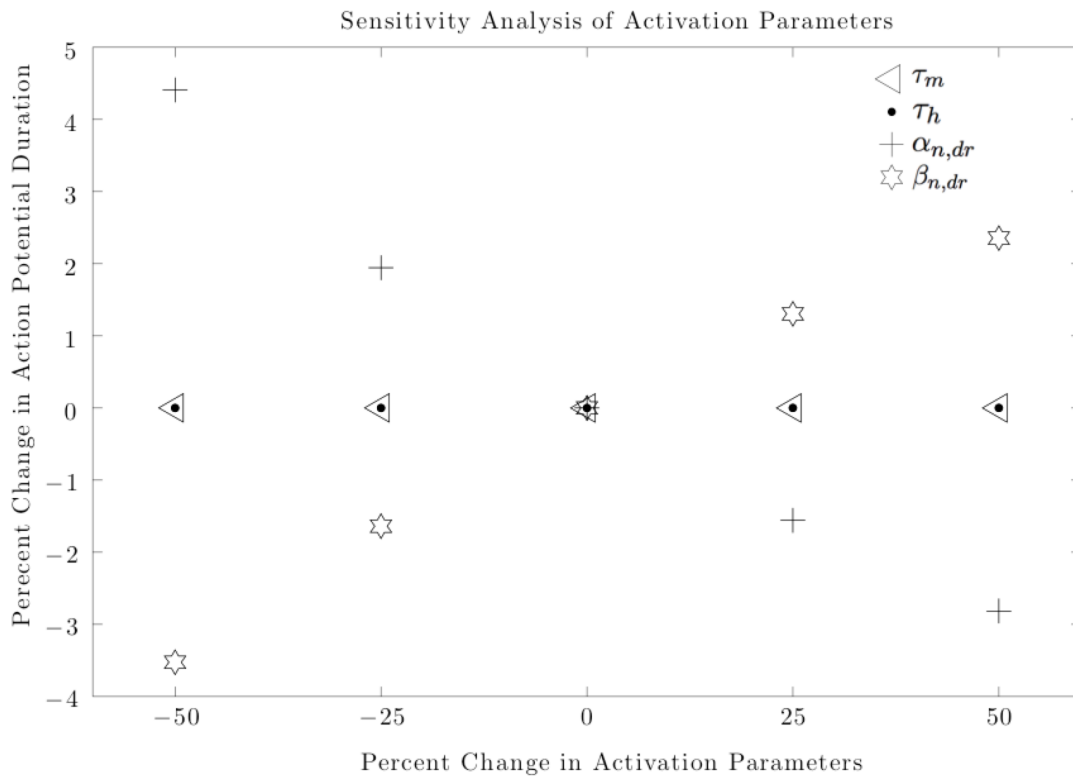


FIGURE 4.2: To study the robustness of the results, a sensitivity analysis was performed. Various activation kinetic parameters were increased and decreased by 25% and 50% individually.

As evident in Figure 4.2, this sensitivity analysis on the mesenchymal stem cell inputs shows the robustness of the results. The action potential duration varies by less than 5%, even when the maximum conductances are increased or decreased by 50%. The maximum action potential duration achieved was still lower than the control action potential duration, which reinforces the fact that mesenchymal stem cells decrease action potential duration. As expected, the activation kinetic parameters of the delayed rectifier potassium channel were most sensitive, as total

currents “A” and “C” affect action potential duration most, and they express this channel.

4.5 Limitations and Future Work

Although the results were robust, and the novel model is capable of successfully describing mesenchymal stem cell electrophysiological behavior, there are several limitations of this study. As a result, there are various areas of improvement for the model, as discussed further in Section 4.5.1. Following these improvements, numerous insights could be developed on the methods and consequences of clinically applying mesenchymal stem cells, as discussed in Section 4.5.2.

4.5.1 Limitations of This Study

Although this model is self-consistent, robust, and valuable, it will need to continue to evolve as electrophysiological data on human mesenchymal stem cells is published. Li *et al* did not cover the activation and inactivation kinetics of the sodium currents, L-type currents, and transient outward currents [45]. Furthermore, the delayed rectifier potassium current activation kinetics were highly variable, which resulted in highly variable activation times for the current [45]. Therefore, it was necessary to approximate these values from the available whole-cell patch clamp experiments for each respective current. Fortunately, these approximations resulted in suitable predictions. Additionally, as discussed in Section 4.4, the cardiomyocyte action potential characteristics were fairly insensitive to variations with these approximated parameters.

Another limiting feature of this model was that ionic pumps, such as the sodium-calcium and sodium-potassium exchangers, were not accounted for in this model. As a result, the intracellular ionic concentration variations were not accounted for over time. However, these effects are expected to be negligible in action potential duration, activation threshold, conduction velocity, and maximum upstroke velocity, making it excessive and unnecessary for the purposes of this study.

4.5.2 Future Work

This promising model leaves opportunity for several future studies. These include: 1) improving the mesenchymal stem cell model; 2) confirming it with patch clamping experiments; 3) coupling the improved model with diseased cardiomyocytes for further insight; 4) determining the functional ion channels that affect the cardiomyocyte action potential duration most; and 5) empirically blocking the functional ion channels that affect the cardiomyocyte action potential duration most.

First, the necessary improvements will be made to the mesenchymal stem cell model, as discussed in Section 4.5.1. Next, this model will be confirmed by empirically coupling mesenchymal stem cells with cardiomyocytes at various ratios. By making the necessary improvements discussed in Section 4.5.1 on the model, numerous insights could be developed on the methods and consequences of clinically applying mesenchymal stem cells. For example, it is subsequently possible to couple the improved mesenchymal stem cell model with diseased cardiomyocyte for further insight into mesenchymal stem cell effects on damaged cardiomyocytes following a myocardial infarction. Furthermore, the functional mesenchymal ion channels that affect the cardiomyocyte action potential duration most can be determined via a more rigorous

parameter sensitivity analysis. Following this analysis, the appropriate modifications would be empirically made to mesenchymal stem cell functional ion channels expressed in order to minimize variation in action potential characteristics. Furthermore, vascular endothelial growth factor (VEGF) could be delivered with this electrically-optimized mesenchymal stem cell system via VEGF gene-transfection [109]. This would result in major improvement of cardiac function, while minimizing potential arrhythmogenic effects of mesenchymal stem cells.

Chapter 5

Conclusion

To better understand the electrical role of mesenchymal stem cells, three novel electrophysiology models were developed. Subsequently, the consequences of electrical interactions between cardiomyocytes and mesenchymal stem cells were predicted by coupling the ten Tusscher cardiomyocyte model to the three novel models developed in this study. Significant electrophysiological consequences were evident when the ten Tusscher model was coupled to each of the mesenchymal stem cell models in ratios of 9:1, 4:1, and 1:1, respectively. These effects include decreases in action potential duration and plateau height, and corresponding variations in ionic current. Furthermore, there was a decrease in both conduction velocity and maximum upstroke velocity. As the ratio of mesenchymal stem cells to cardiomyocytes increased, these effects became even more drastic. Since the membrane potential for mesenchymal stem cells (-42 mV to -12 mV) is greater than for cardiomyocytes (-85 mV), the activation threshold decreased for a cardiomyocyte action potential. These consequences correspond to the *in vitro* electrical effects previously described, and show

mesenchymal stem cells are indeed capable of predisposing re-entrant arrhythmias. A sensitivity analysis on the mesenchymal stem cell inputs shows the robustness of the results. This promising model leaves opportunity for countless future studies. These include: 1) improving the mesenchymal stem cell model; 2) confirming it with patch clamping experiments; 3) coupling the improved model with diseased cardiomyocytes for further insight; 4) determining the functional ion channels that affect the cardiomyocyte action potential duration most; and 5) empirically blocking the functional ion channels that affect the cardiomyocyte action potential duration most.

Appendix A

Sample MATLAB Code

A.1 Sample Data Fitting Code

```
1 % Josh Mayourian
2 % Transient Outward Activation Time Constant Fit
3
4 clc; % Clear command window
5 clear all; % Clear workspace
6 t = 0:10:60; % Voltages (mV) where time constant was evaluated
7 y = [22 9 3.5 3 3.8 4.4 5.7]; %
8
9 format long;
10 y = y;
11 % Plotting empirical data
12 plot(t,y,'black.', 'LineWidth', 1.5, 'MarkerSize', 30);
13
14 % Fitting empirical data
15 F = @(x,xdata) x(1).*exp(-(xdata+x(2)).*(xdata+x(2))/x(3))...
16     +x(4).*exp(-(xdata+x(5)).*(xdata+x(5))/x(6))+x(2);
17
18 x0 = [6 1 180 1 -55 900 1]; %Initial guesses
```

```
19 options = optimset('MaxFunEvals',2000,'MaxIter',400,'TolFun',1e-4);  
20  
21 % Using lsqcurvefit  
22 [x,resnorm,[],exitflag,output] = lsqcurvefit(F,x0,t,y,[],[],options);  
23  
24 hold on;  
25  
26 % Plotting results  
27 tt = -10:.1:60;  
28 plot(tt,F(x,tt),'black','LineWidth',3);  
29 title('Transient Outward Activation Time Constant Fit','interpreter',...
30      'latex', 'FontSize', 20);  
31 xlabel(['Voltage (mV)'],'interpreter','latex', 'FontSize', 20)  
32 ylabel(['Time (ms)'],'interpreter','latex', 'FontSize', 20)  
33 set(gca,'FontSize',20)  
34 hold off;
```

A.2 Sample Individual Ion Channel Current Code

```

1 % Josh Mayourian
2 % Delayed Rectifier Current Simulation
3
4 function current_3
5 clear all; % clear workspace
6 clc; % clear command window
7 V = 10; % Voltage clamp simulation
8
9
10 % Define Constants
11
12 R = 8.314e-3; % Gas constant (J/mmol/K)
13 T = 310; % Temperature (K)
14 F = 96.5; % Faraday's constant (C/mmol)
15 z = 1; % Potassium valence charge
16 Ko = 5.4; % Extracellular Potassium concentration (mmol)
17 Ki = 140; % Intracellular Potassium concentration (mmol)
18
19 domain = [0 300]; % time domain
20 initialvalues = [0 .36 0 0 .64 0]; % initial conditions
21
22 [t,y] = ode45(@ff,domain,initialvalues); % Calling ode function
23 E = 1000*(R.*T./z./F).*log(Ko/Ki);
24 r = 6.5*(V-E).*(y(:,6)); % equivalent to 6x(V+87.0)
25
26 % Plotting results
27 plot(t,r,'black','LineWidth',3);
28 title(['Delayed Rectifier Current Simulation'],'interpreter',...
29 'latex','FontSize',20)
30 xlabel(['Voltage (mV)'],'interpreter','latex','FontSize', 20)
31 ylabel(['Current (pA)'],'interpreter','latex','FontSize', 20)
32 set(gca,'FontSize',20)
33 hold on;
34

```

```
35 % System of ODEs from markov chain model
36 function xdot = ff(t,y)
37
38 xdot = zeros(6,1);
39
40 gamma1 = 2.52.*exp(-(V-53.16).^2/593.7)+2.44;
41 gamma2 = 8.2.*exp(-(V-55.2).^2/659.9);
42 alpha = 0.028./(1+0.86.*exp((V-10.0)./-12.35)).*.6;
43 beta = 3e-4.*((125.5+V)./(1+26.9.*exp(-(V-47.4)/-14.6))).*.6;
44 xdot(1) = 1e-1.*beta.*y(2)-10.*alpha.*y(1); % dp0/dt
45 xdot(2) = (10.*alpha.*y(1)+2*beta.*y(3) - ...
46 (1e-1.*beta+3*alpha).*y(2)); %dp1/dt
47 xdot(3) = (3*alpha.*y(2)+3*beta.*y(4) - ...
48 (2*beta+2*alpha).*y(3)); %dp2/dt
49 xdot(4) = (2*alpha.*y(3)+4*beta.*y(5) - ...
50 (3*beta+alpha).*y(4)); %dp3/dt
51 xdot(5) = (alpha.*y(4)+gamma2.*beta.*y(6) - ...
52 (4*beta+gamma1.*alpha).*y(5)); %dp4/dt
53 xdot(6) = gamma1.*alpha.*y(5)-gamma2.*beta.*y(6); %dp5/dt
54
55 end
56
57
58 end
```

A.3 Sample Total Mesenchymal Stem Cell Current Code

```

1 function current
2
3 % Josh Mayourian
4 % Total Current A
5
6 R = 8.314e-3; % Gas constant (J/mmol/K)
7 T = 310; % Temperature (K)
8 F = 96.5; % Faraday's constant (C/mmol)
9 z = 1; % Potassium valence charge
10 Ko = 5.4; % Extracellular Potassium concentration (mmol)
11 Ki = 140; % Intracellular Potassium concentration (mmol)
12
13
14 % System of ODEs
15 function xdot = current1(t,y)
16
17 xdot = zeros(7,1);
18
19 % Delayed rectifier ODEs
20 gamma1 = 2.52.*exp(-(V-53.16).^2/593.7)+2.44;
21 gamma2 = 8.2.*exp(-(V-55.2).^2/659.9);
22 alpha = 0.028./(1+0.86.*exp((V-10.0)./-12.35));
23 beta = 3e-4.*((125.5+V)./(1+26.9.*exp(-(V-47.4)/-14.6)));
24 xdot(1) = 1e-1.*beta.*y(2)-10.*alpha.*y(1); %dp0/dt
25 xdot(2) = (10.*alpha.*y(1)+2*beta.*y(3) - ...
26 (1e-1.*beta+3*alpha).*y(2)); %dp1/dt
27 xdot(3) = (3*alpha.*y(2)+3*beta.*y(4) - ...
28 (2*beta+2*alpha).*y(3)); %dp2/dt
29 xdot(4) = (2*alpha.*y(3)+4*beta.*y(5) - ...
30 (3*beta+alpha).*y(4)); %dp3/dt
31 xdot(5) = (alpha.*y(4)+gamma2.*beta.*y(6) - ...
32 (4*beta+gamma1.*alpha).*y(5)); %dp4/dt

```

```
33 xdot(6) = gamma1.*alpha.*y(5)-gamma2.*beta.*y(6); %dp5/dt
34
35
36 % KCa ODE
37 Ca = 1e-4;
38 xdot(7) = (1-y(7)).*687.8.*Ca.*exp(V./15.8) - ...
39 y(7).*21.1.*exp(-V./43.5);
40
41 end
42
43 % Plotting results
44 for V = -60:10:60;
45
46 domain = [0 300]; % Time domain
47 initialvalues = [0 .36 0 0 .64 0 0]; % Initial Conditions
48 [t,y] = ode45(@current1,domain,initialvalues);
49 E_k = 1000*(R.*T./z./F).*log(Ko/Ki);
50 r = 3*(V-E_k).*y(:,7) + 6.5*(V-E_k).*(y(:,6)); % I_dr + I_KCa
51 plot(t,r,'black','LineWidth',3);
52 title(['Total Current A Simulation'], 'interpreter',...
53 'latex', 'FontSize', 20)
54 xlabel(['Time (ms)'], 'interpreter', 'latex', 'FontSize', 20)
55 ylabel(['Current (pA)'], 'interpreter', 'latex', 'FontSize', 20)
56 set(gca, 'FontSize', 20)
57 hold on;
58 hold on;
59
60
61 end
62
63 end
```

A.4 Sample CM-hMSC Coupling Code

```
1 % Josh Mayourian
2 % Coupling of CM and hMSC Total Current A
3 % Adaptation of Open-Source cellML model
4
5 % Source: http://models.cellml.org/exposure/
6 %a7179d94365ff0c9c0e6eb7c6a787d3d/ten_tusscher_model_2006_
7 %IK1Ko_M_units.cellml/@@cellml_codegen/MATLAB/raw
8
9 % Typical CellML ‘‘Book keeping’’
10
11
12 function [VOI, STATES, ALGEBRAIC, CONSTANTS] = A
13 clear all;
14 [VOI, STATES, ALGEBRAIC, CONSTANTS] = solveModel();
15
16 end
17
18 function [algebraicVariableCount] = getAlgebraicVariableCount()
19 algebraicVariableCount =81; % Number of variables
20 end
21
22 function [VOI, STATES, ALGEBRAIC, CONSTANTS] = solveModel()
23
24 global algebraicVariableCount;
25 algebraicVariableCount = getAlgebraicVariableCount();
26
27
28 [INIT_STATES, CONSTANTS] = initConsts;
29
30 tspan = [0, 10500]; % Domain to integrate over
31
32 % Integrating options
33 options = odeset('RelTol', 1e-06, 'AbsTol', 1e-06, 'MaxStep', 1);
34
```

```
35 % Ode solver
36 [VOI, STATES] = ode15s(@(VOI, STATES)computeRates(VOI, STATES, ...
37 CONSTANTS), tspan, INIT_STATES, options);
38
39 % Computing the algebraic variables
40 [RATES, ALGEBRAIC] = computeRates(VOI, STATES, CONSTANTS);
41 ALGEBRAIC = computeAlgebraic(ALGEBRAIC, CONSTANTS, STATES, VOI);
42
43 % Plotting the results
44 [LEGEND_STATES, LEGEND_ALGEBRAIC, LEGEND_VOI, LEGEND_CONSTANTS] = ...
45 createLegends();
46
47 plot(VOI-10000, STATES(:,1),'color',[0.5 0.5 0.5], 'linewidth',3);
48 title(['Cardiomyocyte-Mesenchymal Stem Cell Interaction Simulation'], 'interpreter',...
49 'latex', 'FontSize', 20);
50 xlabel(['Time (ms)'], 'interpreter', 'latex', 'FontSize', 20)
51 ylabel(['Voltage (mV)'], 'interpreter', 'latex', 'FontSize', 20)
52 set(gca, 'FontSize', 20);
53 set(legend, 'interpreter', 'latex');
54 legend('Control', '9:1 (CM:hMSC)', '4:1 (CM:hMSC)', '1:1 (CM:hMSC)');
55 hold on;
56
57
58 end
59
60 function [LEGEND_STATES, LEGEND_ALGEBRAIC, LEGEND_VOI, LEGEND_CONSTANTS] ...
61 = createLegends()
62 LEGEND_STATES = ';;'; LEGEND_ALGEBRAIC = ';;'; LEGEND_VOI = ';;'; LEGEND_CONSTANTS = ';;';
63
64 %%% Step 1: ten Tusscher cardiomyocyte model
65
66
67 LEGEND_VOI = strpad('time in component environment (millisecond)');
68 LEGEND_STATES(:,1) = strpad('V in component membrane (millivolt)');
69 LEGEND_CONSTANTS(:,1) = strpad('R in component membrane (joule_per_mole_kelvin)');
70 LEGEND_CONSTANTS(:,2) = strpad('T in component membrane (kelvin)');
```

```

71 LEGEND_CONSTANTS(:,3) = strpad('F in component membrane (coulomb_per_millimole)');
72 LEGEND_CONSTANTS(:,4) = strpad('Cm in component membrane (microF)');
73 LEGEND_CONSTANTS(:,5) = strpad('V_c in component membrane (micrometre3)');
74 LEGEND_ALGEBRAIC(:,48) = strpad('i_K1 in component inward_rectifier_potassium_current (
    picoA_per_picoF)');
75 LEGEND_ALGEBRAIC(:,55) = strpad('i_to in component transient_outward_current (picoA_per_picoF)');
76 LEGEND_ALGEBRAIC(:,49) = strpad('i_Kr in component rapid_time_dependent_potassium_current (
    picoA_per_picoF)');
77 LEGEND_ALGEBRAIC(:,50) = strpad('i_Ks in component slow_time_dependent_potassium_current (
    picoA_per_picoF)');
78 LEGEND_ALGEBRAIC(:,53) = strpad('i_CaL in component L_type_Ca_current (picoA_per_picoF)');
79 LEGEND_ALGEBRAIC(:,56) = strpad('i_NaK in component sodium_potassium_pump_current (picoA_per_picoF)'
);
80 LEGEND_ALGEBRAIC(:,51) = strpad('i_Na in component fast_sodium_current (picoA_per_picoF)');
81 LEGEND_ALGEBRAIC(:,52) = strpad('i_b_Na in component sodium_background_current (picoA_per_picoF)');
82 LEGEND_ALGEBRAIC(:,57) = strpad('i_NaCa in component sodium_calcium_exchanger_current (
    picoA_per_picoF)');
83 LEGEND_ALGEBRAIC(:,54) = strpad('i_b_Ca in component calcium_background_current (picoA_per_picoF)');
84 LEGEND_ALGEBRAIC(:,59) = strpad('i_p_K in component potassium_pump_current (picoA_per_picoF)');
85 LEGEND_ALGEBRAIC(:,58) = strpad('i_p_Ca in component calcium_pump_current (picoA_per_picoF)');
86 LEGEND_ALGEBRAIC(:,13) = strpad('i_Stim in component membrane (picoA_per_picoF)');
87 LEGEND_CONSTANTS(:,6) = strpad('stim_start in component membrane (millisecond)');
88 LEGEND_CONSTANTS(:,7) = strpad('stim_period in component membrane (millisecond)');
89 LEGEND_CONSTANTS(:,8) = strpad('stim_duration in component membrane (millisecond)');
90 LEGEND_CONSTANTS(:,9) = strpad('stim_amplitude in component membrane (picoA_per_picoF)');
91 LEGEND_ALGEBRAIC(:,26) = strpad('E_Na in component reversal_potentials (millivolt)');
92 LEGEND_ALGEBRAIC(:,34) = strpad('E_K in component reversal_potentials (millivolt)');
93 LEGEND_ALGEBRAIC(:,42) = strpad('E_Ks in component reversal_potentials (millivolt)');
94 LEGEND_ALGEBRAIC(:,44) = strpad('E_Ca in component reversal_potentials (millivolt)');
95 LEGEND_CONSTANTS(:,10) = strpad('P_kna in component reversal_potentials (dimensionless)');
96 LEGEND_CONSTANTS(:,11) = strpad('K_o in component potassium_dynamics (millimolar)');
97 LEGEND_CONSTANTS(:,12) = strpad('Na_o in component sodium_dynamics (millimolar)');
98 LEGEND_STATES(:,2) = strpad('K_i in component potassium_dynamics (millimolar)');
99 LEGEND_STATES(:,3) = strpad('Na_i in component sodium_dynamics (millimolar)');
100 LEGEND_CONSTANTS(:,13) = strpad('Ca_o in component calcium_dynamics (millimolar)');
101 LEGEND_STATES(:,4) = strpad('Ca_i in component calcium_dynamics (millimolar)');

```

```

102 LEGEND_CONSTANTS(:,14) = strpad('g_K1 in component inward_rectifier_potassium_current (
    nanoS_per_picoF)');
103 LEGEND_ALGEBRAIC(:,47) = strpad('xK1_inf in component inward_rectifier_potassium_current (
    dimensionless)');
104 LEGEND_ALGEBRAIC(:,45) = strpad('alpha_K1 in component inward_rectifier_potassium_current (
    dimensionless)');
105 LEGEND_ALGEBRAIC(:,46) = strpad('beta_K1 in component inward_rectifier_potassium_current (
    dimensionless)');
106 LEGEND_CONSTANTS(:,15) = strpad('g_Kr in component rapid_time_dependent_potassium_current (
    nanoS_per_picoF)');
107 LEGEND_STATES(:,5) = strpad('Xr1 in component rapid_time_dependent_potassium_current_Xr1_gate (
    dimensionless)');
108 LEGEND_STATES(:,6) = strpad('Xr2 in component rapid_time_dependent_potassium_current_Xr2_gate (
    dimensionless)');
109 LEGEND_ALGEBRAIC(:,1) = strpad('xr1_inf in component rapid_time_dependent_potassium_current_Xr1_gate (
    dimensionless)');
110 LEGEND_ALGEBRAIC(:,14) = strpad('alpha_xr1 in component
    rapid_time_dependent_potassium_current_Xr1_gate (dimensionless)');
111 LEGEND_ALGEBRAIC(:,27) = strpad('beta_xr1 in component
    rapid_time_dependent_potassium_current_Xr1_gate (dimensionless)');
112 LEGEND_ALGEBRAIC(:,35) = strpad('tau_xr1 in component
    rapid_time_dependent_potassium_current_Xr1_gate (millisecond)');
113 LEGEND_ALGEBRAIC(:,2) = strpad('xr2_inf in component rapid_time_dependent_potassium_current_Xr2_gate (
    dimensionless)');
114 LEGEND_ALGEBRAIC(:,15) = strpad('alpha_xr2 in component
    rapid_time_dependent_potassium_current_Xr2_gate (dimensionless)');
115 LEGEND_ALGEBRAIC(:,28) = strpad('beta_xr2 in component
    rapid_time_dependent_potassium_current_Xr2_gate (dimensionless)');
116 LEGEND_ALGEBRAIC(:,36) = strpad('tau_xr2 in component
    rapid_time_dependent_potassium_current_Xr2_gate (millisecond)');
117 LEGEND_CONSTANTS(:,16) = strpad('g_Ks in component slow_time_dependent_potassium_current (
    nanoS_per_picoF)');
118 LEGEND_STATES(:,7) = strpad('Xs in component slow_time_dependent_potassium_current_Xs_gate (
    dimensionless)');
119 LEGEND_ALGEBRAIC(:,3) = strpad('xs_inf in component slow_time_dependent_potassium_current_Xs_gate (
    dimensionless)');

```

```

120 LEGEND_ALGEBRAIC(:,16) = strpad('alpha_xs in component slow_time_dependent_potassium_current_Xs_gate
(dimensionless)');
121 LEGEND_ALGEBRAIC(:,29) = strpad('beta_xs in component slow_time_dependent_potassium_current_Xs_gate
(dimensionless)');
122 LEGEND_ALGEBRAIC(:,37) = strpad('tau_xs in component slow_time_dependent_potassium_current_Xs_gate (
millisecond)');
123 LEGEND_CONSTANTS(:,17) = strpad('g_Na in component fast_sodium_current (nanoS_per_picoF)');
124 LEGEND_STATES(:,8) = strpad('m in component fast_sodium_current_m_gate (dimensionless)');
125 LEGEND_STATES(:,9) = strpad('h in component fast_sodium_current_h_gate (dimensionless)');
126 LEGEND_STATES(:,10) = strpad('j in component fast_sodium_current_j_gate (dimensionless)');
127 LEGEND_ALGEBRAIC(:,4) = strpad('m_inf in component fast_sodium_current_m_gate (dimensionless)');
128 LEGEND_ALGEBRAIC(:,17) = strpad('alpha_m in component fast_sodium_current_m_gate (dimensionless)');
129 LEGEND_ALGEBRAIC(:,30) = strpad('beta_m in component fast_sodium_current_m_gate (dimensionless)');
130 LEGEND_ALGEBRAIC(:,38) = strpad('tau_m in component fast_sodium_current_m_gate (millisecond)');
131 LEGEND_ALGEBRAIC(:,5) = strpad('h_inf in component fast_sodium_current_h_gate (dimensionless)');
132 LEGEND_ALGEBRAIC(:,18) = strpad('alpha_h in component fast_sodium_current_h_gate (per_millisecond)')
;
133 LEGEND_ALGEBRAIC(:,31) = strpad('beta_h in component fast_sodium_current_h_gate (per_millisecond)');
134 LEGEND_ALGEBRAIC(:,39) = strpad('tau_h in component fast_sodium_current_h_gate (millisecond)');
135 LEGEND_ALGEBRAIC(:,6) = strpad('j_inf in component fast_sodium_current_j_gate (dimensionless)');
136 LEGEND_ALGEBRAIC(:,19) = strpad('alpha_j in component fast_sodium_current_j_gate (per_millisecond)')
;
137 LEGEND_ALGEBRAIC(:,32) = strpad('beta_j in component fast_sodium_current_j_gate (per_millisecond)');
138 LEGEND_ALGEBRAIC(:,40) = strpad('tau_j in component fast_sodium_current_j_gate (millisecond)');
139 LEGEND_CONSTANTS(:,18) = strpad('g_bna in component sodium_background_current (nanoS_per_picoF)');
140 LEGEND_CONSTANTS(:,19) = strpad('g_CaL in component L_type_Ca_current (litre_per_farad_second)');
141 LEGEND_STATES(:,11) = strpad('Ca_ss in component calcium_dynamics (millimolar)');
142 LEGEND_STATES(:,12) = strpad('d in component L_type_Ca_current_d_gate (dimensionless)');
143 LEGEND_STATES(:,13) = strpad('f in component L_type_Ca_current_f_gate (dimensionless)');
144 LEGEND_STATES(:,14) = strpad('f2 in component L_type_Ca_current_f2_gate (dimensionless)');
145 LEGEND_STATES(:,15) = strpad('fCass in component L_type_Ca_current_fCass_gate (dimensionless)');
146 LEGEND_ALGEBRAIC(:,7) = strpad('d_inf in component L_type_Ca_current_d_gate (dimensionless)');
147 LEGEND_ALGEBRAIC(:,20) = strpad('alpha_d in component L_type_Ca_current_d_gate (dimensionless)');
148 LEGEND_ALGEBRAIC(:,33) = strpad('beta_d in component L_type_Ca_current_d_gate (dimensionless)');
149 LEGEND_ALGEBRAIC(:,41) = strpad('gamma_d in component L_type_Ca_current_d_gate (millisecond)');
150 LEGEND_ALGEBRAIC(:,43) = strpad('tau_d in component L_type_Ca_current_d_gate (millisecond)');

```

```

151 LEGEND_ALGEBRAIC(:,8) = strpad('f_inf in component L_type_Ca_current_f_gate (dimensionless)');
152 LEGEND_ALGEBRAIC(:,21) = strpad('tau_f in component L_type_Ca_current_f_gate (millisecond)');
153 LEGEND_ALGEBRAIC(:,9) = strpad('f2_inf in component L_type_Ca_current_f2_gate (dimensionless)');
154 LEGEND_ALGEBRAIC(:,22) = strpad('tau_f2 in component L_type_Ca_current_f2_gate (millisecond)');
155 LEGEND_ALGEBRAIC(:,10) = strpad('fCass_inf in component L_type_Ca_current_fCass_gate (dimensionless)');
156 LEGEND_ALGEBRAIC(:,23) = strpad('tau_fCass in component L_type_Ca_current_fCass_gate (millisecond)')
;
157 LEGEND_CONSTANTS(:,20) = strpad('g_bca in component calcium_background_current (nanoS_per_picoF)');
158 LEGEND_CONSTANTS(:,21) = strpad('g_to in component transient_outward_current (nanoS_per_picoF)');
159 LEGEND_STATES(:,16) = strpad('s in component transient_outward_current_s_gate (dimensionless)');
160 LEGEND_STATES(:,17) = strpad('r in component transient_outward_current_r_gate (dimensionless)');
161 LEGEND_ALGEBRAIC(:,11) = strpad('s_inf in component transient_outward_current_s_gate (dimensionless)');
162 LEGEND_ALGEBRAIC(:,24) = strpad('tau_s in component transient_outward_current_s_gate (millisecond)')
;
163 LEGEND_ALGEBRAIC(:,12) = strpad('r_inf in component transient_outward_current_r_gate (dimensionless)');
164 LEGEND_ALGEBRAIC(:,25) = strpad('tau_r in component transient_outward_current_r_gate (millisecond)')
;
165 LEGEND_CONSTANTS(:,22) = strpad('P_NaK in component sodium_potassium_pump_current (picoA_per_picoF)');
;
166 LEGEND_CONSTANTS(:,23) = strpad('K_mk in component sodium_potassium_pump_current (millimolar)');
167 LEGEND_CONSTANTS(:,24) = strpad('K_mNa in component sodium_potassium_pump_current (millimolar)');
168 LEGEND_CONSTANTS(:,25) = strpad('K_NaCa in component sodium_calcium_exchanger_current (
picoA_per_picoF)');
;
169 LEGEND_CONSTANTS(:,26) = strpad('K_sat in component sodium_calcium_exchanger_current (dimensionless)');
;
170 LEGEND_CONSTANTS(:,27) = strpad('alpha in component sodium_calcium_exchanger_current (dimensionless)');
;
171 LEGEND_CONSTANTS(:,28) = strpad('gamma in component sodium_calcium_exchanger_current (dimensionless)');
;
172 LEGEND_CONSTANTS(:,29) = strpad('Km_Ca in component sodium_calcium_exchanger_current (millimolar)');
173 LEGEND_CONSTANTS(:,30) = strpad('Km_Nai in component sodium_calcium_exchanger_current (millimolar)')
;
174 LEGEND_CONSTANTS(:,31) = strpad('g_pCa in component calcium_pump_current (picoA_per_picoF)');
;
```

```

175 LEGEND_CONSTANTS(:,32) = strpad('K_pCa in component calcium_pump_current (millimolar)');
176 LEGEND_CONSTANTS(:,33) = strpad('g_pK in component potassium_pump_current (nanoS_per_picoF)');
177 LEGEND_STATES(:,18) = strpad('Ca_SR in component calcium_dynamics (millimolar)');
178 LEGEND_ALGEBRAIC(:,68) = strpad('i_rel in component calcium_dynamics (millimolar_per_millisecond)');
179 LEGEND_ALGEBRAIC(:,60) = strpad('i_up in component calcium_dynamics (millimolar_per_millisecond)');
180 LEGEND_ALGEBRAIC(:,61) = strpad('i_leak in component calcium_dynamics (millimolar_per_millisecond)')
;
181 LEGEND_ALGEBRAIC(:,62) = strpad('i_xfer in component calcium_dynamics (millimolar_per_millisecond)')
;
182 LEGEND_ALGEBRAIC(:,67) = strpad('0 in component calcium_dynamics (dimensionless)');
183 LEGEND_STATES(:,19) = strpad('R_prime in component calcium_dynamics (dimensionless)');
184 LEGEND_ALGEBRAIC(:,65) = strpad('k1 in component calcium_dynamics (per_millimolar2_per_millisecond)')
);
185 LEGEND_ALGEBRAIC(:,66) = strpad('k2 in component calcium_dynamics (per_millimolar_per_millisecond)')
;
186 LEGEND_CONSTANTS(:,34) = strpad('k1_prime in component calcium_dynamics (
per_millimolar2_per_millisecond)');
187 LEGEND_CONSTANTS(:,35) = strpad('k2_prime in component calcium_dynamics (
per_millimolar_per_millisecond)');
188 LEGEND_CONSTANTS(:,36) = strpad('k3 in component calcium_dynamics (per_millisecond)');
189 LEGEND_CONSTANTS(:,37) = strpad('k4 in component calcium_dynamics (per_millisecond)');
190 LEGEND_CONSTANTS(:,38) = strpad('EC in component calcium_dynamics (millimolar)');
191 LEGEND_CONSTANTS(:,39) = strpad('max_sr in component calcium_dynamics (dimensionless)');
192 LEGEND_CONSTANTS(:,40) = strpad('min_sr in component calcium_dynamics (dimensionless)');
193 LEGEND_ALGEBRAIC(:,63) = strpad('kcavr in component calcium_dynamics (dimensionless)');
194 LEGEND_CONSTANTS(:,41) = strpad('V_rel in component calcium_dynamics (per_millisecond)');
195 LEGEND_CONSTANTS(:,42) = strpad('V_xfer in component calcium_dynamics (per_millisecond)');
196 LEGEND_CONSTANTS(:,43) = strpad('K_up in component calcium_dynamics (millimolar)');
197 LEGEND_CONSTANTS(:,44) = strpad('V_leak in component calcium_dynamics (per_millisecond)');
198 LEGEND_CONSTANTS(:,45) = strpad('Vmax_up in component calcium_dynamics (millimolar_per_millisecond)')
);
199 LEGEND_ALGEBRAIC(:,64) = strpad('Ca_i_bufc in component calcium_dynamics (dimensionless)');
200 LEGEND_ALGEBRAIC(:,69) = strpad('Ca_sr_bufsr in component calcium_dynamics (dimensionless)');
201 LEGEND_ALGEBRAIC(:,70) = strpad('Ca_ss_bufss in component calcium_dynamics (dimensionless)');
202 LEGEND_CONSTANTS(:,46) = strpad('Buf_c in component calcium_dynamics (millimolar)');
203 LEGEND_CONSTANTS(:,47) = strpad('K_buf_c in component calcium_dynamics (millimolar)');

```

```

204 LEGEND_CONSTANTS(:,48) = strpad('Buf_sr in component calcium_dynamics (millimolar)');
205 LEGEND_CONSTANTS(:,49) = strpad('K_buf_sr in component calcium_dynamics (millimolar)');
206 LEGEND_CONSTANTS(:,50) = strpad('Buf_ss in component calcium_dynamics (millimolar)');
207 LEGEND_CONSTANTS(:,51) = strpad('K_buf_ss in component calcium_dynamics (millimolar)');
208 LEGEND_CONSTANTS(:,52) = strpad('V_sr in component calcium_dynamics (micrometre3)');
209 LEGEND_CONSTANTS(:,53) = strpad('V_ss in component calcium_dynamics (micrometre3)');
210 LEGEND_RATES(:,1) = strpad('d/dt V in component membrane (millivolt)');
211 LEGEND_RATES(:,5) = strpad('d/dt Xr1 in component rapid_time_dependent_potassium_current_Xr1_gate (
    dimensionless)');
212 LEGEND_RATES(:,6) = strpad('d/dt Xr2 in component rapid_time_dependent_potassium_current_Xr2_gate (
    dimensionless)');
213 LEGEND_RATES(:,7) = strpad('d/dt Xs in component slow_time_dependent_potassium_current_Xs_gate (
    dimensionless)');
214 LEGEND_RATES(:,8) = strpad('d/dt m in component fast_sodium_current_m_gate (dimensionless)');
215 LEGEND_RATES(:,9) = strpad('d/dt h in component fast_sodium_current_h_gate (dimensionless)');
216 LEGEND_RATES(:,10) = strpad('d/dt j in component fast_sodium_current_j_gate (dimensionless)');
217 LEGEND_RATES(:,12) = strpad('d/dt d in component L_type_Ca_current_d_gate (dimensionless)');
218 LEGEND_RATES(:,13) = strpad('d/dt f in component L_type_Ca_current_f_gate (dimensionless)');
219 LEGEND_RATES(:,14) = strpad('d/dt f2 in component L_type_Ca_current_f2_gate (dimensionless)');
220 LEGEND_RATES(:,15) = strpad('d/dt fCass in component L_type_Ca_current_fCass_gate (dimensionless)');
221 LEGEND_RATES(:,16) = strpad('d/dt s in component transient_outward_current_s_gate (dimensionless)');
222 LEGEND_RATES(:,17) = strpad('d/dt r in component transient_outward_current_r_gate (dimensionless)');
223 LEGEND_RATES(:,19) = strpad('d/dt R_prime in component calcium_dynamics (dimensionless)');
224 LEGEND_RATES(:,4) = strpad('d/dt Ca_i in component calcium_dynamics (millimolar)');
225 LEGEND_RATES(:,18) = strpad('d/dt Ca_SR in component calcium_dynamics (millimolar)');
226 LEGEND_RATES(:,11) = strpad('d/dt Ca_ss in component calcium_dynamics (millimolar)');
227 LEGEND_RATES(:,3) = strpad('d/dt Na_i in component sodium_dynamics (millimolar)');
228 LEGEND_RATES(:,2) = strpad('d/dt K_i in component potassium_dynamics (millimolar)');
229
230
231 % Step 2: hMSC model
232
233 LEGEND_RATES(:,20) = strpad('d/dt p0 in component delayed_rectifier_for_hMSC');
234 LEGEND_RATES(:,21) = strpad('d/dt p1 in component delayed_rectifier_for_hMSC');
235 LEGEND_RATES(:,22) = strpad('d/dt p2 in component delayed_rectifier_for_hMSC');
236 LEGEND_RATES(:,23) = strpad('d/dt p3 in component delayed_rectifier_for_hMSC');

```

```
237 LEGEND_RATES(:,24) = strpad('d/dt p4 in component delayed rectifier for hMSC');
238 LEGEND_RATES(:,25) = strpad('d/dt p5 in component delayed rectifier for hMSC');
239
240 LEGEND_RATES(:,26) = strpad('d/dt m in component calcium activated potassium for hMSC');
241 LEGEND_RATES(:,27) = strpad('d/dt K_i in component potassium dynamics for hMSC');
242
243 LEGEND_STATES(:,20) = strpad('p0 in component delayed rectifier for hMSC');
244 LEGEND_STATES(:,21) = strpad('p1 in component delayed rectifier for hMSC');
245 LEGEND_STATES(:,22) = strpad('p2 in component delayed rectifier for hMSC');
246 LEGEND_STATES(:,23) = strpad('p3 in component delayed rectifier for hMSC');
247 LEGEND_STATES(:,24) = strpad('p4 in component delayed rectifier for hMSC');
248 LEGEND_STATES(:,25) = strpad('p5 in component delayed rectifier for hMSC');
249
250 LEGEND_STATES(:,26) = strpad('m in component calcium activated potassium for hMSC');
251
252 LEGEND_STATES(:,27) = strpad('K_i in component potassium dynamics for hMSC (mmol)');
253
254 LEGEND_STATES(:,28) = strpad('V in component hMSC membrane (mV)');
255
256
257 LEGEND_ALGEBRAIC(:,71) = strpad('gamma1');
258 LEGEND_ALGEBRAIC(:,72) = strpad('gamma2');
259 LEGEND_ALGEBRAIC(:,73) = strpad('alpha');
260 LEGEND_ALGEBRAIC(:,74) = strpad('beta');
261 LEGEND_ALGEBRAIC(:,75) = strpad('theta1');
262 LEGEND_ALGEBRAIC(:,76) = strpad('theta2');
263 LEGEND_ALGEBRAIC(:,77) = strpad('alpha_kca');
264 LEGEND_ALGEBRAIC(:,78) = strpad('beta_kca');
265 LEGEND_ALGEBRAIC(:,79) = strpad('Nernst potential for potassium');
266 LEGEND_ALGEBRAIC(:,80) = strpad('delayed rectifier current');
267 LEGEND_ALGEBRAIC(:,81) = strpad('calcium activated potassium channel current');
268
269
270
271 LEGEND_STATES = LEGEND_STATES';
272 LEGEND_ALGEBRAIC = LEGEND_ALGEBRAIC';
```

```
273 LEGEND_RATES = LEGEND_RATES';  
274 LEGEND_CONSTANTS = LEGEND_CONSTANTS';  
275 end  
276  
277 function [STATES, CONSTANTS] = initConsts()  
278  
279  
280  
281 % Defining constants and initial values  
282  
283  
284 VOI = 0; CONSTANTS = [] ; STATES = [] ; ALGEBRAIC = [] ;  
285  
286  
287 % Cardiomyocyte constants and initial values  
288  
289 STATES(:,1) = -85.423;  
290 CONSTANTS(:,1) = 8314.472;  
291 CONSTANTS(:,2) = 310;  
292 CONSTANTS(:,3) = 96485.3415;  
293 CONSTANTS(:,4) = 0.185;  
294 CONSTANTS(:,5) = 0.016404;  
295 CONSTANTS(:,6) = 10;  
296 CONSTANTS(:,7) = 1000;  
297 CONSTANTS(:,8) = 1;  
298 CONSTANTS(:,9) = 52;  
299 CONSTANTS(:,10) = 0.03;  
300 CONSTANTS(:,11) = 5.4;  
301 CONSTANTS(:,12) = 140;  
302 STATES(:,2) = 138.52;  
303 STATES(:,3) = 10.132;  
304 CONSTANTS(:,13) = 2;  
305 STATES(:,4) = 0.000153;  
306 CONSTANTS(:,14) = 5.405;  
307 CONSTANTS(:,15) = 0.153;  
308 STATES(:,5) = 0.0165;
```

```
309 STATES(:,6) = 0.473;
310 CONSTANTS(:,16) = 0.098;
311 STATES(:,7) = 0.0174;
312 CONSTANTS(:,17) = 14.838;
313 STATES(:,8) = 0.00165;
314 STATES(:,9) = 0.749;
315 STATES(:,10) = 0.6788;
316 CONSTANTS(:,18) = 0.00029;
317 CONSTANTS(:,19) = 0.0000398;
318 STATES(:,11) = 0.00042;
319 STATES(:,12) = 3.288e-5;
320 STATES(:,13) = 0.7026;
321 STATES(:,14) = 0.9526;
322 STATES(:,15) = 0.9942;
323 CONSTANTS(:,20) = 0.000592;
324 CONSTANTS(:,21) = 0.294;
325 STATES(:,16) = 0.999998;
326 STATES(:,17) = 2.347e-8;
327 CONSTANTS(:,22) = 2.724;
328 CONSTANTS(:,23) = 1;
329 CONSTANTS(:,24) = 40;
330 CONSTANTS(:,25) = 1000;
331 CONSTANTS(:,26) = 0.1;
332 CONSTANTS(:,27) = 2.5;
333 CONSTANTS(:,28) = 0.35;
334 CONSTANTS(:,29) = 1.38;
335 CONSTANTS(:,30) = 87.5;
336 CONSTANTS(:,31) = 0.1238;
337 CONSTANTS(:,32) = 0.0005;
338 CONSTANTS(:,33) = 0.0146;
339 STATES(:,18) = 4.272;
340 STATES(:,19) = 0.8978;
341 CONSTANTS(:,34) = 0.15;
342 CONSTANTS(:,35) = 0.045;
343 CONSTANTS(:,36) = 0.06;
344 CONSTANTS(:,37) = 0.005;
```

```
345 CONSTANTS(:,38) = 1.5;
346 CONSTANTS(:,39) = 2.5;
347 CONSTANTS(:,40) = 1;
348 CONSTANTS(:,41) = 0.102;
349 CONSTANTS(:,42) = 0.0038;
350 CONSTANTS(:,43) = 0.00025;
351 CONSTANTS(:,44) = 0.00036;
352 CONSTANTS(:,45) = 0.006375;
353 CONSTANTS(:,46) = 0.2;
354 CONSTANTS(:,47) = 0.001;
355 CONSTANTS(:,48) = 10;
356 CONSTANTS(:,49) = 0.3;
357 CONSTANTS(:,50) = 0.4;
358 CONSTANTS(:,51) = 0.00025;
359 CONSTANTS(:,52) = 0.001094;
360 CONSTANTS(:,53) = 0.00005468;
361
362
363
364
365 % hMSC constants and initial values
366
367 STATES(:,20) = 0;
368 STATES(:,21) = 0.36;
369 STATES(:,22) = 0;
370 STATES(:,23) = 0;
371 STATES(:,24) = 0.64;
372 STATES(:,25) = 0;
373 STATES(:,26) = 0;
374 STATES(:,27) = 5.4;
375 STATES(:,28) = -42;
376
377 if isempty(STATES), warning('Initial values for states not set');, end
378 end
379
380 function [RATES, ALGEBRAIC] = computeRates(VOI, STATES, CONSTANTS)
```

```
381
382 % Computing the rates and variables
383
384
385 global algebraicVariableCount;
386 statesSize = size(STATES);
387 statesColumnCount = statesSize(2);
388 if ( statesColumnCount == 1)
389     STATES = STATES';
390     ALGEBRAIC = zeros(1, algebraicVariableCount);
391 else
392     statesRowCount = statesSize(1);
393     ALGEBRAIC = zeros(statesRowCount, algebraicVariableCount);
394     RATES = zeros(statesRowCount, statesColumnCount);
395 end
396
397 global numbercm
398 numbercm = 1;
399 global numberhmsc
400 numberhmsc = 1;
401
402
403 % Cardiomyocyte calculations
404
405
406 ALGEBRAIC(:,8) = 1.00000./(1.00000+exp((STATES(:,1)+20.0000)./7.00000));
407 ALGEBRAIC(:,21) = 1102.50.*exp( - power(STATES(:,1)+27.0000, 2.00000)./225.000)+200.000./(1.00000+
    exp((13.0000 - STATES(:,1))./10.0000))+180.000./(1.00000+exp((STATES(:,1)+30.0000)./10.0000))
    +20.0000;
408 RATES(:,13) = (ALGEBRAIC(:,8) - STATES(:,13))./ALGEBRAIC(:,21);
409 ALGEBRAIC(:,9) = 0.670000./(1.00000+exp((STATES(:,1)+35.0000)./7.00000))+0.330000;
410 ALGEBRAIC(:,22) = 562.000.*exp( - power(STATES(:,1)+27.0000, 2.00000)./240.000)+31.0000./(1.00000+
    exp((25.0000 - STATES(:,1))./10.0000))+80.0000./(1.00000+exp((STATES(:,1)+30.0000)./10.0000));
411 RATES(:,14) = (ALGEBRAIC(:,9) - STATES(:,14))./ALGEBRAIC(:,22);
412 ALGEBRAIC(:,10) = 0.600000./(1.00000+power(STATES(:,11)./0.0500000, 2.00000))+0.400000;
413 ALGEBRAIC(:,23) = 80.0000./(1.00000+power(STATES(:,11)./0.0500000, 2.00000))+2.00000;
```

```

414 RATES(:,15) = (ALGEBRAIC(:,10) - STATES(:,15))./ALGEBRAIC(:,23);
415 ALGEBRAIC(:,11) = 1.00000./(1.00000+exp((STATES(:,1)+20.0000)./5.00000));
416 ALGEBRAIC(:,24) = 85.0000.*exp( - power(STATES(:,1)+45.0000, 2.00000)./320.000)+5.00000./(1.00000+
    exp((STATES(:,1) - 20.0000)./5.00000))+3.00000;
417 RATES(:,16) = (ALGEBRAIC(:,11) - STATES(:,16))./ALGEBRAIC(:,24);
418 ALGEBRAIC(:,12) = 1.00000./(1.00000+exp((20.0000 - STATES(:,1))./6.00000));
419 ALGEBRAIC(:,25) = 9.50000.*exp( - power(STATES(:,1)+40.0000, 2.00000)./1800.00)+0.800000;
420 RATES(:,17) = (ALGEBRAIC(:,12) - STATES(:,17))./ALGEBRAIC(:,25);
421 ALGEBRAIC(:,1) = 1.00000./(1.00000+exp((- 26.0000 - STATES(:,1))./7.00000));
422 ALGEBRAIC(:,14) = 450.000./(1.00000+exp((- 45.0000 - STATES(:,1))./10.0000));
423 ALGEBRAIC(:,27) = 6.00000./(1.00000+exp((STATES(:,1)+30.0000)./11.5000));
424 ALGEBRAIC(:,35) = 1.00000.*ALGEBRAIC(:,14).*ALGEBRAIC(:,27);
425 RATES(:,5) = (ALGEBRAIC(:,1) - STATES(:,5))./ALGEBRAIC(:,35);
426 ALGEBRAIC(:,2) = 1.00000./(1.00000+exp((STATES(:,1)+88.0000)./24.0000));
427 ALGEBRAIC(:,15) = 3.00000./(1.00000+exp((- 60.0000 - STATES(:,1))./20.0000));
428 ALGEBRAIC(:,28) = 1.12000./(1.00000+exp((STATES(:,1) - 60.0000)./20.0000));
429 ALGEBRAIC(:,36) = 1.00000.*ALGEBRAIC(:,15).*ALGEBRAIC(:,28);
430 RATES(:,6) = (ALGEBRAIC(:,2) - STATES(:,6))./ALGEBRAIC(:,36);
431 ALGEBRAIC(:,3) = 1.00000./(1.00000+exp((- 5.00000 - STATES(:,1))./14.0000));
432 ALGEBRAIC(:,16) = 1400.00./power((1.00000+exp((5.00000 - STATES(:,1))./6.00000)), 1.0 ./ 2);
433 ALGEBRAIC(:,29) = 1.00000./(1.00000+exp((STATES(:,1) - 35.0000)./15.0000));
434 ALGEBRAIC(:,37) = 1.00000.*ALGEBRAIC(:,16).*ALGEBRAIC(:,29)+80.0000;
435 RATES(:,7) = (ALGEBRAIC(:,3) - STATES(:,7))./ALGEBRAIC(:,37);
436 ALGEBRAIC(:,4) = 1.00000./power(1.00000+exp((- 56.8600 - STATES(:,1))./9.03000), 2.00000);
437 ALGEBRAIC(:,17) = 1.00000./(1.00000+exp((- 60.0000 - STATES(:,1))./5.00000));
438 ALGEBRAIC(:,30) = 0.100000./(1.00000+exp((STATES(:,1)+35.0000)./5.00000))+0.100000./(1.00000+exp(
    STATES(:,1) - 50.0000)./200.000));
439 ALGEBRAIC(:,38) = 1.00000.*ALGEBRAIC(:,17).*ALGEBRAIC(:,30);
440 RATES(:,8) = (ALGEBRAIC(:,4) - STATES(:,8))./ALGEBRAIC(:,38);
441 ALGEBRAIC(:,5) = 1.00000./power(1.00000+exp((STATES(:,1)+71.5500)./7.43000), 2.00000);
442 ALGEBRAIC(:,18) = piecewise({STATES(:,1)< - 40.0000, 0.0570000.*exp( -(STATES(:,1)+80.0000)
    ./6.80000 }, 0.00000);
443 ALGEBRAIC(:,31) = piecewise({STATES(:,1)< - 40.0000, 2.70000.*exp( 0.0790000.*STATES(:,1))+310000.*exp(
    0.348500.*STATES(:,1)) }, 0.770000./(- 0.130000.*(1.00000+exp((STATES(:,1)+10.6600)./ - 11.1000)) );
444 ALGEBRAIC(:,39) = 1.00000./(ALGEBRAIC(:,18)+ALGEBRAIC(:,31));

```

```

445 RATES(:,9) = (ALGEBRAIC(:,5) - STATES(:,9))./ALGEBRAIC(:,39);
446 ALGEBRAIC(:,6) = 1.00000./power(1.00000+exp((STATES(:,1)+71.5500)./7.43000), 2.00000);
447 ALGEBRAIC(:,19) = piecewise({STATES(:,1)< - 40.0000, (( ( - 25428.0.*exp( 0.244400.*STATES(:,1)) -
6.94800e-06.*exp( - 0.0439100.*STATES(:,1))).*(STATES(:,1)+37.7800))./1.00000)./(1.00000+exp(
0.311000.*STATES(:,1)+79.2300)) }, 0.00000);
448 ALGEBRAIC(:,32) = piecewise({STATES(:,1)< - 40.0000, ( 0.0242400.*exp( - 0.0105200.*STATES(:,1)))
./(1.00000+exp( - 0.137800.*STATES(:,1)+40.1400)) }, ( 0.600000.*exp( 0.0570000.*STATES(:,1)
))./(1.00000+exp( - 0.100000.*STATES(:,1)+32.0000)));
449 ALGEBRAIC(:,40) = 1.00000./(ALGEBRAIC(:,19)+ALGEBRAIC(:,32));
450 RATES(:,10) = (ALGEBRAIC(:,6) - STATES(:,10))./ALGEBRAIC(:,40);
451 ALGEBRAIC(:,7) = 1.00000./(1.00000+exp(( - 8.00000 - STATES(:,1))./7.50000));
452 ALGEBRAIC(:,20) = 1.40000./(1.00000+exp(( - 35.0000 - STATES(:,1))./13.0000))+0.250000;
453 ALGEBRAIC(:,33) = 1.40000./(1.00000+exp((STATES(:,1)+5.00000)./5.00000));
454 ALGEBRAIC(:,41) = 1.00000./(1.00000+exp((50.0000 - STATES(:,1))./20.0000));
455 ALGEBRAIC(:,43) = 1.00000.*ALGEBRAIC(:,20).*ALGEBRAIC(:,33)+ALGEBRAIC(:,41);
456 RATES(:,12) = (ALGEBRAIC(:,7) - STATES(:,12))./ALGEBRAIC(:,43);
457 ALGEBRAIC(:,56) = (( (( CONSTANTS(:,22).*CONSTANTS(:,11))./(CONSTANTS(:,11)+CONSTANTS(:,23)).*
STATES(:,3))./(STATES(:,3)+CONSTANTS(:,24)))./(1.00000+ 0.124500.*exp(( - 0.100000.*STATES
(:,1).*CONSTANTS(:,3))./( CONSTANTS(:,1).*CONSTANTS(:,2)))+ 0.0353000.*exp(( - STATES(:,1).*CONSTANTS(:,3))./( CONSTANTS(:,1).*CONSTANTS(:,2))));
458 ALGEBRAIC(:,26) = (( CONSTANTS(:,1).*CONSTANTS(:,2))./CONSTANTS(:,3)).*log(CONSTANTS(:,12)./STATES
(:,3));
459 ALGEBRAIC(:,51) = CONSTANTS(:,17).*power(STATES(:,8), 3.00000).*STATES(:,9).*STATES(:,10).*STATES
(:,1) - ALGEBRAIC(:,26));
460 ALGEBRAIC(:,52) = CONSTANTS(:,18).*STATES(:,1) - ALGEBRAIC(:,26));
461 ALGEBRAIC(:,57) = ( CONSTANTS(:,25).*exp(( CONSTANTS(:,28).*STATES(:,1).*CONSTANTS(:,3))./(
CONSTANTS(:,1).*CONSTANTS(:,2))).*power(STATES(:,3), 3.00000).*CONSTANTS(:,13) - exp(( (
CONSTANTS(:,28) - 1.00000).*STATES(:,1).*CONSTANTS(:,3))./( CONSTANTS(:,1).*CONSTANTS(:,2))).*
power(CONSTANTS(:,12), 3.00000).*STATES(:,4).*CONSTANTS(:,27))./(( power(CONSTANTS(:,30),
3.00000)+power(CONSTANTS(:,12), 3.00000)).*(CONSTANTS(:,29)+CONSTANTS(:,13)).*(1.00000+
CONSTANTS(:,26).*exp(( (CONSTANTS(:,28) - 1.00000).*STATES(:,1).*CONSTANTS(:,3))./( CONSTANTS
(:,1).*CONSTANTS(:,2)))));
462 RATES(:,3) = (( - 1.00000.*ALGEBRAIC(:,51)+ALGEBRAIC(:,52)+ 3.00000.*ALGEBRAIC(:,56)+ 3.00000.*ALGEBRAIC(:,57)))./( 1.00000.*CONSTANTS(:,5).*CONSTANTS(:,3)).*CONSTANTS(:,4);
463 ALGEBRAIC(:,34) = (( CONSTANTS(:,1).*CONSTANTS(:,2))./CONSTANTS(:,3)).*log(CONSTANTS(:,11)./STATES
(:,2));

```

```

464 ALGEBRAIC(:,45) = 0.100000./(1.00000+exp( 0.0600000.*((STATES(:,1) - ALGEBRAIC(:,34)) - 200.000)));
465 ALGEBRAIC(:,46) = ( 3.00000.*exp( 0.000200000.*((STATES(:,1) - ALGEBRAIC(:,34))+100.000))+exp(
    0.100000.*((STATES(:,1) - ALGEBRAIC(:,34)) - 10.0000))./(1.00000+exp( - 0.500000.*STATES
    (:,1) - ALGEBRAIC(:,34)))) ;
466 ALGEBRAIC(:,47) = ALGEBRAIC(:,45)./(ALGEBRAIC(:,45)+ALGEBRAIC(:,46));
467 ALGEBRAIC(:,48) = CONSTANTS(:,14).*ALGEBRAIC(:,47).*power((CONSTANTS(:,11)./5.40000), 1.0 ./ 2).*(
    STATES(:,1) - ALGEBRAIC(:,34));
468 ALGEBRAIC(:,55) = CONSTANTS(:,21).*STATES(:,17).*STATES(:,16).*((STATES(:,1) - ALGEBRAIC(:,34)));
469 ALGEBRAIC(:,49) = CONSTANTS(:,15).*power((CONSTANTS(:,11)./5.40000), 1.0 ./ 2).*STATES(:,5).*STATES
    (:,6).*((STATES(:,1) - ALGEBRAIC(:,34));
470 ALGEBRAIC(:,42) = (( CONSTANTS(:,1).*CONSTANTS(:,2))./CONSTANTS(:,3)).*log((CONSTANTS(:,11) +
    CONSTANTS(:,10).*CONSTANTS(:,12))./(STATES(:,2)+CONSTANTS(:,10).*STATES(:,3)));
471 ALGEBRAIC(:,50) = CONSTANTS(:,16).*power(STATES(:,7), 2.00000).*((STATES(:,1) - ALGEBRAIC(:,42)));
472 ALGEBRAIC(:,53) = ( (( CONSTANTS(:,19).*STATES(:,12).*STATES(:,13).*STATES(:,14).*STATES(:,15)
    .*4.00000.*((STATES(:,1) - 15.0000).*power(CONSTANTS(:,3), 2.00000))./( CONSTANTS(:,1).*(
    CONSTANTS(:,2)).*( 0.250000.*STATES(:,11).*exp( 2.00000.*((STATES(:,1) - 15.0000).*CONSTANTS
    (:,3))./( CONSTANTS(:,1).*CONSTANTS(:,2))) - CONSTANTS(:,13)))./(exp( 2.00000.*((STATES(:,1) -
    15.0000).*CONSTANTS(:,3))./( CONSTANTS(:,1).*CONSTANTS(:,2))) - 1.00000);
473 ALGEBRAIC(:,44) = (( 0.500000.*CONSTANTS(:,1).*CONSTANTS(:,2))./CONSTANTS(:,3)).*log(CONSTANTS
    (:,13)./STATES(:,4));
474 ALGEBRAIC(:,54) = CONSTANTS(:,20).*((STATES(:,1) - ALGEBRAIC(:,44)));
475 ALGEBRAIC(:,59) = ( CONSTANTS(:,33).*((STATES(:,1) - ALGEBRAIC(:,34)))./(1.00000+exp(25.0000 -
    STATES(:,1))./5.98000));
476 ALGEBRAIC(:,58) = ( CONSTANTS(:,31).*STATES(:,4))./(STATES(:,4)+CONSTANTS(:,32));
477 ALGEBRAIC(:,13) = .442*piecewise({VOI - floor(VOI./CONSTANTS(:,7)).*CONSTANTS(:,7)>=CONSTANTS(:,6)&
    VOI - floor(VOI./CONSTANTS(:,7)).*CONSTANTS(:,7)<=CONSTANTS(:,6)+CONSTANTS(:,8), - CONSTANTS
    (:,9) }, 0.00000);
478 RATES(:,1) = - (ALGEBRAIC(:,48)+ALGEBRAIC(:,55)+ALGEBRAIC(:,49)+ALGEBRAIC(:,50)+ALGEBRAIC(:,53)+
    ALGEBRAIC(:,56)+ALGEBRAIC(:,51)+ALGEBRAIC(:,52)+ALGEBRAIC(:,57)+ALGEBRAIC(:,54)+ALGEBRAIC(:,59)+
    +ALGEBRAIC(:,58)+ALGEBRAIC(:,13)+(numberhmsc.*1.5./185).*((STATES(:,1)-STATES(:,28)));
479 RATES(:,2) = ( (- 1.00000.*((ALGEBRAIC(:,48)+ALGEBRAIC(:,55)+ALGEBRAIC(:,49)+ALGEBRAIC(:,50)+
    ALGEBRAIC(:,59)+ALGEBRAIC(:,13)) - 2.00000.*ALGEBRAIC(:,56)))./( 1.00000.*CONSTANTS(:,5).*(
    CONSTANTS(:,3))).*CONSTANTS(:,4));
480 ALGEBRAIC(:,60) = CONSTANTS(:,45)./(1.00000+power(CONSTANTS(:,43), 2.00000)./power(STATES(:,4),
    2.00000));
481 ALGEBRAIC(:,61) = CONSTANTS(:,44).*((STATES(:,18) - STATES(:,4));

```

```

482 ALGEBRAIC(:,62) = CONSTANTS(:,42).*(STATES(:,11) - STATES(:,4));
483 ALGEBRAIC(:,64) = 1.00000./(1.00000+( CONSTANTS(:,46).*CONSTANTS(:,47))./power(STATES(:,4)+CONSTANTS
    (:,47), 2.00000));
484 RATES(:,4) = ALGEBRAIC(:,64).*((( ALGEBRAIC(:,61) - ALGEBRAIC(:,60)).*CONSTANTS(:,52))./CONSTANTS
    (:,5)+ALGEBRAIC(:,62)) - ( 1.00000.*((ALGEBRAIC(:,54)+ALGEBRAIC(:,58)) - 2.00000.*ALGEBRAIC
    (:,57)).*CONSTANTS(:,4))./( 2.00000.*1.00000.*CONSTANTS(:,5).*CONSTANTS(:,3)));
485 ALGEBRAIC(:,63) = CONSTANTS(:,39) - (CONSTANTS(:,39) - CONSTANTS(:,40))./(1.00000+power(CONSTANTS
    (:,38)./STATES(:,18), 2.00000));
486 ALGEBRAIC(:,66) = CONSTANTS(:,35).*ALGEBRAIC(:,63);
487 RATES(:,19) = - ALGEBRAIC(:,66).*STATES(:,11).*STATES(:,19)+ CONSTANTS(:,37).* (1.00000 - STATES
    (:,19));
488 ALGEBRAIC(:,65) = CONSTANTS(:,34)./ALGEBRAIC(:,63);
489 ALGEBRAIC(:,67) = ( ALGEBRAIC(:,65).*power(STATES(:,11), 2.00000).*STATES(:,19))./(CONSTANTS(:,36)+
    ALGEBRAIC(:,65).*power(STATES(:,11), 2.00000));
490 ALGEBRAIC(:,68) = CONSTANTS(:,41).*ALGEBRAIC(:,67).* (STATES(:,18) - STATES(:,11));
491 ALGEBRAIC(:,69) = 1.00000./(1.00000+( CONSTANTS(:,48).*CONSTANTS(:,49))./power(STATES(:,18)+
    CONSTANTS(:,49), 2.00000));
492 RATES(:,18) = ALGEBRAIC(:,69).* (ALGEBRAIC(:,60) - (ALGEBRAIC(:,68)+ALGEBRAIC(:,61)));
493 ALGEBRAIC(:,70) = 1.00000./(1.00000+( CONSTANTS(:,50).*CONSTANTS(:,51))./power(STATES(:,11)+
    CONSTANTS(:,51), 2.00000));
494 RATES(:,11) = ALGEBRAIC(:,70).*((( - 1.00000.*ALGEBRAIC(:,53).*CONSTANTS(:,4))./(
    2.00000.*1.00000.*CONSTANTS(:,53).*CONSTANTS(:,3))+ ( ALGEBRAIC(:,68).*CONSTANTS(:,52))./
    CONSTANTS(:,53)) - ( ALGEBRAIC(:,62).*CONSTANTS(:,5))./CONSTANTS(:,53));
495
496 % hMSC calculations
497 ALGEBRAIC(:,71) = 2.52.*exp(-(STATES(:,28)-53.16).^2/593.7)+2.44;
498 ALGEBRAIC(:,72) = 8.2.*exp(-(STATES(:,28)-55.2).^2/659.9);
499 ALGEBRAIC(:,73) = 1.*0.028./(1+0.86.*exp((STATES(:,28)-10.0)./-12.35))*6;
500 ALGEBRAIC(:,74) = 1.*3e-4.*(125.5+STATES(:,28))./(1+26.9.*exp(-(STATES(:,28)-47.4)/-14.6))*6;
501 ALGEBRAIC(:,75) = 1e-1;
502 ALGEBRAIC(:,76) = 10;
503 ALGEBRAIC(:,77) = 687.8.*1e-4.*exp(STATES(:,28)./15.8);
504 ALGEBRAIC(:,78) = 21.1.*exp(-STATES(:,28)./43.5);
505 ALGEBRAIC(:,79) = (8.314.*310./1./96.65).*log(5.4./140);
506 ALGEBRAIC(:,80) = 6.5*(STATES(:,28)-ALGEBRAIC(:,79)).*STATES(:,25);
507 ALGEBRAIC(:,81) = 3*(STATES(:,28)-ALGEBRAIC(:,79)).*STATES(:,26);

```

```

508
509 RATES(:,20) = ALGEBRAIC(:,75).*ALGEBRAIC(:,74).*STATES(:,21)-ALGEBRAIC(:,76).*ALGEBRAIC(:,73).*STATES(:,20);
510 RATES(:,21) = (ALGEBRAIC(:,76).*ALGEBRAIC(:,73).*STATES(:,20)+2*ALGEBRAIC(:,74).*STATES(:,22) - (ALGEBRAIC(:,75).*ALGEBRAIC(:,74)+3*ALGEBRAIC(:,73)).*STATES(:,21));
511 RATES(:,22) = (3.*ALGEBRAIC(:,73).*STATES(:,21)+3*ALGEBRAIC(:,74).*STATES(:,23) - (2.*ALGEBRAIC(:,74)+2*ALGEBRAIC(:,73)).*STATES(:,22));
512 RATES(:,23) = (2.*ALGEBRAIC(:,73).*STATES(:,22)+4*ALGEBRAIC(:,74).*STATES(:,24) - (3.*ALGEBRAIC(:,74)+1*ALGEBRAIC(:,73)).*STATES(:,23));
513 RATES(:,24) = (1.*ALGEBRAIC(:,73).*STATES(:,23)+ALGEBRAIC(:,72).*ALGEBRAIC(:,74).*STATES(:,25) - (4.*ALGEBRAIC(:,74)+ALGEBRAIC(:,71).*ALGEBRAIC(:,73)).*STATES(:,24));
514 RATES(:,25) = ALGEBRAIC(:,71).*ALGEBRAIC(:,73).*STATES(:,24) - ALGEBRAIC(:,72).*ALGEBRAIC(:,74).*STATES(:,25);
515
516 RATES(:,26) = (1-STATES(:,26)).*ALGEBRAIC(:,77)-STATES(:,26).*21.1.*ALGEBRAIC(:,78);
517
518 RATES(:,27) = 0;
519 RATES(:,28) = -(1./59.7).*(ALGEBRAIC(:,80)+ALGEBRAIC(:,81)+59.7*ALGEBRAIC(:,13)+.3*(STATES(:,28)-132.2)+numbercm.*1.5.*((STATES(:,28)-STATES(:,1))));
520
521 RATES = RATES';
522 end
523
524 % Calculate algebraic variables again
525
526
527 function ALGEBRAIC = computeAlgebraic(ALGEBRAIC, CONSTANTS, STATES, VOI)
528
529 % Cardiomyocyte
530
531 ALGEBRAIC(:,8) = 1.00000./(1.00000+exp((STATES(:,1)+20.0000)./7.00000));
532 ALGEBRAIC(:,21) = 1102.50.*exp(-power(STATES(:,1)+27.0000, 2.00000)./225.000)+200.000./(1.00000+exp((13.0000 - STATES(:,1))./10.0000))+180.000./(1.00000+exp((STATES(:,1)+30.0000)./10.0000))+20.0000;
533 ALGEBRAIC(:,9) = 0.670000./(1.00000+exp((STATES(:,1)+35.0000)./7.00000))+0.330000;

```

```

534 ALGEBRAIC(:,22) = 562.000.*exp( - power(STATES(:,1)+27.0000, 2.00000)./240.000)+31.0000./(1.00000+
    exp((25.0000 - STATES(:,1))./10.0000))+80.0000./(1.00000+exp((STATES(:,1)+30.0000)./10.0000));
535 ALGEBRAIC(:,10) = 0.600000./(1.00000+power(STATES(:,11)./0.0500000, 2.00000))+0.400000;
536 ALGEBRAIC(:,23) = 80.0000./(1.00000+power(STATES(:,11)./0.0500000, 2.00000))+2.00000;
537 ALGEBRAIC(:,11) = 1.00000./(1.00000+exp((STATES(:,1)+20.0000)./5.00000));
538 ALGEBRAIC(:,24) = 85.0000.*exp( - power(STATES(:,1)+45.0000, 2.00000)./320.000)+5.00000./(1.00000+
    exp((STATES(:,1) - 20.0000)./5.00000))+3.00000;
539 ALGEBRAIC(:,12) = 1.00000./(1.00000+exp((20.0000 - STATES(:,1))./6.00000));
540 ALGEBRAIC(:,25) = 9.50000.*exp( - power(STATES(:,1)+40.0000, 2.00000)./1800.00)+0.800000;
541 ALGEBRAIC(:,1) = 1.00000./(1.00000+exp((- 26.0000 - STATES(:,1))./7.00000));
542 ALGEBRAIC(:,14) = 450.000./(1.00000+exp((- 45.0000 - STATES(:,1))./10.0000));
543 ALGEBRAIC(:,27) = 6.00000./(1.00000+exp((STATES(:,1)+30.0000)./11.5000));
544 ALGEBRAIC(:,35) = 1.00000.*ALGEBRAIC(:,14).*ALGEBRAIC(:,27);
545 ALGEBRAIC(:,2) = 1.00000./(1.00000+exp((STATES(:,1)+88.0000)./24.0000));
546 ALGEBRAIC(:,15) = 3.00000./(1.00000+exp((- 60.0000 - STATES(:,1))./20.0000));
547 ALGEBRAIC(:,28) = 1.12000./(1.00000+exp((STATES(:,1) - 60.0000)./20.0000));
548 ALGEBRAIC(:,36) = 1.00000.*ALGEBRAIC(:,15).*ALGEBRAIC(:,28);
549 ALGEBRAIC(:,3) = 1.00000./(1.00000+exp((- 5.00000 - STATES(:,1))./14.0000));
550 ALGEBRAIC(:,16) = 1400.00./power((1.00000+exp((5.00000 - STATES(:,1))./6.00000)), 1.0 ./ 2);
551 ALGEBRAIC(:,29) = 1.00000./(1.00000+exp((STATES(:,1) - 35.0000)./15.0000));
552 ALGEBRAIC(:,37) = 1.00000.*ALGEBRAIC(:,16).*ALGEBRAIC(:,29)+80.0000;
553 ALGEBRAIC(:,4) = 1.00000./power(1.00000+exp((- 56.8600 - STATES(:,1))./9.03000), 2.00000);
554 ALGEBRAIC(:,17) = 1.00000./(1.00000+exp((- 60.0000 - STATES(:,1))./5.00000));
555 ALGEBRAIC(:,30) = 0.100000./(1.00000+exp((STATES(:,1)+35.0000)./5.00000))+0.100000./(1.00000+exp(
    STATES(:,1) - 50.0000)./200.0000);
556 ALGEBRAIC(:,38) = 1.00000.*ALGEBRAIC(:,17).*ALGEBRAIC(:,30);
557 ALGEBRAIC(:,5) = 1.00000./power(1.00000+exp((STATES(:,1)+71.5500)./7.43000), 2.00000);
558 ALGEBRAIC(:,18) = piecewise({STATES(:,1)< - 40.0000, 0.0570000.*exp( -(STATES(:,1)+80.0000)
    ./6.80000) }, 0.00000);
559 ALGEBRAIC(:,31) = piecewise({STATES(:,1)< - 40.0000, 2.70000.*exp( 0.0790000.*STATES(:,1)+
    310000.*exp( 0.348500.*STATES(:,1)) }, 0.770000./ ( 0.130000.* (1.00000+exp((STATES(:,1)
    +10.6600)./ - 11.1000)) );
560 ALGEBRAIC(:,39) = 1.00000./(ALGEBRAIC(:,18)+ALGEBRAIC(:,31));
561 ALGEBRAIC(:,6) = 1.00000./power(1.00000+exp((STATES(:,1)+71.5500)./7.43000), 2.00000);

```

```

562 ALGEBRAIC(:,19) = piecewise({STATES(:,1)< - 40.0000, (( ( - 25428.0.*exp( 0.244400.*STATES(:,1)) -
6.94800e-06.*exp( - 0.0439100.*STATES(:,1))).*(STATES(:,1)+37.7800))./1.00000)./(1.00000+exp(
0.311000.*STATES(:,1)+79.2300)) }, 0.00000);
563 ALGEBRAIC(:,32) = piecewise({STATES(:,1)< - 40.0000, ( 0.0242400.*exp( - 0.0105200.*STATES(:,1)))
./(1.00000+exp( - 0.137800.*STATES(:,1)+40.1400)) }, ( 0.600000.*exp( 0.0570000.*STATES(:,1))
)./(1.00000+exp( - 0.100000.*STATES(:,1)+32.00000)));
564 ALGEBRAIC(:,40) = 1.00000./ (ALGEBRAIC(:,19)+ALGEBRAIC(:,32));
565 ALGEBRAIC(:,7) = 1.00000./ (1.00000+exp(( - 8.00000 - STATES(:,1))./7.50000));
566 ALGEBRAIC(:,20) = 1.40000./ (1.00000+exp(( - 35.0000 - STATES(:,1))./13.0000))+0.250000;
567 ALGEBRAIC(:,33) = 1.40000./ (1.00000+exp((STATES(:,1)+5.00000)./5.00000));
568 ALGEBRAIC(:,41) = 1.00000./ (1.00000+exp((50.0000 - STATES(:,1))./20.0000));
569 ALGEBRAIC(:,43) = 1.00000.*ALGEBRAIC(:,20).*ALGEBRAIC(:,33)+ALGEBRAIC(:,41);
570 ALGEBRAIC(:,56) = (( (( CONSTANTS(:,22).*CONSTANTS(:,11))./(CONSTANTS(:,11)+CONSTANTS(:,23))).*
STATES(:,3))./(STATES(:,3)+CONSTANTS(:,24)))./(1.00000+ 0.124500.*exp(( - 0.100000.*STATES
(:,1).*CONSTANTS(:,3))./( CONSTANTS(:,1).*CONSTANTS(:,2)))+ 0.0353000.*exp(( - STATES(:,1).*CONSTANTS(:,3))./( CONSTANTS(:,1).*CONSTANTS(:,2))));;
571 ALGEBRAIC(:,26) = (( CONSTANTS(:,1).*CONSTANTS(:,2))./CONSTANTS(:,3)).*log(CONSTANTS(:,12)./STATES
(:,3));
572 ALGEBRAIC(:,51) = CONSTANTS(:,17).*power(STATES(:,8), 3.00000).*STATES(:,9).*STATES(:,10).*STATES
(:,1) - ALGEBRAIC(:,26));
573 ALGEBRAIC(:,52) = CONSTANTS(:,18).*STATES(:,1) - ALGEBRAIC(:,26));
574 ALGEBRAIC(:,57) = ( CONSTANTS(:,25).* ( exp(( CONSTANTS(:,28).*STATES(:,1).*CONSTANTS(:,3))./(
CONSTANTS(:,1).*CONSTANTS(:,2))).*power(STATES(:,3), 3.00000).*CONSTANTS(:,13) - exp(( (
CONSTANTS(:,28) - 1.00000).*STATES(:,1).*CONSTANTS(:,3))./( CONSTANTS(:,1).*CONSTANTS(:,2))).*power(
CONSTANTS(:,12), 3.00000).*STATES(:,4).*CONSTANTS(:,27))./ ( power(CONSTANTS(:,30),
3.00000)+power(CONSTANTS(:,12), 3.00000)).*(CONSTANTS(:,29)+CONSTANTS(:,13)).*(1.00000+
CONSTANTS(:,26).*exp(( (CONSTANTS(:,28) - 1.00000).*STATES(:,1).*CONSTANTS(:,3))./( CONSTANTS
(:,1).*CONSTANTS(:,2))))));
575 ALGEBRAIC(:,34) = (( CONSTANTS(:,1).*CONSTANTS(:,2))./CONSTANTS(:,3)).*log(CONSTANTS(:,11)./STATES
(:,2));
576 ALGEBRAIC(:,45) = 0.100000./ (1.00000+exp( 0.0600000.*((STATES(:,1) - ALGEBRAIC(:,34)) - 200.0000)));
577 ALGEBRAIC(:,46) = ( 3.00000.*exp( 0.000200000.*((STATES(:,1) - ALGEBRAIC(:,34))+100.0000))+exp(
0.100000.*((STATES(:,1) - ALGEBRAIC(:,34)) - 10.00000))./(1.00000+exp( - 0.500000.*STATES
(:,1) - ALGEBRAIC(:,34))));
578 ALGEBRAIC(:,47) = ALGEBRAIC(:,45)./(ALGEBRAIC(:,45)+ALGEBRAIC(:,46));

```

```

579 ALGEBRAIC(:,48) = CONSTANTS(:,14).*ALGEBRAIC(:,47).*power((CONSTANTS(:,11)./5.40000), 1.0 ./ 2).*(
    STATES(:,1) - ALGEBRAIC(:,34));
580 ALGEBRAIC(:,55) = CONSTANTS(:,21).*STATES(:,17).*STATES(:,16).*(STATES(:,1) - ALGEBRAIC(:,34));
581 ALGEBRAIC(:,49) = CONSTANTS(:,15).*power((CONSTANTS(:,11)./5.40000), 1.0 ./ 2).*STATES(:,5).*STATES
    (:,6).*(STATES(:,1) - ALGEBRAIC(:,34));
582 ALGEBRAIC(:,42) = (( CONSTANTS(:,1).*CONSTANTS(:,2))./CONSTANTS(:,3)).*log((CONSTANTS(:,11)+
    CONSTANTS(:,10).*CONSTANTS(:,12))./(STATES(:,2)+ CONSTANTS(:,10).*STATES(:,3)));
583 ALGEBRAIC(:,50) = CONSTANTS(:,16).*power(STATES(:,7), 2.00000).*((STATES(:,1) - ALGEBRAIC(:,42));
584 ALGEBRAIC(:,53) = ( (( CONSTANTS(:,19).*STATES(:,12).*STATES(:,13).*STATES(:,14).*STATES(:,15)
    .*4.00000.*STATES(:,1) - 15.0000).*power(CONSTANTS(:,3), 2.00000))./(( CONSTANTS(:,1).*CONSTANTS(:,2)).*( 0.250000.*STATES(:,11).*exp(( 2.00000.*STATES(:,1) - 15.0000).*CONSTANTS
    (:,3))./( CONSTANTS(:,1).*CONSTANTS(:,2))) - CONSTANTS(:,13)))./((exp(( 2.00000.*STATES(:,1) - 15.0000).*CONSTANTS(:,3))./(( CONSTANTS(:,1).*CONSTANTS(:,2))) - 1.00000);
585 ALGEBRAIC(:,44) = (( 0.500000.*CONSTANTS(:,1).*CONSTANTS(:,2))./CONSTANTS(:,3)).*log(CONSTANTS
    (:,13)./STATES(:,4));
586 ALGEBRAIC(:,54) = CONSTANTS(:,20).*((STATES(:,1) - ALGEBRAIC(:,44));
587 ALGEBRAIC(:,59) = ( CONSTANTS(:,33).*((STATES(:,1) - ALGEBRAIC(:,34)))./(1.00000+exp((25.0000 -
    STATES(:,1))./5.98000));
588 ALGEBRAIC(:,58) = ( CONSTANTS(:,31).*STATES(:,4))./(STATES(:,4)+CONSTANTS(:,32));
589 ALGEBRAIC(:,13) = 1*piecewise({VOI - floor(VOI./CONSTANTS(:,7)).*CONSTANTS(:,7)>=CONSTANTS(:,6)&VOI
    - floor(VOI./CONSTANTS(:,7)).*CONSTANTS(:,7)<=CONSTANTS(:,6)+CONSTANTS(:,8), - CONSTANTS
    (:,9) }, 0.00000);
590 ALGEBRAIC(:,60) = CONSTANTS(:,45)./(1.00000+power(CONSTANTS(:,43), 2.00000)./power(STATES(:,4),
    2.00000));
591 ALGEBRAIC(:,61) = CONSTANTS(:,44).*((STATES(:,18) - STATES(:,4));
592 ALGEBRAIC(:,62) = CONSTANTS(:,42).*((STATES(:,11) - STATES(:,4));
593 ALGEBRAIC(:,64) = 1.00000./(1.00000+( CONSTANTS(:,46).*CONSTANTS(:,47))./power(STATES(:,4)+CONSTANTS
    (:,47), 2.00000));
594 ALGEBRAIC(:,63) = CONSTANTS(:,39) - ((CONSTANTS(:,39) - CONSTANTS(:,40))./(1.00000+power(CONSTANTS
    (:,38)./STATES(:,18), 2.00000));
595 ALGEBRAIC(:,66) = CONSTANTS(:,35).*ALGEBRAIC(:,63);
596 ALGEBRAIC(:,65) = CONSTANTS(:,34)./ALGEBRAIC(:,63);
597 ALGEBRAIC(:,67) = ( ALGEBRAIC(:,65).*power(STATES(:,11), 2.00000).*STATES(:,19))./((CONSTANTS(:,36)+
    ALGEBRAIC(:,65).*power(STATES(:,11), 2.00000));
598 ALGEBRAIC(:,68) = CONSTANTS(:,41).*ALGEBRAIC(:,67).*((STATES(:,18) - STATES(:,11)));

```

```
599 ALGEBRAIC(:,69) = 1.00000./(1.00000+ (CONSTANTS(:,48).*CONSTANTS(:,49))./power(STATES(:,18)+  
    CONSTANTS(:,49), 2.00000));  
600 ALGEBRAIC(:,70) = 1.00000./(1.00000+ (CONSTANTS(:,50).*CONSTANTS(:,51))./power(STATES(:,11)+  
    CONSTANTS(:,51), 2.00000));  
601  
602  
603 % hMSC  
604  
605 ALGEBRAIC(:,71) = 2.52.*exp(-(STATES(:,28)-53.16).^2/593.7)+2.44;  
606 ALGEBRAIC(:,72) = 8.2.*exp(-(STATES(:,28)-55.2).^2/659.9);  
607 ALGEBRAIC(:,73) = 0.028./(1+0.86.*exp((STATES(:,28)-10.0)./-12.35)).*.6;  
608 ALGEBRAIC(:,74) = 3e-4.* (125.5+STATES(:,28))./(1+26.9.*exp(-(STATES(:,28)-47.4)/-14.6)).*.6;  
609 ALGEBRAIC(:,75) = 1e-1;  
610 ALGEBRAIC(:,76) = 10;  
611 ALGEBRAIC(:,77) = 687.8.*1e-4.*exp(STATES(:,28)./15.8);  
612 ALGEBRAIC(:,78) = 21.1.*exp(-STATES(:,28)./43.5);  
613 ALGEBRAIC(:,79) = (8.314.*310./1./96.65).*log(5.4./140);  
614 ALGEBRAIC(:,80) = 6*(STATES(:,28)-ALGEBRAIC(:,79)).*STATES(:,25);  
615 ALGEBRAIC(:,81) = 3*(STATES(:,28)-ALGEBRAIC(:,79)).*STATES(:,26);  
616  
617  
618 end  
619  
620 % Piecewise functions are part of this model. They are calculated here  
621  
622 function x = piecewise(cases, default)  
623 set = [0];  
624 for i = 1:2:length(cases)  
625 if (length(cases{i+1}) == 1)  
626 x(cases{i} & ~set,:) = cases{i+1};  
627 else  
628 x(cases{i} & ~set,:) = cases{i+1}(cases{i} & ~set);  
629 end  
630 set = set | cases{i};  
631 if(set), break, end  
632 end
```

```
633 if (length(default) == 1)
634     x(~set,:) = default;
635 else
636     x(~set,:) = default(~set);
637 end
638 end
639
640
641 function strout = strpad(strin)
642 req_length = 160;
643 insize = size(strin,2);
644 if insize > req_length
645     strout = strin(1:req_length);
646 else
647     strout = [strin, blanks(req_length - insize)];
648 end
649 end
```

A.5 Sample Conduction Velocity Code

```
1 function [AA, BB, maxcv] = Total_A_CV
2
3
4 % A modification of the code from:
5 % http://www.mathworks.com/matlabcentral/fileexchange/40813-rgdspracticalguide/content/pdepeHH.m
6
7
8 clear all;
9
10 % parameters to apply pde solver over
11
12 L     = 2;    % length (cm)
13 dx    = .02;   % step size (cm)
14 x     = 0:dx:L; % distance vector (cm)
15
16 global tmax
17 global dt
18 tmax = 450; % maximum time (ms)
19 dt   = .005;  % time step size (ms)
20 t = 0:dt:tmax; % time vector (ms)
21
22
23 m = 0; % geometry for pde
24 % pde solver function
25 S = pdepe(m, @pdehh, @pdeinic, @pdebouc, x, t, []);
26
27 % voltage
28 V = S(:,:,1);
29
30 % plotting the solution
31 solutionV = figure;
32 set(axes, 'FontSize',15);
33 set(solutionV, 'Position',[190 50 560 420]);
34 surf(x, t, V, 'FaceColor','interp', 'EdgeColor','none','FaceLighting','phong');
```



```
70 CONSTANTS(:,1) = 8314.472;
71 CONSTANTS(:,2) = 310;
72 CONSTANTS(:,3) = 96485.3415;
73 CONSTANTS(:,4) = 0.185;
74 CONSTANTS(:,5) = 0.016404;
75 CONSTANTS(:,6) = 10;
76 CONSTANTS(:,7) = 1000;
77 CONSTANTS(:,8) = 1;
78 CONSTANTS(:,9) = 52;
79 CONSTANTS(:,10) = 0.03;
80 CONSTANTS(:,11) = 5.4;
81 CONSTANTS(:,12) = 140;
82 CONSTANTS(:,13) = 2;
83 CONSTANTS(:,14) = 5.405;
84 CONSTANTS(:,15) = 0.153;
85 CONSTANTS(:,16) = 0.098;
86 CONSTANTS(:,17) = 14.838;
87 CONSTANTS(:,18) = 0.00029;
88 CONSTANTS(:,19) = 0.0000398;
89 CONSTANTS(:,20) = 0.000592;
90 CONSTANTS(:,21) = 0.294;
91 CONSTANTS(:,22) = 2.724;
92 CONSTANTS(:,23) = 1;
93 CONSTANTS(:,24) = 40;
94 CONSTANTS(:,25) = 1000;
95 CONSTANTS(:,26) = 0.1;
96 CONSTANTS(:,27) = 2.5;
97 CONSTANTS(:,28) = 0.35;
98 CONSTANTS(:,29) = 1.38;
99 CONSTANTS(:,30) = 87.5;
100 CONSTANTS(:,31) = 0.1238;
101 CONSTANTS(:,32) = 0.0005;
102 CONSTANTS(:,33) = 0.0146;
103 CONSTANTS(:,34) = 0.15;
104 CONSTANTS(:,35) = 0.045;
105 CONSTANTS(:,36) = 0.06;
```

```
106 CONSTANTS(:,37) = 0.005;
107 CONSTANTS(:,38) = 1.5;
108 CONSTANTS(:,39) = 2.5;
109 CONSTANTS(:,40) = 1;
110 CONSTANTS(:,41) = 0.102;
111 CONSTANTS(:,42) = 0.0038;
112 CONSTANTS(:,43) = 0.00025;
113 CONSTANTS(:,44) = 0.00036;
114 CONSTANTS(:,45) = 0.006375;
115 CONSTANTS(:,46) = 0.2;
116 CONSTANTS(:,47) = 0.001;
117 CONSTANTS(:,48) = 10;
118 CONSTANTS(:,49) = 0.3;
119 CONSTANTS(:,50) = 0.4;
120 CONSTANTS(:,51) = 0.00025;
121 CONSTANTS(:,52) = 0.001094;
122 CONSTANTS(:,53) = 0.00005468;
123 STATES = u;
124
125
126 % cm calculation
127 ALGEBRAIC(8) = 1.00000./(1.00000+exp((STATES(1)+20.0000)./7.00000));
128 ALGEBRAIC(21) = 1102.50.*exp( - power(STATES(1)+27.0000, 2.00000)./225.000)+200.000./(1.00000+exp
    ((13.0000 - STATES(1))./10.0000))+180.000./(1.00000+exp((STATES(1)+30.0000)./10.0000))+20.0000;
129 RATES(13) = (ALGEBRAIC(8) - STATES(13))./ALGEBRAIC(21);
130 ALGEBRAIC(9) = 0.670000./(1.00000+exp((STATES(1)+35.0000)./7.00000))+0.330000;
131 ALGEBRAIC(22) = 562.000.*exp( - power(STATES(1)+27.0000, 2.00000)./240.000)+31.0000./(1.00000+exp
    ((25.0000 - STATES(1))./10.0000))+80.0000./(1.00000+exp((STATES(1)+30.0000)./10.0000));
132 RATES(14) = (ALGEBRAIC(9) - STATES(14))./ALGEBRAIC(22);
133 ALGEBRAIC(10) = 0.600000./(1.00000+power(STATES(11)./0.0500000, 2.00000))+0.400000;
134 ALGEBRAIC(23) = 80.0000./(1.00000+power(STATES(11)./0.0500000, 2.00000))+2.00000;
135 RATES(15) = (ALGEBRAIC(10) - STATES(15))./ALGEBRAIC(23);
136 ALGEBRAIC(11) = 1.00000./(1.00000+exp((STATES(1)+20.0000)./5.00000));
137 ALGEBRAIC(24) = 85.0000.*exp( - power(STATES(1)+45.0000, 2.00000)./320.000)+5.00000./(1.00000+exp(
    STATES(1) - 20.0000)./5.00000))+3.00000;
138 RATES(16) = (ALGEBRAIC(11) - STATES(16))./ALGEBRAIC(24);
```

```

139 ALGEBRAIC(12) = 1.00000./(1.00000+exp((20.0000 - STATES(1))./6.00000));
140 ALGEBRAIC(25) = 9.50000.*exp(- power(STATES(1)+40.0000, 2.00000)./1800.00)+0.800000;
141 RATES(17) = (ALGEBRAIC(12) - STATES(17))./ALGEBRAIC(25);
142 ALGEBRAIC(1) = 1.00000./(1.00000+exp((- 26.0000 - STATES(1))./7.00000));
143 ALGEBRAIC(14) = 450.000./(1.00000+exp((- 45.0000 - STATES(1))./10.0000));
144 ALGEBRAIC(27) = 6.00000./(1.00000+exp((STATES(1)+30.0000)./11.5000));
145 ALGEBRAIC(35) = 1.00000.*ALGEBRAIC(14).*ALGEBRAIC(27);
146 RATES(5) = (ALGEBRAIC(1) - STATES(5))./ALGEBRAIC(35);
147 ALGEBRAIC(2) = 1.00000./(1.00000+exp((STATES(1)+88.0000)./24.0000));
148 ALGEBRAIC(15) = 3.00000./(1.00000+exp((- 60.0000 - STATES(1))./20.0000));
149 ALGEBRAIC(28) = 1.12000./(1.00000+exp((STATES(1) - 60.0000)./20.0000));
150 ALGEBRAIC(36) = 1.00000.*ALGEBRAIC(15).*ALGEBRAIC(28);
151 RATES(6) = (ALGEBRAIC(2) - STATES(6))./ALGEBRAIC(36);
152 ALGEBRAIC(3) = 1.00000./(1.00000+exp((- 5.00000 - STATES(1))./14.0000));
153 ALGEBRAIC(16) = 1400.00./power((1.00000+exp((5.00000 - STATES(1))./6.00000)), 1.0 ./ 2);
154 ALGEBRAIC(29) = 1.00000./(1.00000+exp((STATES(1) - 35.0000)./15.0000));
155 ALGEBRAIC(37) = 1.00000.*ALGEBRAIC(16).*ALGEBRAIC(29)+80.0000;
156 RATES(7) = (ALGEBRAIC(3) - STATES(7))./ALGEBRAIC(37);
157 ALGEBRAIC(4) = 1.00000./power(1.00000+exp((- 56.8600 - STATES(1))./9.03000), 2.00000);
158 ALGEBRAIC(17) = 1.00000./(1.00000+exp((- 60.0000 - STATES(1))./5.00000));
159 ALGEBRAIC(30) = 0.100000./(1.00000+exp((STATES(1)+35.0000)./5.00000))+0.100000./(1.00000+exp((STATES
(1) - 50.0000)./200.000));
160 ALGEBRAIC(38) = 1.00000.*ALGEBRAIC(17).*ALGEBRAIC(30);
161 RATES(8) = (ALGEBRAIC(4) - STATES(8))./ALGEBRAIC(38);
162 ALGEBRAIC(5) = 1.00000./power(1.00000+exp((STATES(1)+71.5500)./7.43000), 2.00000);
163 ALGEBRAIC(18) = piecewise({STATES(1)< - 40.0000, 0.0570000.*exp(- (STATES(1)+80.0000)./6.80000 },
0.00000);
164 ALGEBRAIC(31) = piecewise({STATES(1)< - 40.0000, 2.70000.*exp(0.0790000.*STATES(1))+ 310000.*exp(
0.348500.*STATES(1) }, 0.770000./((0.130000.*exp((STATES(1)+10.6600)./- 11.1000)));
;
165 ALGEBRAIC(39) = 1.00000./(ALGEBRAIC(18)+ALGEBRAIC(31));
166 RATES(9) = (ALGEBRAIC(5) - STATES(9))./ALGEBRAIC(39);
167 ALGEBRAIC(6) = 1.00000./power(1.00000+exp((STATES(1)+71.5500)./7.43000), 2.00000);
168 ALGEBRAIC(19) = piecewise({STATES(1)< - 40.0000, (((- 25428.0.*exp(0.244400.*STATES(1)) -
6.94800e-06.*exp(- 0.0439100.*STATES(1))).*(STATES(1)+37.7800)./1.00000)./(1.00000+exp(
0.311000.*STATES(1)+79.2300))), 0.00000);

```

```

169 ALGEBRAIC(32) = piecewise({STATES(1)< - 40.0000, ( 0.0242400.*exp( - 0.0105200.*STATES(1)))
    ./(1.00000+exp( - 0.137800.*STATES(1)+40.1400))}, ( 0.600000.*exp( 0.0570000.*STATES(1)))
    ./(1.00000+exp( - 0.100000.*STATES(1)+32.0000)));
170 ALGEBRAIC(40) = 1.00000./(ALGEBRAIC(19)+ALGEBRAIC(32));
171 RATES(10) = (ALGEBRAIC(6) - STATES(10))./ALGEBRAIC(40);
172 ALGEBRAIC(7) = 1.00000./(1.00000+exp((- 8.00000 - STATES(1))./7.50000));
173 ALGEBRAIC(20) = 1.40000./(1.00000+exp((- 35.0000 - STATES(1))./13.0000))+0.250000;
174 ALGEBRAIC(33) = 1.40000./(1.00000+exp((STATES(1)+5.00000)./5.00000));
175 ALGEBRAIC(41) = 1.00000./(1.00000+exp((50.0000 - STATES(1))./20.0000));
176 ALGEBRAIC(43) = 1.00000.*ALGEBRAIC(20).*ALGEBRAIC(33)+ALGEBRAIC(41);
177 RATES(12) = (ALGEBRAIC(7) - STATES(12))./ALGEBRAIC(43);
178 ALGEBRAIC(56) = (( (( CONSTANTS(:,22).*CONSTANTS(:,11))./(CONSTANTS(:,11)+CONSTANTS(:,23))).*STATES
    (3))./(STATES(3)+CONSTANTS(:,24)))./(1.00000+ 0.124500.*exp((- 0.100000.*STATES(1).*CONSTANTS
    (:,3))./( CONSTANTS(:,1).*CONSTANTS(:,2)))+ 0.0353000.*exp((- - STATES(1).*CONSTANTS(:,3))./
    CONSTANTS(:,1).*CONSTANTS(:,2))));
179 ALGEBRAIC(26) = (( CONSTANTS(:,1).*CONSTANTS(:,2))./CONSTANTS(:,3)).*log(CONSTANTS(:,12)./STATES(3)
    );
180 ALGEBRAIC(51) = CONSTANTS(:,17).*power(STATES(8), 3.00000).*STATES(9).*STATES(10).*STATES(1) -
    ALGEBRAIC(26));
181 ALGEBRAIC(52) = CONSTANTS(:,18).*STATES(1) - ALGEBRAIC(26);
182 ALGEBRAIC(57) = ( CONSTANTS(:,25).*( exp(( CONSTANTS(:,28).*STATES(1).*CONSTANTS(:,3))./( CONSTANTS
    (:,1).*CONSTANTS(:,2))).*power(STATES(3), 3.00000).*CONSTANTS(:,13) - exp(( (CONSTANTS(:,28) -
    1.00000).*STATES(1).*CONSTANTS(:,3))./( CONSTANTS(:,1).*CONSTANTS(:,2))).*power(CONSTANTS
    (:,12), 3.00000).*STATES(4).*CONSTANTS(:,27))./( (power(CONSTANTS(:,30), 3.00000)+power(
    CONSTANTS(:,12), 3.00000)).*(CONSTANTS(:,29)+CONSTANTS(:,13)).*(1.00000+ CONSTANTS(:,26).*exp(
    (CONSTANTS(:,28) - 1.00000).*STATES(1).*CONSTANTS(:,3))./( (CONSTANTS(:,1).*CONSTANTS(:,2))))));
183 RATES(3) = (( - 1.00000.*ALGEBRAIC(51)+ALGEBRAIC(52)+ 3.00000.*ALGEBRAIC(56)+ 3.00000.*ALGEBRAIC
    (57)))./( 1.00000.*CONSTANTS(:,5).*CONSTANTS(:,3)).*CONSTANTS(:,4);
184 ALGEBRAIC(34) = (( CONSTANTS(:,1).*CONSTANTS(:,2))./CONSTANTS(:,3)).*log(CONSTANTS(:,11)./STATES(2)
    );
185 ALGEBRAIC(45) = 0.100000./(1.00000+exp( 0.0600000.*((STATES(1) - ALGEBRAIC(34)) - 200.000)));
186 ALGEBRAIC(46) = ( 3.00000.*exp( 0.000200000.*((STATES(1) - ALGEBRAIC(34))+100.000))+exp(
    0.100000.*((STATES(1) - ALGEBRAIC(34)) - 10.0000))./(1.00000+exp( - 0.500000.*((STATES(1) -
    ALGEBRAIC(34)))));
187 ALGEBRAIC(47) = ALGEBRAIC(45)./(ALGEBRAIC(45)+ALGEBRAIC(46));

```

```

188 ALGEBRAIC(48) = CONSTANTS(:,14).*ALGEBRAIC(47).*power((CONSTANTS(:,11)./5.40000), 1.0 ./ 2).*(
    STATES(1) - ALGEBRAIC(34));
189 ALGEBRAIC(55) = CONSTANTS(:,21).*STATES(17).*STATES(16).*((STATES(1) - ALGEBRAIC(34));
190 ALGEBRAIC(49) = CONSTANTS(:,15).*power((CONSTANTS(:,11)./5.40000), 1.0 ./ 2).*STATES(5).*STATES(6)
    .*(STATES(1) - ALGEBRAIC(34));
191 ALGEBRAIC(42) = ((CONSTANTS(:,1).*CONSTANTS(:,2))./CONSTANTS(:,3)).*log((CONSTANTS(:,1)+
    CONSTANTS(:,10).*CONSTANTS(:,12))./(STATES(2)+CONSTANTS(:,10).*STATES(3)));
192 ALGEBRAIC(50) = CONSTANTS(:,16).*power(STATES(7), 2.00000).*((STATES(1) - ALGEBRAIC(42));
193 ALGEBRAIC(53) = ( ((CONSTANTS(:,19).*STATES(12).*STATES(13).*STATES(14).*STATES(15).*4.00000.*(
    STATES(1) - 15.0000).*power(CONSTANTS(:,3), 2.00000))./(CONSTANTS(:,1).*CONSTANTS(:,2))).*(
    0.250000.*STATES(11).*exp(( 2.00000.*((STATES(1) - 15.0000).*CONSTANTS(:,3))./(CONSTANTS(:,1).*(
    CONSTANTS(:,2))) - CONSTANTS(:,13)))./(exp(( 2.00000.*((STATES(1) - 15.0000).*CONSTANTS(:,3))./(
    CONSTANTS(:,1).*CONSTANTS(:,2))) - 1.00000));
194 ALGEBRAIC(44) = (( 0.500000.*CONSTANTS(:,1).*CONSTANTS(:,2))./CONSTANTS(:,3)).*log(CONSTANTS(:,13)
    ./STATES(4));
195 ALGEBRAIC(54) = CONSTANTS(:,20).*((STATES(1) - ALGEBRAIC(44));
196 ALGEBRAIC(59) = ( CONSTANTS(:,33).*((STATES(1) - ALGEBRAIC(34)))./(1.00000+exp((25.0000 - STATES(1))
    ./5.98000));
197 ALGEBRAIC(58) = ( CONSTANTS(:,31).*STATES(4))./(STATES(4)+CONSTANTS(:,32));
198 RATES(1) = - (ALGEBRAIC(48)+ALGEBRAIC(55)+ALGEBRAIC(49)+ALGEBRAIC(50)+ALGEBRAIC(53)+ALGEBRAIC(56)+
    ALGEBRAIC(51)+ALGEBRAIC(52)+ALGEBRAIC(57)+ALGEBRAIC(54)+ALGEBRAIC(59)+ALGEBRAIC(58)+(numberhmsc
    .*1.5./185).*((STATES(1)-STATES(28)));
199 RATES(2) = (( - 1.00000.*((ALGEBRAIC(48)+ALGEBRAIC(55)+ALGEBRAIC(49)+ALGEBRAIC(50)+ALGEBRAIC(59)+
    ALGEBRAIC(13)) - 2.00000.*ALGEBRAIC(56)))./( 1.00000.*CONSTANTS(:,5).*CONSTANTS(:,3))).*
    CONSTANTS(:,4);
200 ALGEBRAIC(60) = CONSTANTS(:,45)./(1.00000+power(CONSTANTS(:,43), 2.00000)./power(STATES(4), 2.00000)
    );
201 ALGEBRAIC(61) = CONSTANTS(:,44).*((STATES(18) - STATES(4));
202 ALGEBRAIC(62) = CONSTANTS(:,42).*((STATES(11) - STATES(4));
203 ALGEBRAIC(64) = 1.00000./(1.00000+( CONSTANTS(:,46).*CONSTANTS(:,47))./power(STATES(4)+CONSTANTS
    (:,47), 2.00000));
204 RATES(4) = ALGEBRAIC(64).*((( (ALGEBRAIC(61) - ALGEBRAIC(60)).*CONSTANTS(:,52))./CONSTANTS(:,5)+
    ALGEBRAIC(62)) - ( 1.00000.*((ALGEBRAIC(54)+ALGEBRAIC(58)) - 2.00000.*ALGEBRAIC(57)).*
    CONSTANTS(:,4))./( 2.00000.*1.00000.*CONSTANTS(:,5).*CONSTANTS(:,3)));
205 ALGEBRAIC(63) = CONSTANTS(:,39) - (CONSTANTS(:,39) - CONSTANTS(:,40))./(1.00000+power(CONSTANTS
    (:,38)./STATES(18), 2.00000));

```

```

206 ALGEBRAIC(66) = CONSTANTS(:,35).*ALGEBRAIC(63);
207 RATES(19) = - ALGEBRAIC(66).*STATES(11).*STATES(19)+ CONSTANTS(:,37).*(1.00000 - STATES(19));
208 ALGEBRAIC(65) = CONSTANTS(:,34)./ALGEBRAIC(63);
209 ALGEBRAIC(67) = ( ALGEBRAIC(65).*power(STATES(11), 2.00000).*STATES(19))./(CONSTANTS(:,36) +
    ALGEBRAIC(65).*power(STATES(11), 2.00000));
210 ALGEBRAIC(68) = CONSTANTS(:,41).*ALGEBRAIC(67).*(STATES(18) - STATES(11));
211 ALGEBRAIC(69) = 1.00000./(1.00000+( CONSTANTS(:,48).*CONSTANTS(:,49))./power(STATES(18)+CONSTANTS
    (:,49), 2.00000));
212 RATES(18) = ALGEBRAIC(69).*((ALGEBRAIC(60) - (ALGEBRAIC(68)+ALGEBRAIC(61))));
213 ALGEBRAIC(70) = 1.00000./(1.00000+( CONSTANTS(:,50).*CONSTANTS(:,51))./power(STATES(11)+CONSTANTS
    (:,51), 2.00000));
214 RATES(11) = ALGEBRAIC(70).*((( - 1.00000.*ALGEBRAIC(53).*CONSTANTS(:,4))./( 2.00000.*1.00000.*
    CONSTANTS(:,53).*CONSTANTS(:,3))+(( ALGEBRAIC(68).*CONSTANTS(:,52))./CONSTANTS(:,53)) - (
    ALGEBRAIC(62).*CONSTANTS(:,5))./CONSTANTS(:,53));
215
216 % hMSC calculations
217 ALGEBRAIC(71) = 2.52.*exp(-(STATES(28)-53.16).^2/593.7)+2.44;
218 ALGEBRAIC(72) = 8.2.*exp(-(STATES(28)-55.2).^2/659.9);
219 ALGEBRAIC(73) = 0.028./(1+0.86.*exp((STATES(28)-10.0)./-12.35)).*.6;
220 ALGEBRAIC(74) = 3e-4.*(125.5+STATES(28))./(1+26.9.*exp(-(STATES(28)-47.4)/-14.6)).*.6;
221 ALGEBRAIC(75) = 1e-1;
222 ALGEBRAIC(76) = 10;
223 ALGEBRAIC(77) = 687.8.*1e-4.*exp(STATES(28)./15.8);
224 ALGEBRAIC(78) = 21.1.*exp(-STATES(28)./43.5);
225 ALGEBRAIC(79) = (8.314.*310./1./96.65).*log(5.4./140);
226 ALGEBRAIC(80) = 6.5*(STATES(28)-ALGEBRAIC(79)).*STATES(25);
227 ALGEBRAIC(81) = 3*(STATES(28)-ALGEBRAIC(79)).*STATES(26);
228
229 RATES(20) = ALGEBRAIC(75).*ALGEBRAIC(74).*STATES(21)-ALGEBRAIC(76).*ALGEBRAIC(73).*STATES(20);
230 RATES(21) = (ALGEBRAIC(76).*ALGEBRAIC(73).*STATES(20)+2*ALGEBRAIC(74).*STATES(22) - (ALGEBRAIC(75).*ALGEBRAIC(74)+3*ALGEBRAIC(73)).*STATES(21));
231 RATES(22) = (3.*ALGEBRAIC(73).*STATES(21)+3*ALGEBRAIC(74).*STATES(23) - (2.*ALGEBRAIC(74)+2*ALGEBRAIC(73)).*STATES(22));
232 RATES(23) = (2.*ALGEBRAIC(73).*STATES(22)+4*ALGEBRAIC(74).*STATES(24) - (3.*ALGEBRAIC(74)+1*ALGEBRAIC(73)).*STATES(23));

```

```
233 RATES(24) = (1.*ALGEBRAIC(73).*STATES(23)+ALGEBRAIC(72).*ALGEBRAIC(74).*STATES(25) - (4.*ALGEBRAIC  
    (74)+ALGEBRAIC(71).*ALGEBRAIC(73)).*STATES(24));  
234 RATES(25) = ALGEBRAIC(71).*ALGEBRAIC(73).*STATES(24) - ALGEBRAIC(72).*ALGEBRAIC(74).*STATES(25);  
235  
236 RATES(26) = (1-STATES(26)).*ALGEBRAIC(77)-STATES(26).*21.1.*ALGEBRAIC(78);  
237  
238 RATES(27) = 0;  
239 RATES(28) = -(1./59.7).*(ALGEBRAIC(80)+ALGEBRAIC(81)+.014*(STATES(28)-130)+numbercm.*1.5.*(STATES  
    (28)-STATES(1)));  
240  
241 s = RATES;  
242  
243  
244 end  
245  
246 % initial conditions  
247  
248 function u0 = pdeinic(~, p)  
249  
250  
251 INIT(1) = -85.423;  
252 INIT(2) = 138.52;  
253 INIT(3) = 10.132;  
254 INIT(4) = 0.000153;  
255 INIT(5) = 0.0165;  
256 INIT(6) = 0.473;  
257 INIT(7) = 0.0174;  
258 INIT(8) = 0.00165;  
259 INIT(9) = 0.749;  
260 INIT(10) = 0.6788;  
261 INIT(11) = 0.00042;  
262 INIT(12) = 3.288e-5;  
263 INIT(13) = 0.7026;  
264 INIT(14) = 0.9526;  
265 INIT(15) = 0.9942;  
266 INIT(16) = 0.999998;
```

```

267 INIT(17) = 2.347e-8;
268 INIT(18) = 4.272;
269 INIT(19) = 0.8978;
270 INIT(20) = 0;
271 INIT(21) = 0.36;
272 INIT(22) = 0;
273 INIT(23) = 0;
274 INIT(24) = 0.64;
275 INIT(25) = 0;
276 INIT(26) = 0;
277 INIT(27) = 5.4;
278 INIT(28) = -42;
279
280 u0 = INIT;
281 end
282
283 % boundary conditions
284
285 function [pl,ql,pr,qr] = pdebouc(~, ~, ~, ur, t, p)
286
287 Istim = 10*(heaviside(t)- heaviside(t - .2));
288 pl = [Istim; 0; 0; 0; 0; 0; 0; 0; 0; 0; 0; 0; 0; 0; 0; 0; 0; 0; 0; 0; 0; 0; 0; 0; 0; 0; 0; 0; Istim];
289 ql = [1; 1; 1; 1; 1; 1; 1; 1; 1; 1; 1; 1; 1; 1; 1; 1; 1; 1; 1; 1; 1; 1; 1; 1; 1; 1; 1; 1; 1; 1; 1];
290 pr = [0; 0; 0; 0; 0; 0; 0; 0; 0; 0; 0; 0; 0; 0; 0; 0; 0; 0; 0; 0; 0; 0; 0; 0; 0; 0; 0; 0];
291 qr = [1; 1; 1; 1; 1; 1; 1; 1; 1; 1; 1; 1; 1; 1; 1; 1; 1; 1; 1; 1; 1; 1; 1; 1; 1; 1; 1; 1];
292
293 end
294
295
296 function x = piecewise(cases, default)
297 set = [0];
298 for i = 1:2:length(cases)
299     if (length(cases{i+1}) == 1)
300         x(cases{i} & ~set,:) = cases{i+1};
301     else
302         x(cases{i} & ~set,:) = cases{i+1}(cases{i} & ~set);

```

```
303     end
304
305     set = set | cases{i};
306
307     if(set), break, end
308
309 end
310
311 else
312
313
314
315 function strout = strpad(strin)
316
317 req_length = 160;
318
319 insize = size(strin,2);
320
321 if insize > req_length
322
323 strout = strin(1:req_length);
324
325 else
326
327 strout = [strin, blanks(req_length - insize)];
328
329 end
330
331 end
```

Bibliography

- [1] Schulman IH and Hare JM. Key developments in stem cell therapy in cardiology. *Regenerative medicine*, 7(6 Suppl):17–24, Nov 2012. ISSN 1746-076X.
URL <http://www.ncbi.nlm.nih.gov/pubmed/23346572>.
- [2] Roger VL, Go AS, Lloyd-Jones DM, Benjamin EJ, Berry JD, Borden WB, Bravata DM, Dai S, Ford ES, Fox CS, Fullerton HJ, Gillespie C, Hailpern SM, Heit JA, Howard VJ, Kissela BM, Kittner SJ, Lackland DT, Lichtman JH, Lisabeth LD, Makuc DM, Marcus GM, Marelli A, Matchar DB, Moy CS, Mozaffarian D, Mussolino ME, Nichol G, Paynter NP, Soliman EZ, Sorlie PD, Sotoodehnia N, Turan TN, Virani SS, Wong ND, Woo D, Turner MB, and American Heart Association Statistics Committee and Stroke Statistics Subcommittee. Heart disease and stroke statistics—2012 update: a report from the american heart association. *Circulation*, 125(1):e2–e220, Jan 2012. ISSN 1524-4539. doi: 10.1161/CIR.0b013e31823ac046. URL <http://www.ncbi.nlm.nih.gov/pubmed/22179539>.
- [3] Garben JC and Lee RT. Cardiac stem cell therapy and the promise of heart regeneration. *Cell Stem Cell*, 12:689–698, June 2013.

- [4] Wei HJ, Chen CH, Lee WY, Chiu I, Hwang SM, Lin WW, Huang CC, Yeh YC, Chang Y, and Sung HW. Bioengineered cardiac patch constructed from multilayered mesenchymal stem cells for myocardial repair. *Biomaterials*, 29(26):3547–3556, Sep 2008. ISSN 0142-9612. doi: 10.1016/j.biomaterials.2008.05.009. URL <http://www.ncbi.nlm.nih.gov/pubmed/18538386>.
- [5] Aguirre A, Sancho-Martinez I, and Izpisua Belmonte JC. Reprogramming toward heart regeneration: stem cells and beyond. *Cell Stem Cell*, 12(3):275–84, 2013.
- [6] Hare JM, Traverse JH, Henry TD, Dib N, Strumpf RK, Schulman SP, Gerstenblith G, DeMaria AN, Denktas AE, Gammon RS, Hermiller JB Jr, Reisman MA, Schaer GL, and Sherman W. A randomized, double-blind, placebo-controlled, dose-escalation study of intravenous adult human mesenchymal stem cells (prochymal) after acute myocardial infarction. *Journal of the American College of Cardiology*, 54(24):2277–2286, Dec 2009. ISSN 1558-3597. doi: 10.1016/j.jacc.2009.06.055. URL <http://www.ncbi.nlm.nih.gov/pubmed/19958962>.
- [7] Boyle AJ, Schulman SP, and Hare JM. Stem cell therapy for cardiac repair: Ready for the next step. *Controversies in Cardiovascular Medicine*, 114:339–352, July 2006.
- [8] Mazo M, Arana M, Pelacho B, and Prosper F. Mesenchymal stem cells and cardiovascular disease: Bench to bedside roadmap. *Stem Cells International*, 2012(175979):11, Oct 2012.

- [9] Meregalli M, Farini A, and Torrente Y. Mesenchymal stem cells as muscle reservoir. *Journal of Stem Cell Research and Therapy*, 1(2), July 2011.
- [10] Pittenger MF, Mackay AM, Beck SC, Jaiswal RK, Douglas R, Mosca JD, Moorman MA, Simonetti DW, Craig S, and Marshak DR. Multilineage potential of adult human mesenchymal stem cells. *Science*, 284(5411):143–7, Apr 1999.
- [11] Acquistapace A, Bru T, Lesault PF, Figeac F, Courdert AE, Ie Coz O, Christov C, Baudin X, Auber F, Yiou R, Dubois-Rande JL, and Rodriguez AM. Human mesenchymal stem cells reprogram adult cardiomyocytes toward a progenitor-like state through partial cell fusion and mitochondria transfer. *Stem cells (Dayton, Ohio)*, 29(5):812–824, May 2011. ISSN 1549-4918. doi: 10.1002/stem.632. URL <http://www.ncbi.nlm.nih.gov/pubmed/21433223>.
- [12] Gaebel R, Furlani D, Sorg H, Polchow B, Frank J, Bieback K, Wang W, Klöpsch C, Ong L, Li W, Ma N, and Steinhoff G. Cell origin of human mesenchymal stem cells determines a different healing performance in cardiac regeneration. *PLoS one*, 6(2):e15652, Feb 2011. ISSN 1932-6203. doi: 10.1371/journal.pone.0015652. URL <http://www.ncbi.nlm.nih.gov/pubmed/21347366>.
- [13] Bayes-Genis A, Soler-Botija C, Farre J, Sepulveda P, Raya A, Roura S, Prat-Vidal C, Galvez-Monton C, Montero JA, Buscher D, and Izpisua Belmonte JC. Human progenitor cells derived from cardiac adipose tissue ameliorate myocardial infarctions in rats. *Journal of Molecular and Cellular Cardiology*, 49(5):771–80, Nov 2010.

- [14] Miyahara Y, Nagaya N, Kataoka M, Yanagawa B, Tanaka K, Hao H, Ishino K, Ishida H, Shimizu T, Kangawa K, Sano S, Okano T, Kitamura S, and Mori H. Monolayered mesenchymal stem cells repair scarred myocardium after myocardial infarction. *Nature medicine*, 12(4):459–465, Apr 2006. ISSN 1078-8956. doi: 10.1038/nm1391. URL <http://www.ncbi.nlm.nih.gov/pubmed/16582917>.
- [15] Zhao Z, Chen Z, Zhao X, Pan F, Cai M, Wang T, Zhang H, Lu JR, and Lei M. Sphingosine-1-phosphate promotes the differentiation of human umbilical cord mesenchymal stem cells into cardiomyocytes under the designated culturing conditions. *Journal of Biomedical Science*, 18(37), Jun 2011.
- [16] Kurth TB, Dell’accio F, Crouch V, Augello A, Sharpe PT, and De Bari C. Functional mesenchymal stem cell niches in adult mouse knee joint synovium in vivo. *Arthritis and Rheumatism*, 63(5):1289, 300 2011.
- [17] Sabatini F, Petecchia L, Tavian M, Jodon de Villeroché V, Rossi GA, and Brouty-Boyé D. Human bronchial fibroblasts exhibit a mesenchymal stem cell phenotype and multilineage differentiating potentialities. *Laboratory investigation; a journal of technical methods and pathology*, 85(8):962–971, Aug 2005. ISSN 0023-6837. doi: 10.1038/labinvest.3700300. URL <http://www.ncbi.nlm.nih.gov/pubmed/15924148>.
- [18] Tsuji H, Miyoshi S, Ikegami Y, Hida N, Asada H, Togashi I, Suzuki J, Satake M, Nakamizo H, Tanaka M, Mori T, Segawa K, Nishiyama N, Inoue J, Makino H, Miyado K, Ogawa S, Yoshimura Y, and Umezawa A. Xenografted human

- amniotic membrane-derived mesenchymal stem cells are immunologically tolerated and transdifferentiated into cardiomyocytes. *Circulation research*, 106(10):1613–1623, May 2010. ISSN 1524-4571. doi: 10.1161/CIRCRESAHA.109.205260. URL <http://www.ncbi.nlm.nih.gov/pubmed/20508201>.
- [19] Zvaifler NJ, Marinova-Mutafchieva L, Adams G, Edwards CJ, Moss J, Burger JA, and Maini RN. Mesenchymal precursor cells in the blood of normal individuals. *Arthritis Research*, 2(6):477–88, Aug 2000.
- [20] Lipinski MJ, Biondi-Zocca GG, Abbate A, Khianey R, Sheiban I, Bartunek J, Vanderheyden M, Kim HS, Hang HJ, Strauer BE, and Vetrovec GW. Impact of intracoronary cell therapy on left ventricular function in the setting of acute myocardial infarction: a collaborative systematic review and meta-analysis of controlled clinical trials. *J Am Coll Cardiol*, 30;50(18):1761–7, Oct 2007.
- [21] Wollert KC and Drexler H. Clinical applications of stem cells for the heart. *Circ Res*, 96:151–163, 2005.
- [22] Terrovitis JV, Smith RR, and Marban E. Assessment and optimization of cell engraftment after transplantation into the heart. *Circ Res*, 19;106(3):479–94, Feb 2010.
- [23] Chen S, Liu Z, Tian N, Zhang J, Yei F, Duan B, Zhu Z, Lin S, and Kwan TW. Intracoronary transplantation of autologous bone marrow mesenchymal stem cells for ischemic cardiomyopathy due to isolated chronic occluded left anterior descending artery. *The Journal of invasive cardiology*, 18(11):552–556,

- Nov 2006. ISSN 1557-2501. URL <http://www.ncbi.nlm.nih.gov/pubmed/17090821>.
- [24] Katritsis DG, Sotiropoulou PA, Karvouni E, Karabinos I, Korovesis S, Perez SA, Vordinis EM, and Papamichail M. Transcoronary transplantation of autologous mesenchymal stem cells and endothelial progenitors into infarcted human myocardium. *Catheterization and cardiovascular interventions : official journal of the Society for Cardiac Angiography & Interventions*, 65(3):321–329, Jul 2005. ISSN 1522-1946. doi: 10.1002/ccd.20406. URL <http://www.ncbi.nlm.nih.gov/pubmed/15954106>.
- [25] Chen SL, Fang WW, Ye F, Liu YH, Qian J, Shan SJ, Zhang JJ, Chunhua RZ, Liao LM, Lin S, and Sun JP. Effect on left ventricular function of intracoronary transplantation of autologous bone marrow mesenchymal stem cell in patients with acute myocardial infarction. *The American journal of cardiology*, 94(1):92–95, Jul 2004. ISSN 0002-9149. doi: 10.1016/j.amjcard.2004.03.034. URL <http://www.ncbi.nlm.nih.gov/pubmed/15219514>.
- [26] Dib N, Henry T, DeMaria A, Itescu S, McCarthy MM, and Jaggar SC. The first us study to assess the feasibility and safety of endocardial delivery of allogenic mesenchymal precursor cells in patient with heart failure: three-month interim analysis. *J Am Coll Cardiol*, 55(10A), March 2010.
- [27] Cashman TJ, Gouon-Evans V, and Costa KD. Mesenchymal stem cells for cardiac therapy: Practical challenges and potential mechanisms. *Stem Cell Rev and Rep*, 9(3):254–65, Jun 2012.

- [28] Wollert KC, Meyer GP, Lotz J, Ringes-Lichtenberg S, Lippolt P, Breidenbach C, Fichtner S, Korte T, Hornig B, Messinger D, Arseniev L, Hertenstein B, Ganser A, and Drexler H. Intracoronary autologous bone-marrow cell transfer after myocardial infarction: the boost randomised controlled clinical trial. *Lancet*, 364(9429):141–148, Jul 2004. ISSN 1474-547X. doi: 10.1016/S0140-6736(04)16626-9. URL <http://www.ncbi.nlm.nih.gov/pubmed/15246726>.
- [29] Schaefer A, Zwadlo C, Fuchs M, Meyer GP, Lippolt P, Wollert KC, and Drexler H. Long-term effects of intracoronary bone marrow cell transfer on diastolic function in patients after acute myocardial infarction: 5-year results from the randomized-controlled boost trial—an echocardiographic study. *European journal of echocardiography : the journal of the Working Group on Echocardiography of the European Society of Cardiology*, 11(2):165–171, Mar 2010. ISSN 1532-2114. doi: 10.1093/ejechocard/jep191. URL <http://www.ncbi.nlm.nih.gov/pubmed/19946118>.
- [30] Meyer GP, Wollert KC, Lotz J, Steffens J, Lippolt P, Fichtner S, Hecker H, Schaefer A, Arseniev L, Hertenstein B, Ganser A, and Drexler H. Intracoronary bone marrow cell transfer after myocardial infarction: 5-year follow-up from the randomized-controlled boost trial. *European heart journal*, 30(24):2978–2984, Dec 2009. ISSN 1522-9645. doi: 10.1093/eurheartj/ehp374. URL <http://www.ncbi.nlm.nih.gov/pubmed/19773226>.
- [31] Meyer GP, Wollert KC, Lotz J, Steffens J, Lippolt P, Fichtner S, Hecker H,

- Schaefer A, Arseniev L, Hertenstein B, Ganser A, and Drexler H. Intracoronary bone marrow cell transfer after myocardial infarction: eighteen months' follow-up data from the randomized, controlled boost (bone marrow transfer to enhance st-elevation infarct regeneration) trial. *Circulation*, 113(10):1287–1294, Mar 2006. ISSN 1524-4539. doi: 10.1161/CIRCULATIONAHA.105.575118. URL <http://www.ncbi.nlm.nih.gov/pubmed/16520413>.
- [32] Friis T, Haack-Sorensen M, Mathiasen AB, Ripa RS, Kristoffersen US, Jorgensen E, Hansen L, Bindslev L, Kjaer A, Hesse B, and Kastrup J Dickmeiss E. Mesenchymal stromal cell derived endothelial progenitor treatment in patients with refractory angina. *Scandinavian cardiovascular journal : SCJ*, 45(3):161–168, Jun 2011. ISSN 1651-2006. doi: 10.3109/14017431.2011.569571. URL <http://www.ncbi.nlm.nih.gov/pubmed/21486102>.
- [33] Williams AR, Trachtberg B, Velazquez DL, McNiece I, Altman P, Menzabal AM Rouy D, Pattany PM, Lopera GA, Fishman J, Zambrano JP, Heldman AW, and Hare JM. Intramyocardial stem cell injection in patients with ischemic cardiomyopathy: functional recovery and reverse remodeling. *Circulation research*, 108(7):792–796, Apr 2011. ISSN 1524-4571. doi: 10.1161/CIRCRESAHA.111.242610. URL <http://www.ncbi.nlm.nih.gov/pubmed/21415390>.
- [34] Penn MS, Ellis S, Gandhi S, Greenbaum A, Hodes Z, Mendelsohn FO, Strasser D, Ting AE, and Sherman W. Adventitial delivery of an allogeneic bone marrow-derived adherent stem cell in acute myocardial infarction: phase i

- clinical study. *Circulation research*, 110(2):304–311, Jan 2012. ISSN 1524-4571. doi: 10.1161/CIRCRESAHA.111.253427. URL <http://www.ncbi.nlm.nih.gov/pubmed/22052917>.
- [35] Segers VF and Lee RT. Stem-cell therapy for cardiac disease. *Nature*, 451: 937–942, Feb 2008.
- [36] Abdel-Latif A, Bolli R, Tleyjeh IM, Montori VM, Perin EC, Hornung CA, Zuba-Surma EK, Al-Mallah M, and Dawn B. Adult bone marrow-derived cells for cardiac repair: a systematic review and meta-analysis. *Archives of internal medicine*, 167(10):989–997, May 2007. ISSN 0003-9926. doi: 10.1001/archinte.167.10.989. URL <http://www.ncbi.nlm.nih.gov/pubmed/17533201>.
- [37] Chang MG, Tung L, Sekar RB, Chang CY, Cysyk J, Dong P, Marbán E, and Abraham MR. Proarrhythmic potential of mesenchymal stem cell transplantation revealed in an in vitro coculture model. *Circulation*, 113(15):1832–1841, Apr 2006. ISSN 1524-4539. doi: 10.1161/CIRCULATIONAHA.105.593038. URL <http://www.ncbi.nlm.nih.gov/pubmed/16606790>.
- [38] Janse MJ and Wit AL. Electrophysiological mechanisms of ventricular arrhythmias resulting from myocardial ischemia and infarction. *Physiol Rev.*, 69(4):1049–169, Oct 1989.
- [39] Numasawa Y, Kimura T, Miyoshi S, Nishiyama N, Hida N, Tsuji H, Tsuruta H, Segawa K, Ogawa S, and Umezawa A. Treatment of human mesenchymal stem cells with angiotensin receptor blocker improved efficiency of cardiomyogenic transdifferentiation and improved cardiac function via angiogenesis. *Stem cells*

- (Dayton, Ohio), 29(9):1405–1414, Sep 2011. ISSN 1549-4918. doi: 10.1002/stem.691. URL <http://www.ncbi.nlm.nih.gov/pubmed/21755575>.
- [40] Serrao GW, Turnbull IC, Ancukiewicz D, Kim DE, Kao E, Cashman TJ, Hadri L, Hajjar RJ, and Costa KD. Myocyte-depleted engineered cardiac tissues support therapeutic potential of mesenchymal stem cells. *Tissue engineering. Part A*, 18(13-14):1322–1333, Jul 2012. ISSN 1937-335X. doi: 10.1089/ten.TEA.2011.0278. URL <http://www.ncbi.nlm.nih.gov/pubmed/22500611>.
- [41] Hui-Nam Pak, Mohammed Qayyum, Dave T. Kim, Akira Hamabe, Yasushi Miyauchi, Michael C. Lill, Malkar Frantzen, Kaname Takizawa, Lan S. Chen, Michael C. Fishbein, Behrooz G. Sharifi, Peng-Sheng Chen, and Raj Makkar. Mesenchymal stem cell injection induces cardiac nerve sprouting and increased tenascin expression in a swine model of myocardial infarction. *Journal of cardiovascular electrophysiology*, 14(8):841–848, Aug 2003. ISSN 1045-3873. URL <http://www.ncbi.nlm.nih.gov/pubmed/12890047>.
- [42] Rosen MR, Brink PR, Cohen IS, and Robinson RB. Gene, stem cells and biological pacemakers. *Cardiovascular Research*, 64:12–23, May 2004.
- [43] Klabunde RE. Action potentials.
- [44] Adeniran A. *Biophysically Detailed Modelling of the Functional Impact of Gene Mutations Associated with the 'Short QT Syndrome'*. PhD thesis, University of Manchester, 2012.

- [45] Li GR, Sun H, Deng X, and Lau CP. Characterization of ionic currents in human mesenchymal stem cells from bone marrow. *Stem Cells*, 23(3):371–82, March 2005.
- [46] Heubach JF, Graf EM, Leutheuser J, Bock M, Balana B, Zahanich I, Christ T, Boxberger S, Wettwer E, and Ravens U. Electrophysiological properties of human mesenchymal stem cells. *The Journal of physiology*, 554(Pt 3):659–672, Feb 2004. ISSN 0022-3751. doi: 10.1113/jphysiol.2003.055806. URL <http://www.ncbi.nlm.nih.gov/pubmed/14578475>.
- [47] Li GR and Deng XL. Functional ion channels in stem cells. *World Journal of Stem Cells*, 3(3):19–24, Mar 2011.
- [48] Firth AL and Yuan JX. "ether-a-go-go" proliferation of ipsc-derived mesenchymal stem cells. focus on "regulation of cell proliferation of human induced pluripotent stem cell-derived mesenchymal stem cells via ether-a-go-go 1 (heag1) potassium channel. *Am J Physiol Cell Physiol*, 303(2):C113–4, Jul 2012.
- [49] Purves D, Augustine GJ, Fitzpatrick D, Katz LC, LaMantia AS, McNamara JO, and Williams S. *Neuroscience*, volume 2. Sinauer Associates, 2001.
- [50] Yuan P, Leonetti MD, Pico AR, Hsiung Y, and MacKinnon R. Structure of the human bk channel ca₂₊-activation apparatus at 3.0 Å resolution. *Science*, 329(5988):182–6, Jul 2010.
- [51] Wallner M, Meera P, and Toro L. Determinant for beta-subunit regulation in high-conductance voltage-activated and ca₂₊-sensitive k⁺ channels: an

- additional transmembrane region at the n terminus. *Proc. Natl. Acad. Sci. U.S.A.*, 93:14922–14927, Dec 1996.
- [52] Wu Y, Yang Y, Ye S, and Jian Y. Structure of the gating ring from the human large-conductance Ca^{2+} gated K^+ channel. *Nature*, 466(7304):393–397, July 2010.
- [53] Jiang Y, Pico A, Cadene M, Chait BT, and MacKinnon R. Structure of the rck domain from the *e. coli* K^+ channel and demonstration of its presence in the human bk channel. *Neuron*, 29(3):593–601, March 2001.
- [54] Pico AR. Rck domain model of calcium activation in bk channels. *PhD Thesis*, 2003.
- [55] Yusifov T, Savalli N, Gandhi CS, Ottolia M, and Olcese R. The rck2 domain of the human bkca channel is a calcium sensor. *Proc. Natl. Acad. Sci. U.S.A.*, 105(1):376–81, Jan 2008.
- [56] Schreiber M and Salkoff L. A novel calcium-sensing domain in the bk channel. *Biophysical Journal*, 73(3):1355–63, September 1997.
- [57] Yuan P, Leonetti MD, Hsiung Y, and MacKinnon R. Open structure of the Ca^{2+} gating ring in the high-conductance Ca^{2+} -activated K^+ channel. *Nature*, 481(7379):94–7, Dec 2012.
- [58] Sanguinetti MC and Tristani-Firouzi M. herg potassium channels and cardiac arrhythmia. *Nature*, 440(7083):463–9, March 2006.

- [59] Sanguinetti MC, Jiang C, Curran ME, and Keating MT. A mechanistic link between an inherited and an acquired cardiac arrhythmia: herg encodes the delayed rectifier potassium channel. *Cell*, 81(2):299–307, Apr 1995.
- [60] Moss AJ, Zareba W, Kaufman ES, Gartman E, Peterson DR, Benhorin J, Towbin JA, Keating MT, Priori SG, Schwartz PJ, Vincent GM, Robinson Jl, Andrews ML, Feng C, Hall WJ, Medina A, Zhang L, and Wang Z. Increased risk of arrhythmic events in long-qt syndrome with mutations in the pore region of the human ether-a-go-go-related gene potassium channel. *Circulation*, 105(7):794–799, Feb 2002. ISSN 1524-4539. URL <http://www.ncbi.nlm.nih.gov/pubmed/11854117>.
- [61] Heinemann SH. Regulation of eag potassium channels by cytosolic proteins. URL [http://www.sfb604.uni-jena.de/Aims/Area+A/Project+A4+\(Heinemann\).html](http://www.sfb604.uni-jena.de/Aims/Area+A/Project+A4+(Heinemann).html).
- [62] Barros F, Dominguez P, and de la Pena P. Cytoplasmic domains and voltage-dependent potassium channel gating. *Frontiers in Pharmacology*, 3(49):1–15, March 2012.
- [63] Soldatov NM. Molecular determinants of cav1.2 calcium channel inactivation. *ISRN Molecular Biology*, 2012:1–10, September 2012.
- [64] Dib-Hajj SD, Yang Y, Waxman B, and Waxman SG. The nav1.7 sodium channel: from molecule to man. *Nature*, 14:49–62, Jan 2013.
- [65] Genetics Home Reference. Scn5a. URL <http://ghr.nlm.nih.gov/gene/SCN5A>.

- [66] ten Tusscher KHWJ, Noble D, Noble PJ, and Panfilov AV. A model for human ventricular tissue. *American Journal of Physiology*, 286(4):H1573–89, Apr 2004.
- [67] MacCannell AK, Bazzazi H, Chilton L, Shibukawa Y, and Giles WR Clark R. A mathematical model of electrotonic interactions between ventricular myocytes and fibroblasts. *Biophysical Journal*, 92:4121–4132, June 2007.
- [68] Dayan P and Abbott LF. *Theoretical Neuroscience: Computational and Mathematical Modeling of Neural Systems*. MIT Press, 2001.
- [69] Heubach JF, Graf EM, Leutheuser J, Bock M, Balana B, Zahanich I, Christ T, Boxberger S, Wettwer E, and Ravens U. Electrophysiological properties of human mesenchymal stem cells. *J. Physiol.*, 554:659–72, Feb 2003.
- [70] Valiunas V, Doronin S, Valiuniene L, Potapova I, Zuckerman J, Walcott B, Robinson RB, Rosen MR, Brink PR, and Cohen IS. Human mesenchymal stem cells make cardiac connexins and form functional gap junctions. *J. Physiol.*, 555(3):617–626, Feb 2004.
- [71] Dill KA and Bromberg S. *Molecular Driving Forces: Statistical Thermodynamics in Chemistry and Biology*. Science, 2003.
- [72] Kirby BJ. *Micro- and Nanoscale Fluid Mechanics: Transport in Microfluidic Devices*. Cambridge University Press, 2010.
- [73] Probstein R. *Physicochemical Hydrodynamics*. John Wiley and Sons, 1994.

- [74] Plonsey R and Barr RC. *Bioelectricity: A Quantitative Approach*. Springer, 2007.
- [75] Kandel ER, Schwartz JH, and Jessell TM. *Principles of Neural Science*. McGraw-Hill, Year.
- [76] Hille B. *Ion Channels of Excitable Membranes*. Sinauer Associates, 3rd edition, 2001.
- [77] Priebe L and Beuckelmann DJ. Simulation study of cellular electric properties in heart failure. *Circ Res*, 82(11):1206–23, Jun 1998.
- [78] Luo C and Rudy Y. A model of the ventricular cardiac action potential, depolarization, repolarization, and their interaction. *Circ Res*, 68(6):1501–26, Jun 1991.
- [79] ten Tusscher KHWJ and Panfilov AV. Alternans and spiral breakup in a human ventricular tissue model. *American Journal of Physiology - Heart and Circulatory Physiology*, 291:H1088–H1100, March 2006.
- [80] Antzelevitch C. M cells in the human heart. *Circ Res*, 106:815–817, March 2010.
- [81] Williams AR and Hare JR. Mesenchymal stem cells: Biology, pathophysiology, translational findings, and therapeutic implications for cardiac disease. *Circ Res*, 109:923–940, August 2011.
- [82] ten Tusscher KHWJ and Panfilov AV. Alternans and spiral breakup in a human ventricular tissue model. URL <http://models.cellml.org/>

exposure/de5058f16f829f91a1e4e5990a10ed71/tentusscher_panfilov_2006_c.cellml/view.

- [83] Sachse FB, Moreno AP, and Abildskov JA. Electrophysiological modeling of fibroblasts and their interaction with myocytes. *Annals of Biomedical Engineering*, 36(1):41–56, Jan 2008.
- [84] Hodgkin AL and Huxley AF. A quantitative description of membrane current and its application to conduction and excitation in nerve. *J. Physiol.*, 117(4):500–544, Aug 1952.
- [85] Meech RW and Standen NB. Potassium activation in helix aspersa neurones under voltage clamp: a component mediated by calcium influx. *J. Physiol.*, 249(2):211–259, Jul 1975.
- [86] Wilson WA and Goldner MM. Voltage clamping with a single microelectrode. *J. Neurobiology*, 6(4):411–422, Oct 1975.
- [87] Neher E and Sakmann B. Single-channel currents recorded from membrane of denervated frog muscle fibers. *Nature*, 260:799–802, April 1976.
- [88] Lehmann-Horn F, Fauler M, Holzherr B, and Jurkat-Rott K. *Cardiac Electrophysiology Methods and Models*. Springer, 2010.
- [89] Gerstner W and Kistler WM. *Spiking Neuron Models: Single Neurons, Populations, Plasticity*. Cambridge University Press, 2002.
- [90] Beeler GW and Reuter H. Reconstruction of the action potential of ventricular myocardial fibers. *J. Physiol.*, 268(1):177–210, Jun 1977.

- [91] Courtemanche M, Ramirez RJ, and Nattel S. Ionic mechanisms underlying human atrial action potential properties: insights from a mathematical model. *American Journal of Physiology - Heart and Circulatory Physiology*, 275:H301–21, Jul 1998.
- [92] Koch C and Segev I. *Methods in Neuronal Modeling: From Ions to Networks*. A Bradford Book, 1998.
- [93] Klemic KG, Durand DM, and Jones SW. Activation kinetics of the delayed rectifier potassium current of bullfrog sympathetic neurons. *Journal of Neurophysiology*, 79(5):2345–57, May 1998.
- [94] Kawano S, Otsu K, and Shoji S. Calcium oscillations regulated by sodium-calcium exchanger and plasma membrane calcium pump induce fluctuations of membrane currents and potentials in human mesenchymal stem cells. *Cell Calcium*, 34(2):145–56, Aug 2003.
- [95] Karp G. *Cell and Molecular Biology*. Wiley, 2008.
- [96] Borlin N. Nonlinear optimization: Trust-region methods.
- [97] Hung J. Energy optimization of a diatomic system.
- [98] Burden RL and Faires JD. *Numerical Analysis*. Brooks-Cole, 2010.
- [99] Mathews JH. Runge-kutta-fehlberg method.
- [100] Sachse FB, Moreno AP, Seemann G, and Abildskov JA. A model of electrical conduction in cardiac tissue including fibroblasts. *Annals of Biomedical Engineering*, 37(5):874–89, May 2009.

- [101] Jongsma HJ and Wilders R. Gap junctions in cardiovascular disease. *Circulation Research*, 86(12):1193–7, Jun 2006.
- [102] Jongsma HJ and Wilders R. Limitations of the dual voltage clamp method in assaying conductance and kinetics of gap junction channels. *Biophysical Journal*, 63(4):942–953, Oct 1992.
- [103] Mohr P, Taylor BN, and Newell D. Codata recommended values of the fundamental physical constants: 2006. *Rev. Mod. Phys.*, 80:633–730, June 2006.
- [104] Bard Ermentrout G. Passive cell models: Comp neuroscience.
- [105] Docheva D, Padula D, Popov C, Mutschler W, Clausen-Schaumann H, and Schieker M. Researching into the cellular shape, volume and elasticity of mesenchymal stem cells, osteoblasts and osteosarcoma cells by atomic force microscopy. *J. Cell. Mol. Med.*, 12(2):537–52, April 2008.
- [106] Stewart P, Aslanidi OV, Noble D, Noble PJ, Boyett MR, and Zhang H. Mathematical models of the electrical action potential of purkinje fibre cells. *The Royal Society*, 367:2225–2255, May 2009.
- [107] Wang Z, Fermini B, and Nattel S. Sustained depolarization-induced outward current in human atrial myocytes. *Circulation Research*, 73(6):1061–76, Dec 1993.
- [108] Clayton RH, Bernus O, Cherry EM, Dierckx H, Fenton FH, Mirabella L, Panfilov AV, Sachse FB, Seemann G, and Zhang H. Models of cardiac tissue electrophysiology: Progress, challenges and open questions. *Progress in Biophysics and Molecular Biology*, 104(1-3):22–48, Jan 2010.

- [109] Wang J and Xie X. *Mesenchymal Stem Cells for the Heart*. Springer, 2009.
- [110] Pijnappels DA, Schalij MJ, van Tuyn J, Ypey DL, de Vries AAF, van der Wall EE, van der Laarse A, and Atsma DE. Progressive increase in conduction velocity across human mesenchymal stem cells is mediated by enhanced electrical coupling. *Cardiovascular Research*, 1;72(2):282–91, Nov 2006.